Aus dem
Lehrstuhl für Stoffwechselbiochemie, Biomedizinisches Centrum (BMC)
Institut der Ludwig-Maximilians-Universität München

Dissertation

zum Erwerb des Doctor of Philosophy (Ph.D.)

an der Medizinischen Fakultät der

Ludwig-Maximilians-Universität zu München

Mis-localization of endogenous TDP-43 leads to ALS-like early-stage metabolic dysfunction and progressive motor deficits

vorgelegt von:

Yiying Hu

aus:

Xuzhou, China

Jahr:

2024

Mit Genehmigung der Medizinischen Fakultät der

Ludwig-Maximilians-Universität zu München

Erstes Gutachten:	Prof. Dr. Dr. h.c. Christian Haass
Zweites Gutachten:	Dr. Bettina Schmid
Drittes Gutachten:	Priv. Doz. Dr. Heike Beck
Viertes Gutachten:	Prof. Dr. Paul Lingor
Dekan:	Prof. Dr. med. Thomas Gudermann
Tag der mündlichen Prüfung:	17.07.2024

Table of contents

Abstract

The key pathological signature of ALS/ FTLD is the aggregation of the Tar-DNA binding protein of 43 kDa (TDP-43, TARDBP). TDP-43 is an RNA- and DNA-binding protein expressed in all cell types. In physiological condition, TDP-43 is located in the nucleus. In disease conditions, mis-localization of TDP-43 from the nucleus to the cytoplasm results in cytoplasmic TDP-43 aggregation and nuclear clearing of TDP-43. Overexpression of TDP-43 in animal models has so far mainly been used to recapitulate features of ALS. However, these models likely generate unspecific toxicity and only poorly recapitulate the disease state since endogenous TDP-43 levels are very tightly regulated by autoregulatory feedback loops and high levels of wildtype and mutant TDP-43 are toxic.

An animal model that combines both features of nuclear clearing of endogenous TDP-43 and increased cytoplasmic TDP-43 would provide a valuable opportunity to gain further insights into early ALS pathology *in vivo* and develop more effective treatments. For my thesis, I generated a novel animal model, called CytoTDP, where nuclear TDP-43 is forced to locate to the cytoplasm by genetically inactivating a nuclear localization signal. CytoTDP fish exhibit early-stage phenotypes, similar to clinical features of ALS, including progressive motor defects, neuromuscular junction degeneration and muscle atrophy. Taking advantage of the fact that zebrafish embryonic development depends entirely on yolk consumption before 5 days post fertilization, I identified that microglia proliferation and activation in the hypothalamus (the metabolic regulatory center) is independent from food intake. I also compared transcript levels in the CytoTDP line to our previously generated TDP-43 knockout line and found that cytoplasmic toxic gain of function of TDP-43, rather than TDP-43 loss of function, leads to early onset glycogen mis-regulation.

Overall, the CytoTDP line mimics the ALS/FTLD hallmark of progressive motor defects. The results from my thesis suggest that weight loss and metabolic alterations observed in ALS patients might be caused by TDP-43 cytoplasmic gain of function as a direct consequence of dysfunction in the hypothalamus.

Therefore, the CytoTDP line can provide an important opportunity to investigate mis-regulated targets for therapeutic intervention at the early stages of disease progression.

List of figures

List of abbreviations

5-HT: 5-hydroxytryptamine

aa: amino acids

ALS: amyotrophic lateral sclerosis

ASOs: antisense oligonucleotides

BTX: bungarotoxin

BV-FTD: behavioral-variant frontotemporal dementia

C9ORF72: Chromosome 9 open reading frame 72

CNS: central nervous system

dpf: days post fertilization

DNA: deoxyribonucleic acid

DTI: Diffusion tensor imaging

fALS: familial ALS

FLAIR: fluid-attenuated inversion recovery

FTD: frontotemporal dementia

FTLD: frontotemporal lobar degeneration

FTD-MND: frontotemporal dementia-motor neuron disease

FTLD-MND: frontotemporal lobar degeneration-motor neuron disease

FTLD-TDP: TDP-43-positive FTLD

GO: gene ontology

GRN: progranulin

IBMPFD: inclusion body myopathy associated with Paget disease of bone and frontotemporal dementia

IF: immunofluorescence

IHC: immunohistochemistry

KI: knockin

KO: knockout

LCD: low-complexity domain

MAPT: microtubule-associated protein tau

MRI: magnetic resonance imaging

mRNA: messenger RNA

nAChR: nicotinic acetylcholine receptor

NFV-PPA: non-fluent variant primary progressive aphasia

NES: nuclear export signal

NLS: nuclear localization signal

NMJ: neuromuscular junction

PBS: phosphate-buffered saline

PCA: principal component analysis

PCR: polymerase chain reaction

PFA: paraformaldehyde

PPA: primary progressive aphasia

RFLP: restriction fragment length polymorphism

RNA: ribonucleic acid

RRM: RNA recognition motif

sALS: sporadic ALS

SD: semantic dementia

SEM: scanning electron microscopy

SOD1: superoxide dismutase 1

SR: sarcoplasmic reticulum

SV-PPA: semantic-variant primary progressive aphasia

TARDBP: transactive response DNA binding protein

Tardbpl: Tar DNA-binding protein of 43 kDa-like

Tardbpl_tv1: Tardbpl transcript variant 1

TDP-43: TAR DNA-binding protein of 43 kDa

UTR: untranslated region

WB: Western blotting

1. Introduction

1.1 Amyotrophic lateral sclerosis and frontotemporal dementia

Amyotrophic lateral sclerosis (ALS) and frontotemporal dementia (FTD) are considered to be two different neurodegenerative disease. However, an increasing amount of evidence suggests ALS and FTD can have overlapping clinical features (including movement deficits, dementia, weight loss and metabolic dysfunction), genetics and pathologies (Figure 1.1) (*1-3*). Thus, ALS and FTD are clinically, genetically, and pathologically interrelated.

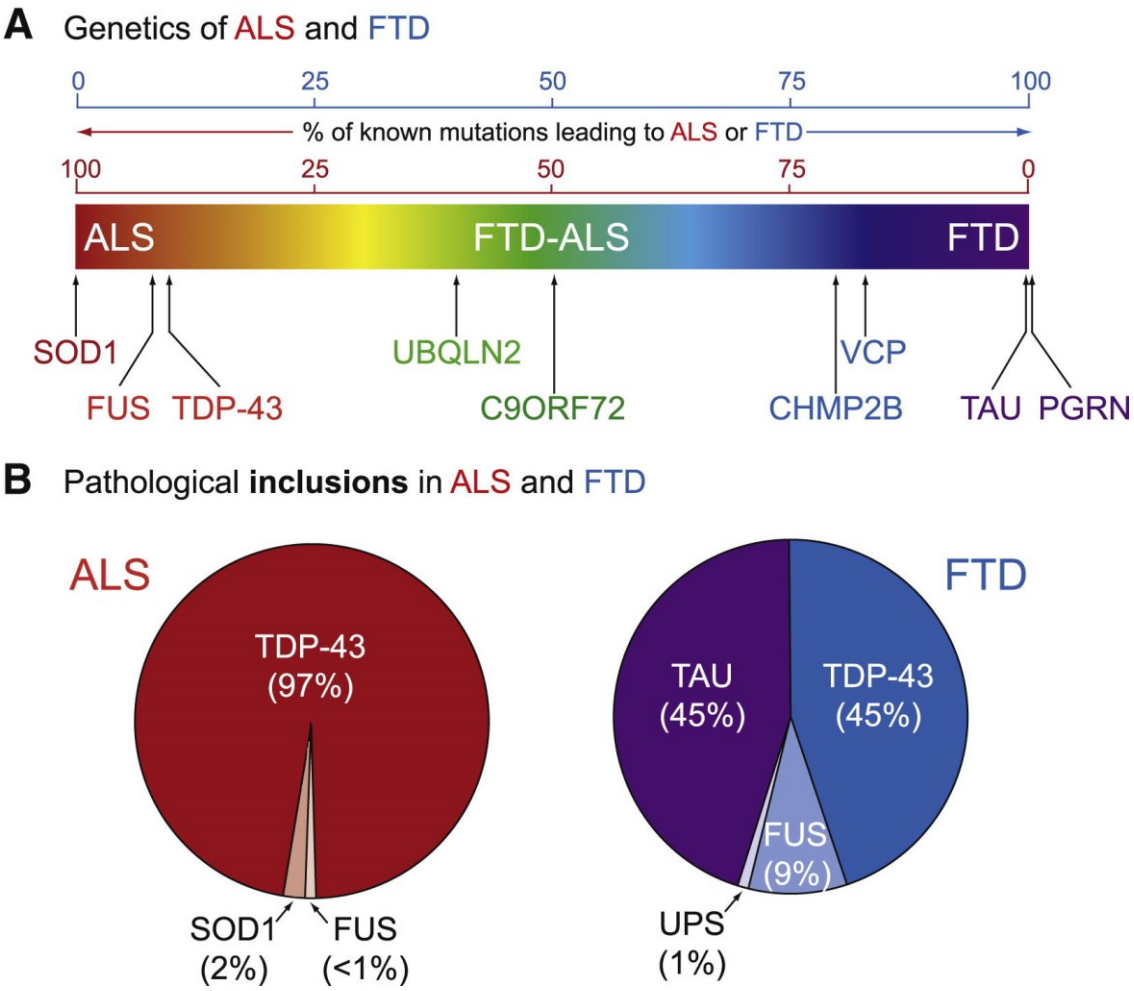

Figure 1.1: Genetic and pathological overlap between ALS and FTD (*4*).

(A) Predominant known genetic causes for ALS and FTD are graphed based on the proportion of known mutations leading to ALS or FTD. (B) Schematic diagram shows major pathological protein inclusions' proportion in ALS and FTD.

1.1.1 ALS

ALS is a fatal neurodegenerative disease characterized by upper motor neuron (UMN) and/or lower motor neuron (LMN) dysfunction (*5*). Most ALS patients die due to respiratory failure within 2-4 years from symptoms' onset (*5*-*7*). However, ALS is easily mis-diagnosed, because ALS is relatively rare and its clinical presentations are heterogeneous (*5*). ALS has more than 10 clinical phenotypes, including classical ALS, cervical onset ALS, lumbar onset ALS, flail arm, flail leg, pyramidal, respiratory onset, hemiplegic, cachexia, lower motor neurons, upper motor neurons, bulbar ALS, pseudobulbar palsy, and pseudobulbar affect (Table 1) (*5, 6*). Although ALS is relatively rare, the burden on the patient's family and the society is enormous. Delays in the early diagnosis of ALS can have an impact on caregiving and support, so the discovery of an early ALS biomarker could have big implications for ALS patients.

Table 1: ALS phenotypes (modified from Feldman, et al. 2022) **(*2*).**

Classical ALS	Phenotype presents with LMN and UMN signs. Muscle weakness begins in the limbs.
Cervical onset ALS	Phenotype belongs to classical ALS, but muscle weakness begins in the upper limbs, particularly hand.
Lumbar onset ALS	Phenotype belongs to classical ALS, but muscle weakness begins in the lower limbs, particularly foot.
Flail arm	Proximal muscle weakness is stronger compared to distal muscle weakness, patients with flail arm have LMN and UMN signs.
Flail leg	Muscle weakness in the legs caused by LMN dysfunction.
Pyramidal	Phenotype presents with UMN and LMN signs. UMN dysfunction can cause muscle weakness in controlling limbs, swallowing, and speaking.
Respiratory onset	Respiratory muscles' weakness caused by LMN and UMN dysfunction.
Hemiplegic	Phenotype presents with muscle weakness in one side of the body. Muscle weakness is caused by UMN dysfunction.
Cachexia	Weight loss and muscle loss with unknown cause.
Lower motor neurons	Muscle weakness, atrophy, and fasciculations are the characterizations of LMN dysfunction.
Upper motor neurons	UMN dysfunction is characterized by alterations in reflexes.
Bulbar ALS	Phenotype presents with LMN and UMN signs, begins with muscle weakness in controlling speaking and swallowing.
Pseudobulbar palsy	Phenotype starts from UMN signs and then spreads to limbs.
Pseudobulbar affect	Phenotype presents outbursts of emotions that cannot be controlled.

1.1.1.1 Epidemiology

The incidence of ALS is highest between the ages of 60 and 79 years (*8*), and the global annual incidence of ALS is approximately 1.9 cases per 100,000 people (*9*). The incidence of ALS varies by region. The incidence rate in Europe is slightly higher than on a global level (*10*), while it is lower in Asia (*11*). However, there is currently a rapid increase in the world's population over the age of 60 years, particularly in developing countries, where United Nations reports indicate that the proportion of older people will increase from around 9% in 2015 to 16% in 2040. Thus, there are epidemiologic studies that suggest a significant increase in the number of people with ALS between 2015 and 2040 and a shift in the weight of the disease from developed to developing countries (*12*). In the United States, the ALS Registry Act has been passed by the US Congress in 2008 which benefits epidemiologic estimates of ALS (*13*). While in developing countries, there is still a lack of such systematic registries of ALS patients, which raises a challenge for developing countries to predict and face the rise of ALS patients in the future.

1.1.1.2 Clinical presentation

1.1.1.2.1 Motor symptoms

The clinical presentation of ALS manifests as a combination of UMN and/ or LMN dysfunction leading to muscle wasting (*5*). Historically, ALS was therefore considered a relatively uniform disease of progressive muscle weakness. However, clinicians have demonstrated the heterogeneity of the clinical presentation of ALS over the past decades, and subdivided ALS into dozens of subtypes based on clinical manifestations and location of disease onset (*5, 6*). Among these ALS phenotypes, the most common ALS phenotypes are bulbar, cervical and lumbar onset. Motor neuron dysfunctions in ALS result in progressive

weakness of skeletal muscles involved in limb movement, swallowing and food intake, speech, and respiratory functions. ALS clinical phenotypes correlate with median survival, e.g., patients with the pseudobulbar palsy subtype have longer survival, patients with the flail arm subtype have slower disease progression, and patients with medullary onset of disease have a higher risk of developing FTD (*14, 15*). Therefore, understanding the heterogeneity of the clinical manifestations of ALS provides important information for the early diagnosis and prognosis of ALS. At the same time, this also illustrates the difficulty of conducting clinical studies on ALS.

1.1.1.2.2 Cognitive and behavioral dysfunction

Historically, it was thought that ALS was a pure motor disease. After decades of research on ALS, it has been found that approximately 50% of individuals with ALS have cognitive and/or behavioral dysfunction and 15% of individuals with ALS have FTD (*5*). Patients with ALS can experience a loss of normal language ability and executive functions, including weakened working memory, inhibition, and fluency. However, in ALS patients, long-term memory and spatial function remain unaffected (*16-19*).

In addition, patients with ALS may also experience depression, anxiety, and sleep disturbances, as well as emotional instability (*16, 20-22*).

1.1.1.2.3 Metabolic dysfunction

Weight loss has been recognized as one of the hallmarks of ALS, which is thought to be associated with malnutrition and hypermetabolism. On the one hand, it has been suggested that as ALS disease progresses, patients may experience decrease in nutritional intake for a variety of reasons, especially in patients who

develop cognitive impairment (*19, 23*). Reasons for decreased nutritional intake in ALS patients may include difficulty swallowing due to weakness of the pharyngeal muscles, loss of appetite due to altered hypothalamic function or depression, and difficulty eating due to hand weakness (*24, 25*). On the other hand, it has been shown that ALS patients suffer from hypermetabolism (*26*). Some studies report that about 50% of ALS patients have increased resting energy expenditure (*27, 28*). Therefore, the causes of weight loss in ALS patients are very complex.

Consistent with other neurodegenerative diseases, ALS has also been found to be associated with insulin resistance (*29*). Interestingly, several studies have suggested that insulin resistance may be protective against ALS (*30, 31*). In a Swedish study, type 2 diabetes was associated with a reduced risk of ALS, while type 1 diabetes was associated with an increased risk of ALS (*30*). However, large, prospective, multicenter studies in multiple countries are needed to further define the relationship between insulin resistance and ALS.

1.1.1.3 Genetics

ALS is categorized as familial ALS (fALS) or sporadic ALS (sALS). Approximately 10% of all ALS patients have a family history of ALS. However, pathogenic mutations found in fALS are also reported in sALS patients (*32*). Of the more than 40 ALS-associated genes identified to date, the most common are superoxide dismutase 1 (*SOD1*), chromosome 9 open reading frame 72 (*C9ORF72*), TAR DNA-binding protein (*TARDBP*), and fused in sarcoma (*FUS*) (*7, 33*) (Figure 1.2).

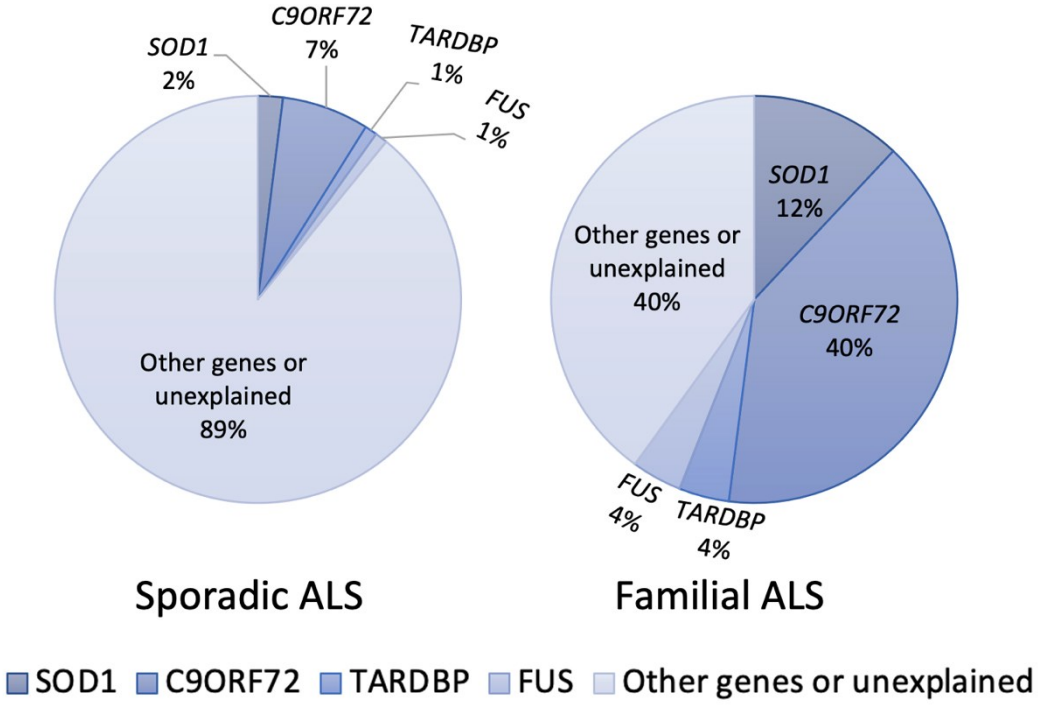

Figure 1.2: Contributions of *SOD1*, *C9ORF72*, *TARDBP* and *FUS* mutations in sporadic and familial ALS (modified from Akçimen, et al. 2023) **(*34*).**

In 1993, the superoxide dismutase 1 (*SOD1*) gene was the first gene shown to be associated with ALS (*35*). Pathogenic variants of SOD1 account for approximately 12-30% of fALS cases and less than 2% of sALS cases (*34, 36, 37*). More than 100 disease associated SOD1 variants have been identified since 1993 (*38*). In addition, almost all of the SOD1 variants are inherited in an autosomal dominant manner (except the D90A variant) (*37*). ALS patients with

SOD1 mutations lack TDP-43 pathology, which is found in more than 97% of all ALS cases. The SOD1 pathomechanism is therefore thought to be distinct from TDP-43 (*39, 40*).

Two independent studies demonstrated that expansions of the hexanucleotide repeat (GGGGCC) in the non-coding region of the Chromosome 9 open reading frame 72 (*C9ORF72*) gene are the most common genetic cause of ALS in European populations (*41, 42*). The hexanucleotide sequence GGGGCC is repeated in the *C9ORF72* gene about five times in healthy individuals, whereas an expansion of hundreds to thousands hexanucleotide repeats can be found in ALS patients. Gain of function (including RNA toxicity and toxic protein aggregates) and loss of function were considered to be relevant to the disease mechanisms. However, if the repeat size has a correlation with the clinical heterogeneity of ALS patients remains unclear (*43-45*). This hexanucleotide repeat expansion occurs in about 40% of fALS and about 7% of sALS cases in European populations, while is relatively rare in Asian populations (*34, 36*). Interestingly, cases with a GGGGCC expansion also showed TDP-43 pathology (*46*).

Researchers discovered in 2006 that the main component of the ubiquitinated protein inclusions present in most ALS patients is TDP-43 (*47, 48*), which was a landmark discovery in the field of ALS. Two years later, researchers found that mutations in the *TARDBP* gene can lead to ALS, which suggested that TDP-43 can also be a cause of ALS (*49-52*). *TARDBP* mutations account for only around 4% of fALS and 1% of sALS, which is less frequent than *C9ORF72* and *SOD1* mutations (*32, 53*). So far, more than 50 mutations in the *TARDBP* gene have been shown to be associated with ALS and most of them are in the carboxy-terminal low-complexity domain (LCD) (*50, 51, 54, 55*). This domain interacts with other heterologous ribonucleoproteins and is very important for TDP-43's solubility and localization in the cell (*47, 56, 57*). Some human TDP-43 mutations (including G294A, A315T, Q331K, M337V, Q343R, R361S, N390D, and N390S) have been shown to be related to toxicity and enhancing aggregation (*58-60*). Therefore, LCD is important in forming TDP-43 aggregates.

Similar to TDP-43, FUS is an RNA-binding protein. In 2009, it was discovered that mutations in the *FUS* gene also cause ALS (*61, 62*). The discovery of FUS-causing mutations in ALS patients further illustrate the important role of RNA metabolism in the pathogenesis of ALS. *FUS* mutations account for 4% of fALS cases and 1% of sALS cases (*32, 63*).

1.1.1.4 Pathology of ALS

In ALS patients, neurodegeneration affects primarily UMN and LMN (*64*). Various types of cytoplasmic inclusions can be found in degenerated motor neurons. The main protein component of these inclusion are either SOD1, TDP-43 or FUS (*65-69*).

Motor neurons loss leads to muscle denervation. Thus, ALS patients' muscles can have neurogenic atrophy and pseudohypertrophy (particularly affecting type 2 muscle fibers) (*65, 66, 68-70*).

1.1.2 FTD

FTD is an umbrella term characterized by progressive deficits in behavior, language, or executive function. The diagnosis of frontotemporal dementia can easily be confused with other mental illnesses, which can delay caregiving support. Frontotemporal lobar degeneration (FTLD) is the pathological condition of FTD (*71*). Classification of FTLD neuropathology is based on the identification of the major protein aggregates. Aggregation of TDP-43 in the cytoplasm occurs in approximately 45% of FTLD (*71*).

1.1.2.1 Epidemiology

The incidence of FTD is approximately 9.4 cases per 100,000 people (*72*). FTD is the second or third most common dementia in dementia patients younger than 65 years of age (*73*). However, the prevalence of FTD is most likely underestimated because it is easily misdiagnosed. 60% of patients with FTD have an onset age of 45-64 years, and only 10% have an onset age younger than 45 years (*74, 75*). The median survival time for FTD patients from diagnosis is 6 years but varies according to subtypes. For instance, the survival time for patients with frontotemporal dementia-motor neuron disease (FTD-MND) is only 2 years from diagnosis (*76*).

1.1.2.2 Clinical variants of FTD

FTD is classified into 3 subtypes according to clinical presentations: behavioral-variant frontotemporal dementia (BV-FTD), non-fluent variant primary progressive aphasia (NFV-PPA), semantic-variant primary progressive aphasia (SV-PPA) (Figure 1.3) (*77, 78*). FTD patients develop cognitive deficits. Some patients develop additional motor deficits at later disease stages, including

symptoms similar to motor neuron disease. Difficulties with moving, eating, and swallowing are present in these FTD patients at end-stage. Death in patients with FTD is usually caused by secondary infections such as pneumonia.

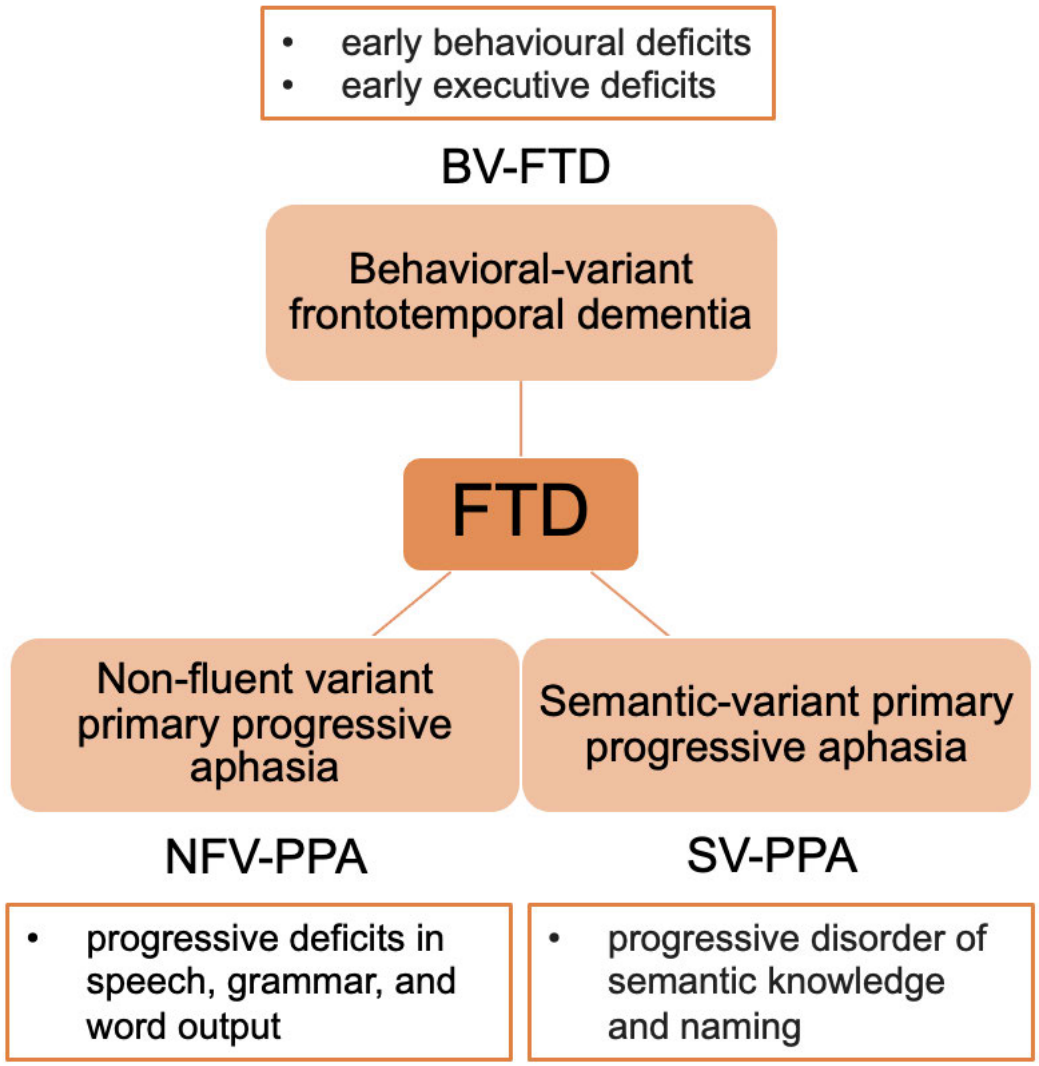

Figure 1.3: Clinical variants of FTD (modified from Bang, et al. 2015) ***(3)*.**

1.1.2.3 Clinical features

1.1.2.3.1 Cognitive, executive and language dysfunction

Cognitive-related common clinical symptoms in patients with FTD include social symptoms, emotional symptoms, compulsive behaviors, sensory symptoms, executive symptoms, neuropsychiatric symptoms (Figure 1.4) and language symptoms (Figure 1.5).

The most obvious early symptoms of BV-FTD include disinhibition, apathy, and personality changes (*3, 78*). Behavioral disinhibition can lead to inappropriate social behavior or even criminal behavior. Apathy manifests as decreased interest in hobbies, a behavior similar to symptoms of depression. At the same time, patients may lose empathy for family and friends. However, the patients themselves do not have much awareness of these changes. Since both Alzheimer's disease and BV-FTD have executive dysfunction, it can easily be misdiagnosed as Alzheimer's disease.

Patients with primary progressive aphasia (PPA) have language deficits at early stage and activities in daily living are impaired due to language dysfunction. Language dysfunction in patients with PPA includes object naming, speech production, and grammar or word comprehension. However, patients do not develop behavioral deficits at early stages of the disease (*79*).

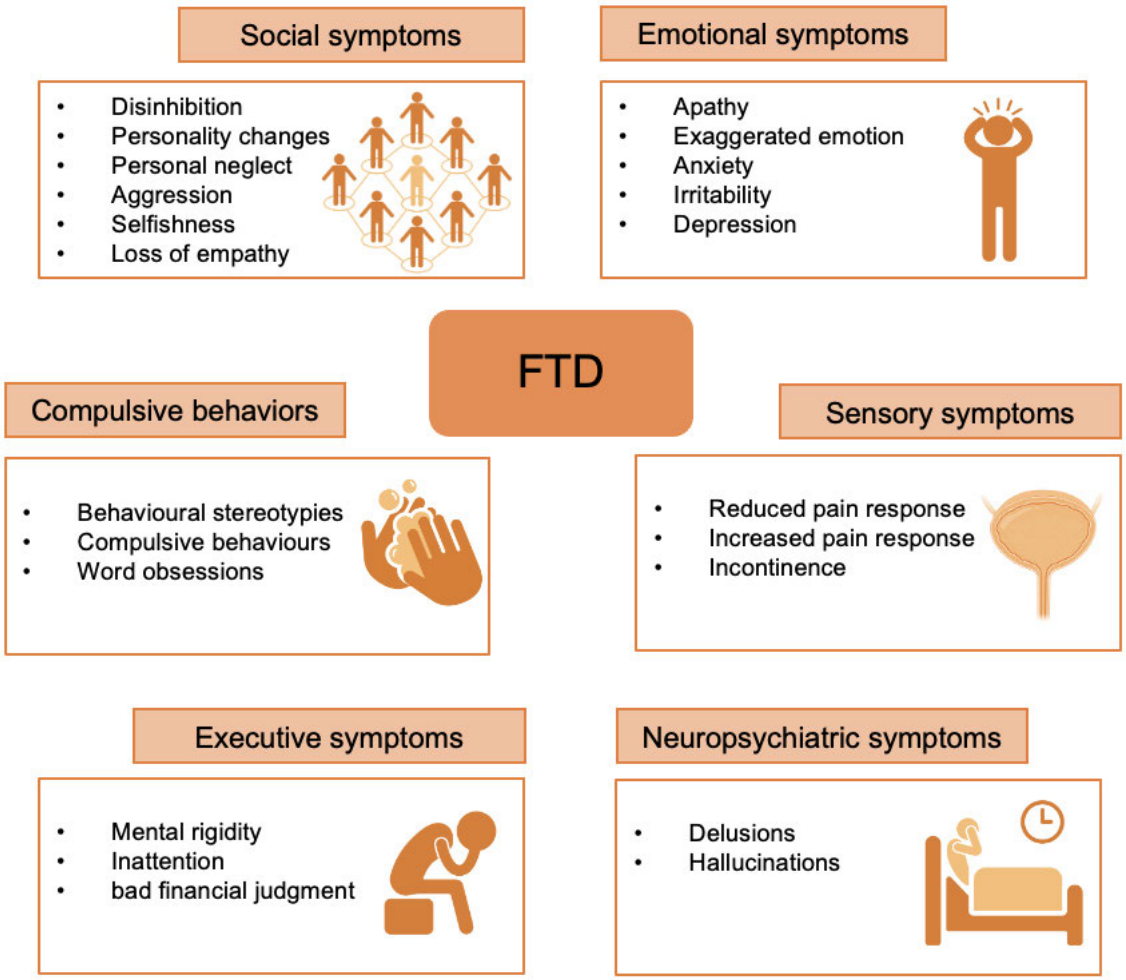

Figure 1.4: Cognitive and executive symptoms in FTD (*80*) (generated by Biorender).

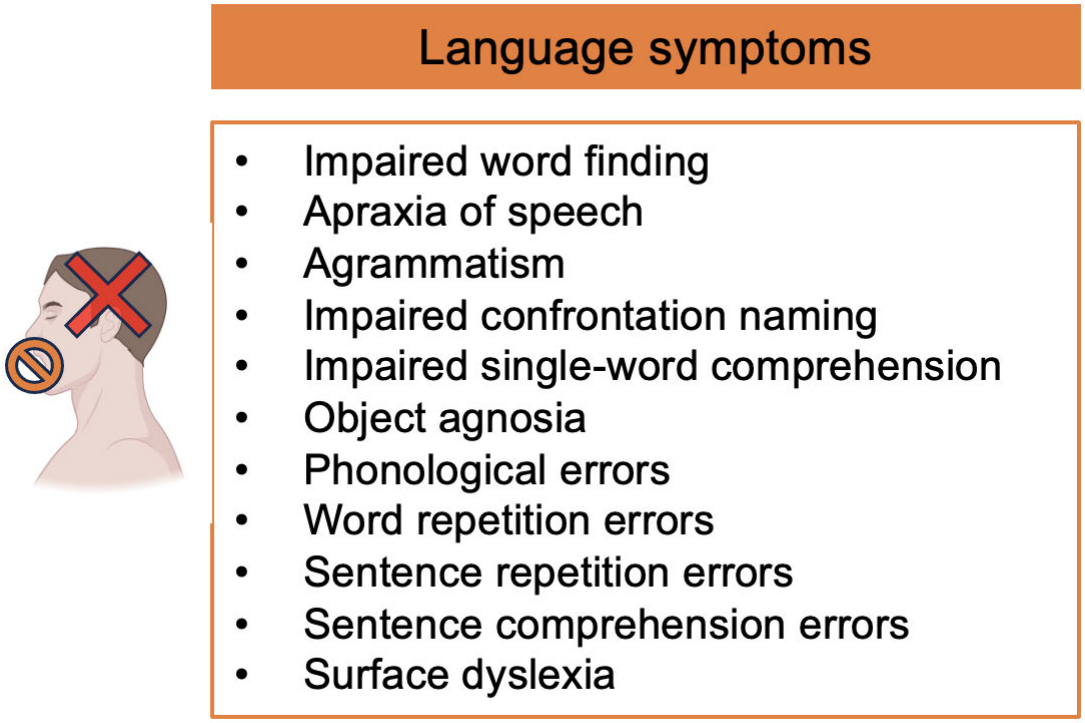

Figure 1.5: Language symptoms in FTD (*80*) (generated by Biorender)**.**

1.1.2.3.2 Motor symptoms

About 30% of FTD patients have mild motor dysfunctions (*81*). Motor neuron disease is most prominent in patients with BV-FTD rather than patients with PPA. It has been shown that about 12.5% of patients with BV-FTD can develop motor neuron disease (*81*). In addition, researchers have found pathology of frontotemporal lobar degeneration-motor neuron disease (FTLD-MND) in patients with clinically diagnosed as only FTD but not FTD-MND (*82*).

1.1.2.3.3 Metabolic dysfunction

Patients with FTD can have altered eating behaviors, including overeating, dietary changes, and other symptoms. These symptoms help differentiate FTD from Alzheimer's disease (*78, 83*). Strikingly, more than 60% of patients with BV-FTD have symptoms of altered eating behavior at initial presentation (*84*). However, changes in eating habits differ between FTD clinical subtypes, e.g., patients with BV-FTD showed mainly increased appetite, whereas patients with SV-PPA show mainly increased food selectivity (*85-87*). However, the changes in eating behavior of FTD patients are very complex and may be related to neuroendocrine pathological changes, cognitive changes, and cultural traditions, so the findings are easily confounded (*88*). In addition, dysphagia has been reported in all three subtypes of FTD, which can also affect eating behaviors of FTD patients (*89*).

Similar to ALS, insulin resistance has been found in patients with FTD (*90*) and the prevalence of diabetes is increased in patients with FTD (*91*), but the impact of diabetes on FTD progression and survival still requires further study.

1.1.2.4 Genetics

Approximately 40% of FTD patients have a family history, and mutations in the *C9ORF72*, Microtubule-Associated Protein Tau (*MAPT*) and Progranulin (*GRN*) genes account for approximately 60% of all fFTD cases (*3, 92*).

Mutations in the *C9ORF72* gene account for approximately 25% of fFTD patients and are the most common mutation in fFTD (*41*). Mutations in *MAPT* were the first mutations shown to be associated with FTD (*93-95*) and account for

approximately 20% of fFTD (*96*). Patients with *MAPT* mutants have pathologic manifestations of Tau-positive inclusions (*97*). Mutations in the *GRN* gene cause approximately 20% of fFTD (*96*), and the pathology is characterized by TDP-43 inclusion (*98*).

1.1.2.5 Pathology of FTD

FTLD is the pathological condition of FTD (*71*). The pathology of the FTLD brain is atrophy of the frontal and anterior temporal lobes. In addition, FTLD is a proteinopathy and is divided into different subtypes based on different abnormal protein inclusions. FTLD was initially divided into two categories: FTLD-tau (patients with Tau-positive inclusion) and FTLD-U (patients with Tau-negative ubiquitin-positive inclusions) (*99-101*). Later FTLD-TDP (patients with TDP-43 inclusion) was found to account for the majority of FTLD-U and FTLD-FUS (patients with FUS inclusions) was found in only a small subset of FTLD-U (*47, 102*). To date there are still unknown inclusion proteins in a small group of FTLD-U patients (*100*).

1.2 TDP-43

It was discovered that ALS and FTD are characterized by the abnormal aggregation of the TDP-43 (*47*). Inclusions of TDP-43 are found in around 97% ALS and around 45% FTD patients (*4*). A notable feature of these aggregates is that TDP-43 is abnormally phosphorylated, proteolytically processed, ubiquitinated and predominantly localized to the cytoplasm (*47*).

1.2.1 Physiological function of TDP-43

TDP-43 is a 414 amino acids (aa) protein encoded by the *TARDBP* gene, which is highly conserved and widely expressed. It contains two RNA recognition motifs (RRM1 and RRM2), and a low-complexity domain (LCD) at the C-terminus (Figure 1.6) (*103-105*). TDP-43 is expressed in almost every tissue and binds DNA, RNA and proteins (*103*). Under physiological condition, the protein is mainly localized to the nucleus. In addition, TDP-43 contains a nuclear localization signal (NLS) and nuclear export signal (NES) and shuttles between the cytoplasm and the nucleus. It has been shown that disruption of the NLS or NES can alter the subcellular localization of TDP-43 (*57, 106*).

Figure 1.6: Schematic diagram of human TARDBP (Figure from Hu, et al. Mol Neurodegener. 2024 (*107*)).

TDP-43 has important roles in regulating splicing, RNA transport, RNA stability, microRNA biogenesis and transcription (*56, 108-111*). It has been shown that

TDP-43 has essential functions in normal development since TDP-43 knockout (KO) mice are embryonic lethal (*112-114*).

Furthermore, TDP-43 function is very dose-sensitive, since endogenous TDP-43 levels are tightly regulated through an autoregulatory negative feedback loop. High levels of TDP-43 protein lead to a decrease in TDP-43 RNA levels by binding to its own 3' UTR and promoting mRNA destabilization (*115-117*).

1.2.2 TDP-43 proteinopathies

The hallmark features of TDP-43 proteinopathies are the clearance of endogenous TDP-43 from the nucleus with aggregation in the cytoplasm (*4*). Aggregates of TDP-43 are generally found in the motor cortex as well as in the spinal cord in ALS patients (*118-120*), and in the frontotemporal neocortex and the hippocampus in FTD patients (*47, 48, 121*). TDP-43 aggregates can also be found as a co-pathology in other neurodegenerative diseases (*122-127*) and has been recently categorized as Limbic-predominant age-related TDP-43 encephalopathy (LATE) (*128*).

In most ALS patients, the pathologic manifestations of TDP-43 are predominantly seen in neurons and glial cells (*40*), and the morphology of TDP-43 inclusions varies, including small granules, filamentous skeins, and Lewy body-like inclusions (Figure 1.7) (*129*). In addition, TDP-43 pathology in ALS patients with *TARDBP* mutations are difficult to be distinguished from ALS patients without *TARDBP* mutations (*51, 52, 130, 131*).

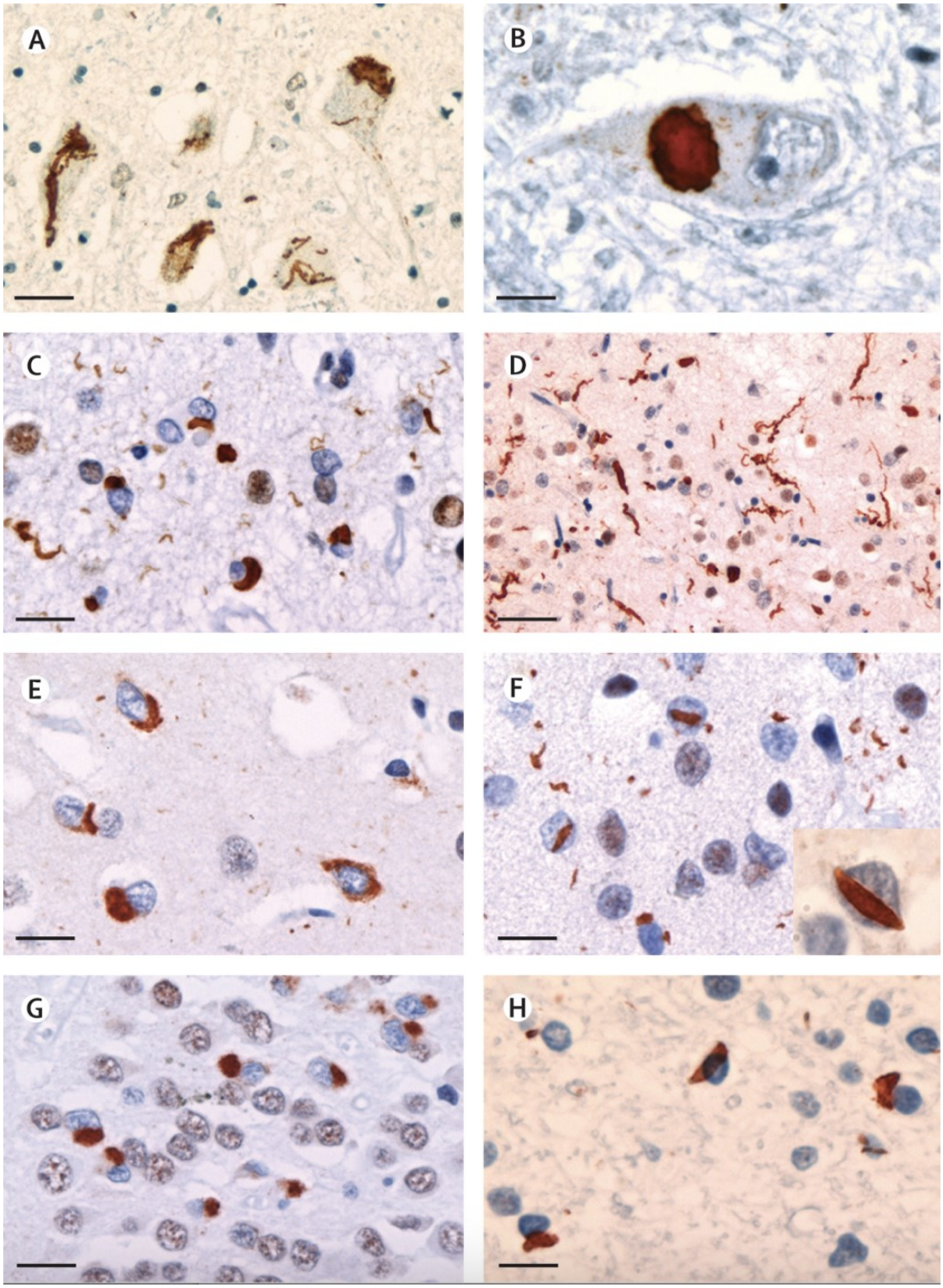

Reprinted with permission from [Elsevier and Copyright Clearance Center] [I. R. Mackenzie, R. Rademakers, M. Neumann, TDP-43 and FUS in amyotrophic

lateral sclerosis and frontotemporal dementia. Lancet Neurol 9, 995-1007 (2010), https://doi.org/10.1016/S1474-4422(10)70195-2]. Copyright [2010].

Figure 1.7: TDP-43 pathological characteristics in ALS and FTLD (Figure from Mackenzie, et al. 2010) (*129*).

(A-B) IHC stainings on ALS-TDP patients' tissues showing TDP-43-immunoreactive motor neuron with (A) skein-like and (B) round inclusions. Scale bars: A= 20 μm, B= 10 μm. (C-H) IHC stainings on FTLD-TDP patients' tissues showing TDP-43-immunoreactive (C) compact neuronal cytoplasmic inclusions and short neurites (type 1), (D) long neurites (type 2), (E) compact and granular cytoplasmic inclusions (type 3) and (F) abundant neuronal intranuclear inclusions (type 4). (G) Inclusions in the cytoplasm of dentate granule cells of the hippocampus. (H) Glial inclusions. Scale bars: B, H = 10 μm, C, G = 20 μm, D = 40 μm, E, F = 15 μm.

Interestingly, FTLD-TDP has four pathological subtypes (Figure 1.7): subtype 1 is predominantly found in patients with BV-FTD or NFV-PPA; subtype 2 is usually manifested as semantic dementia; subtype 3 is mainly associated with ALS accompanied by FTD; and subtype 4 is only found in the inclusion body myopathy associated with Paget disease of bone and frontotemporal dementia (IBMPFD) (*101, 132-135*). This suggests that patients with TDP-43 proteinopathies do not necessarily develop motor symptoms.

1.2.3 Zebrafish Tardbp and Tardbpl

tardbp and *tardbpl* are known as two orthologs of the human *TARDBP* gene in zebrafish. The *tardbp* gene encodes Tardbp (Tar DNA binding protein of 43 kDa). Zebrafish Tardbp is highly homologous to human TDP-43 and contains a RRM1, RRM2 and LCD. The *tardbpl* gene is either spliced to Tardbpl (Tar DNA binding protein of 43 kDa-like), that contains RRM1 and RRM2, but lacks the LCD, or to

Tardbpl_tv1 (*tardbpl* transcript variant 1), which contains RRM1, RRM2 and LCD (Figure 1.8) (*136, 137*).

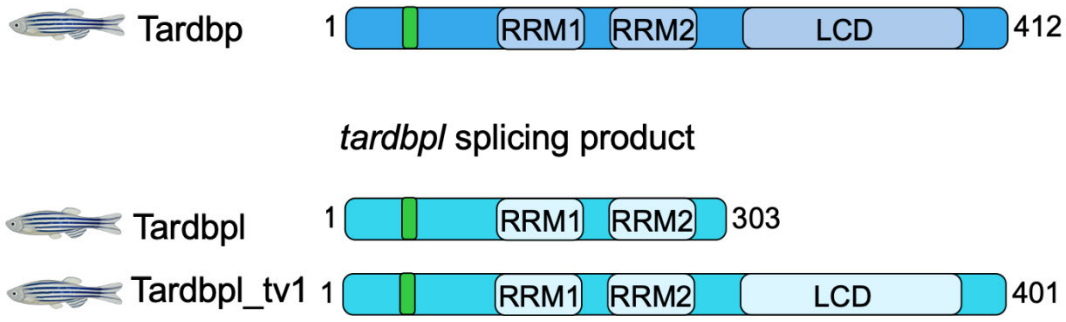

Figure 1.8: Splicing products from the zebrafish orthologs of human *TARDBP*, *tardbp* and *tardbpl* (Figure from Hu, et al. Mol Neurodegener. 2024(*107*)).

In wildtype fish, only very low amounts of Tardbpl_tv1 level are expressed. However, our group and others have previously shown that in Tardbp KO zebrafish, *tardbpl* splicing is changed in favor of Tardbpl_tv1 to compensate loss of Tardbp function (*136, 137*).

1.3 TDP-43 animal models

TDP-43 pathology is very common in ALS/FTD as stated previously. Therefore, using animal models to mimic TDP-43 proteinopathies can be very helpful investigating molecular and cellular disease mechanisms. Over the past decades, researchers have developed many animal models for ALS and FTD to gain more information related to the molecular pathomechanisms (*138*). Current TDP-43 animal models mainly include TDP-43 KO models, overexpression models and knockin (KI) models.

TDP-43 KO mice are embryonic lethal and heterozygotes develop motor deficits in later life (*114*). TDP-43 conditional KO mice develop pronounced ALS/FTD-like phenotypes, including dementia-like behavior, motor dysfunction, brain atrophy and neuronal loss (*139, 140*). In addition, ALS/FTD-like phenotypes have been found in zebrafish TDP-43 KO models (*136, 137*). These TDP-43 KO animal models have made important contributions to the understanding of the *in vivo* function of TDP-43. However, KO animals do not fully mimic the pathological manifestations of ALS/FTD due to the lack of cytoplasmic TDP-43 mis-localization and inclusions.

It has been shown that human TDP-43-ΔNLS overexpression in mice exhibit gain of cytoplasmic function of TDP-43 and are able to sequester nuclear TDP-43 in the cytoplasm which also mimics a nuclear loss of function at the same time (*141*). However, overexpression of TDP-43 brings unspecific toxicity because, as previously described, TDP-43 levels in cells are tightly regulated in auto-regulatory negative feedback loops. Other mouse model has previously demonstrated that even overexpression of WT TDP-43 can lead to toxicity (*117*).

To circumvent overexpression-associated toxicity, several TDP-43 patient mutation KI models have been generated, such as TDP43-A315T, TDP43-M337V, TDP43-G298S and TDP43-Q331K KI mice (*142-146*). Unfortunately, these knockin animal models showed very mild or late onset phenotypes, including mitochondria dysfunction with no other obvious phenotype. Behavioral

phenotypes started from 6 months of age onward. Therefore, we need new animal models to mimic the full TDP-43 pathology with nuclear clearing and a shift of TDP-43 to the cytoplasm as seen in ALS and FTD patients.

1.4 Goals of the study

TDP-43 is mainly localized in the nucleus under physiological conditions. However, in approximately 97% of ALS patients and 45% of FTD patients, TDP-43 can become mis-localized from the nucleus to the cytoplasm forming aggregates (*4*). Thus, whether loss of TDP-43 nuclear function or gain of cytotoxic function in the cytoplasm plays a crucial role in TDP-43-mediated neurodegenerative diseases is an important but unsolved question. Several studies have shown the connections between the loss of TDP-43 nuclear function and disease (*147-149*). However, progress in understanding the toxic functions of cytoplasmic TDP-43 has been slow, partly due to the lack of animal models that mimic this aspect of TDP-43 pathology. To investigate the loss of function and gain of function at a same time *in vivo*, our lab used a vertebrate model to generate a new TDP-43 disease model recapitulating both aspects of the pathology.

Therefore, the first goal of this thesis is to discover if the mis-localization of endogenous TDP-43 causes disease-like phenotypes. The second goal of this thesis is to identify dysregulated pathways in early ALS through transcriptomic analysis of this animal model.

2. Material and Methods

2.1 Material

2.1.1 Zebrafish lines

Zebrafish line	Origin
Wildtype AB	G. Streisinger, Institute of Neuroscience, University of Oregon, Eugene, USA
ΔNLS-Tardbp	DZNE, Munich, Germany
Tardbpl ^{mde114} used for Tardbpl -/-	Bettina Schmid & Alexander Hruscha, DZNE, Munich, Germany (*136*)
Tardbp ^{mde150}*/ Tardbpl* ^{mde114} used for TDP DKO	Bettina Schmid & Alexander Hruscha, DZNE, Munich, Germany (*136*)
Tg(mpeg1.1:EGFP-CAAX)	Ambra Villani, EMBL, Developmental Biology Unit, Heidelberg (*150*)

2.1.2 Genome editing of ΔNLS-Tardbp line

donor construct (ssDNA:
tgtgtatatatagcaattgagtttttctttttctagAAACTGTTCTGCCAGATAATgcagcagcaATG
GATGAGATCGATGCTTCATCTGCGACCAAGATCAAGAGAGGAGATCAGAA
GAC)

Cas9 protein (IDT Alt-R® S.p. Cas9 Nuclease V3)

crRNA:tracrRNA duplex (IDT,crRNA sequence:
CTGTTCTGCCAGATAATAAG).

2.1.3 Primer for sequencing and genotyping

T30	CCTTCTGAATTCTTTTAGCTGTCCA
T31	GCACCATGATGACTTCCCCA
T32	TCCTTCTGAATTCTTTTAGCTGTCC
T42	TCTCATCCATTGCTGCTGC

2.1.4 Antibodies

The following antibodies were used for Western blotting (WB).

Primary antibody	Dilution	Company
α-tubulin, T6199 (Mouse)	1:10000	Sigma
Tardbp 4A12-111 (Rat)	1:1	Helmholtz Center Munich
Tardbp 30G5-1-1 (Mouse)	1:20	Helmholtz Center Munich
Tardbpl_tv1 16C8-11 (Rat)	2:5	Helmholtz Center Munich

Secondary antibody	Dilution	Company
Anti-rat IgG2a, HRP conj.	1:1000	Helmholtz Center Munich
Anti-mouse IgG3, HRP conj.	1:1000	Helmholtz Center Munich
Anti-rabbit IgG, HRP conj. W4011	1:5000	Promega
Anti-mouse IgG, HRP conj. W4021	1:5000	Promega

The following antibodies were used for immunofluorescence (IF) and immunohistochemistry (IHC)

Primary antibody	Dilution	Company
Tardbp 30G5-1-1 (Mouse)	1:50	Helmholtz Center Munich
Rabbit anti-GFP, A-11122,	1:200	ThermoFisher
Rat anti-serotonin antibody, MAB352	1:200	Sigma
Mouse monoclonal antibody ZNP-1	1:200	DSHB
Tardbpl_tv1 16C8-11 (Rat)	2:5	Helmholtz Center Munich
anti-ubiquitin antibody #04-263 clone FK2	1:40,000	Merck

Secondary antibody	Dilution	Company
Goat anti-rabbit IgG Alexa 488, A-11034	1:200	ThermoFisher

Goat anti-rat IgG Alexa 546, A-11081	1:200	ThermoFisher
Donkey anti-mouse IgG Alexa 647, A-31571	1:200	ThermoFisher
Goat anti-mouse Alexa Fluor antibody, A-11029	1:200	Invitrogen

2.1.5 Reagents and consumables

Alexa Fluor 488-α-bungarotoxin, B-13422	ThermoFisher
ApeKI, R0643L	NEB
β-Mercaptoethanol, 4227.1	Roth
bromo phenol blue, 18030	Fluga
blotting Paper, MN218B	Macherey-Nagel
benzyl alcohol, 24122	Sigma
benzyl benzoate, W213802	Sigma

collagenase, C7657	Sigma
deoxynucleoside triphosphates (dATP, dCTP, dGTP, dTTP)	ThermoFisher
DAPI, D8417	Sigma
dimethyl sulfoxide, 317275	Merck
Dimethyl sulfoxide (DMSO), 317275	Merck
ECLplus, 1863031	ThermoFisher
GeneRuler DNA Ladder Mix, SM0333	ThermoFisher
goat serum, 16210072	Gibco
H_2O_2, LC-4458.2	neoLab
I-Block, T2015	Invitrogen
KOH, 221473	Sigma
low melting point agarose, 50180	MetaPhor
methanol, 4627.1	Carl Roth

newborn calf serum (NCS), N4762	Sigma
MG132, 474790	Millipore
N,N,N′,N′-Tetrakis-(2-hydroxyethyl)-ethylendiamin, 87600	Sigma
osmium tetroxide, 19152	EMS
paraffin, 6642.2	Carl Roth
petri dishes, 82.1473	Sarstedt
petri dish, 81156	ibidi
potassium ferricyanide, P8131	Sigma
precision Plus Protein All Blue Standard, 1610373	Bio-Rad
propidium iodide, P4864	Sigma
PVDF membrane, IPVH00010	Millipore
QIAzol Lysis Reagent, 79306	QIAGEN
tricaine, A5040	Sigma

thiocarbohydrazide, 223220	Sigma
triton X-100, X100	Sigma
urea, 3941.1	Carl Roth
X-ray films Super RX, 47410	Fujifilm

2.1.5 Commercial assays

Glycogen Assay Kit II (colorimetric), ab169558	Abcam
LX112 embedding kit	LADD
TruSeq stranded total RNA Sample Preparation kit	Illumina
ultraView diaminobenzidine (DAB) detection kit	Roche

2.1.6 Equipment and software

Agilent 2100 BioAnalyzer	Agilent

ATLAS5 Array Tomography	Fibics
centrifuge, 5427 R	Eppendorf
Crossbeam Gemini 340 SEM	Zeiss
Cytoscape	Cytoscape team
Fiji	NIH
ImageJ 2.3.0.	NIH
laboratory microwave	PELCO BioWave
LSM800 confocal	Zeiss
Leica S4E, KL200 LCD	Leica
Leica TCS SP5 II	Leica
Novaseq6000 sequencer	Illumina
GraphPad Prism 9.3.0.	Dotmatics
R langurage	The R-foundation
Ventana BenchMark ULTRA	Roche
ultra-diamond knife	Diatome
Ultramicrotome, UC7	Leica
Zebrabox tracking device, ZebraLabv3	Viewpoint

2.2 Methods

Please note: some figures and descriptions used in this part have similarities to a paper in the journal "Molecular Neurodegeneration", where I am the first author and wrote the first draft of the manuscript. As the first author of this paper, I was involved in all of the experiments and designed and performed most of the experiments. Experiments that are not mainly produced by me are marked clearly in this thesis.

2.2.1 Fish maintenance

All zebrafish used in this thesis were raised in the fish facility (DZNE, Munich) based on local animal welfare regulations. All the experiments performed with fish got approval from the District Government of Upper Bavaria, Germany. E3 medium was used to raise larvae from 0 dpf to 5 dpf in 28.5°C incubators (no more than 60 embryos per petri dish). For larvae older than 5 dpf, cocultures with rotifers were used to raise them until 16 dpf (*151-153*). Larvae were staged based on descriptions from Kimmel et al (*154*).

2.2.2 Generation of genome edited fish

P0 and F1 ΔNLS-Tardbp fish were generated by Alexander Hruscha, DZNE Munich. Generation and breeding of the ΔNLS-Tardbp fish line had approval from the government of upper Bavaria. To generate the ΔNLS-Tardbp line, CRISPR-Cas9 technology was used. A donor construct, Cas9 protein and a crRNA:tracrRNA duplex was injected into one cell stage wildtype embryos. Injected P0 fish were raised to 3 months of age and fins of injected P0 fish were clipped for restriction fragment length polymorphism (RFLP) analysis to check if DNA integration of the donor plasmid was successful as described (*155*). P0 positive founder fish were used for outcrosses and their offspring was screened

for germline transmission of the donor construct. From 60 pre-screened positive founder fish, 4 positive F1 fish were selected based on successful germline transmission. Sanger sequencing was used to confirm successful mutation of NLS1 (Figure 2.1).

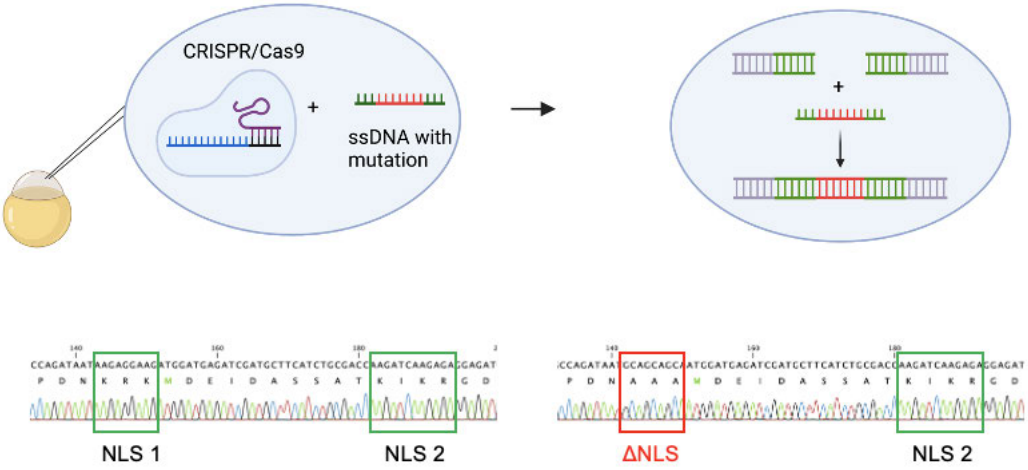

P0 and F1 ΔNLS-Tardbp fish were generated by Alexander Hruscha

Figure 2.1: Generation and confirmation of the zebrafish ΔNLS-Tardbp line (Figure from Hu, et al. Mol Neurodegener. 2024 (*107*))

Schematic drawing shows CRISPR/Cas9 genome editing approach to generate the ΔNLS-Tardbp line (top). Genome editing of NLS1 was confirmed by sequence reads in ΔNLS-Tardbp homozygous fish (bottom).

2.2.3 Immunohistochemistry

Ventana BenchMark ULTRA machine was operated by Michael Schmidt from the Zentrum für Neuropathologie, Munich. Freshly prepared 4% paraformaldehyde (PFA) in phosphate-buffered saline (PBS) was used for zebrafish embryos (5 dpf) fixation. All embryos (mutants and controls) were fixed in 4% PFA for 36 hours at 4 °C. After fixation, all embryos were washed thoroughly with PBS and then embedded with paraffin. Paraffin blocks with embryos were cut in 2 µm thick

sections. Immunohistochemistry (IHC) for TDP-43 was performed in a Ventana BenchMark ULTRA automated staining machine using the ultraView diaminobenzidine (DAB) detection kit. All IHC experiments were done based on the instructions of the manufacturer. The TDP-43 primary antibody was incubated at 37°C for 32 min.

2.2.4 Western blotting

Liquid nitrogen was used to freeze embryos or larvae. Frozen embryos or larvae were stored in a -80°C freezer. To lyse embryos or larvae samples, 4 X Lämmli buffer (20-40 µl of 4 X Lämmli buffer per fish) was added followed by sonication. Lysates were then boiled at 95 °C for 5 min with 800 rpm shaking. After the lysates were centrifuged at room temperature (5 min spin at 13,000 rpm), the supernatants were loaded on gels. For each lane on the 12% Tris glycine gel, ~10-20 µl of supernatant from each sample was loaded. Proteins were separated by electrophoresis and transferred to PVDF membranes. The PVDF membranes were blocked in 0.2% I-Block solution in PBST (0.1% Tween 20) for 1 h at room temperature. The PVDF membranes were then incubated in primary antibody in blocking solution for at least 15 hours at 4 °C. The following commercial primary antibodies were used for WB: anti-ubiquitin antibody clone FK2, α-tubulin. The following antibodies were generated by the Institute of Molecular Immunology, Helmholtz Center Munich: Tardbpl_tv1 16C8-11; Tardbp 4A12-111; Tardbp 30G5-1-1. After washing the PVDF membranes 4 X 15 min with 0.2% I-Block solution in PBST they were incubated in secondary antibody in PBST with blocking solution for 1 h. The following secondary antibodies were used to perform WB: Anti-rabbit IgG, HRP conj.; Anti-mouse IgG, HRP conj.; Anti-rat IgG2a; Anti-mouse IgG3, HRP conj. At last, the membranes were developed by ECLplus after 6 × 15min PBST washes.

2.2.5 MG132 treatment of zebrafish

Zebrafish embryos were collected at 2 dpf (48 CytoTDP fish and 48 Control fish). The chorion of the embryos was removed manually and dechorionated embryos were placed in a 24-well plate, with 6 embryos per well. 100µl of solution (treatment solution or control solution) was added to each well. For the treatment solution, 100µM or 200µM MG132 were prepared from a 5mM MG132 stock solution (in DMSO) diluted in E3 medium. For the control solution, the corresponding amount of DMSO was added to E3 medium. All the embryos were incubated in a 24-well plate at 28.5°C for 24 hours. The samples were collected at 3 dpf. Each sample contained 5 larvae, which were frozen in liquid nitrogen.

2.2.6 Tissue clearing and whole-mount immunofluorescence

This experiment was performed by Dr. Chenchen Pan, DKFZ Heidelberg.
CytoTDP fish with the Tg(mpeg1.1:EGFP-CAAX) transgene labeling microglia with membrane bound GFP were used for tissue clearing and whole-mount immunofluorescence. 5 dpf and 8 dpf zebrafish larvae from this cross were collected and 4% PFA used for fixation. Zebrafish samples were fixed at 4°C overnight. A modified protocol from DEEP-Clear was applied after short PBS washes of the samples (*156*). Samples were treated overnight with acetone that was prechilled at -20 °C, then gently washed 3 X 10 mins at room temperature with PBS. Then, 3% H_2O_2 in 0.8% KOH was used for depigmentation. Samples were placed in 3% H_2O_2 for 5-10 minutes. This depigmentation step was done under a dissection microscope (to closely monitor the depigmentation step). Accumulation of bubbles was avoided by manual rotating the tubes containing the fish samples. After five short PBS washes, the fish samples were treated with Solution-1.1 (10% (v/v) N,N,N′,N′-Tetrakis-(2-hydroxyethyl)-ethylendiamin, 5%

(w/v) urea and 5% (v/v) Triton X-100) at room temperature for 5-10 minutes. Samples were subsequently shortly washed in PBS 5 times. The blocking solution (10% goat serum in PBS) was added to samples and then gently shaken at RT for 3 hours. Samples were then incubated in primary antibody solution (5% goat serum in PBS) for 5 days at 4°C. The following commercial primary antibodies were used for this experiment: rabbit anti-GFP antibody, rat anti- 5-hydroxytryptamine, mouse monoclonal antibody ZNP-1. After several rounds of short PBS washes, the secondary antibodies with propidium iodide or DAPI in blocking solution (5% goat serum in PBS) were added to the samples and gently shaken at 4°C for 5 days. The following commercial secondary antibodies were used for this experiment: goat anti-rabbit IgG Alexa 488, goat anti-rat IgG Alexa 546, donkey anti-mouse IgG Alexa 647.

All zebrafish samples were shortly washed five times with PBS after immunofluorescence staining, then placed in agarose (1% agarose in PBS) and carefully aligned before solidification. Agarose gel blocks containing zebrafish samples were cut out and were collected in Eppendorf tubes. Gradient dehydration steps were conducted by incubation in 20%, 40%, 60% and 80% methanol solutions (in dH_2O) followed by incubation in 100% methanol overnight at RT. After 3 hours incubation in 100% methanol, BABB (1:2 mixture of benzyl alcohol and benzyl benzoate) was used for refractive index matching. The samples were covered with aluminum foil to prevent bleaching of fluorescence. Once samples achieved optical transparency, the samples were processed using further imaging steps.

2.2.7 Confocal microscopy and microglia quantification

This experiment was performed by Dr. Chenchen Pan, DKFZ Heidelberg.
Cleared agarose gel blocks that contained mounted zebrafish samples were put on a glass bottom petri dish. Zebrafish samples' entire heads were scanned using a 10x air objective of a confocal microscopy (step size 5 µm). A 4 X zoom was

used to image the hypothalamic region of zebrafish (step size 2 µm). FIJI was used for loading the imaging files with the ‘Split channels’ option for opening the files. Each channel of each file was saved as a separate ‘tiff’ file. The ‘Synchronize Windows’ function in FIJI was used for quantification of the microglia cell number in zebrafish whole-brain and in the hypothalamus. The nuclei staining channel was used for characterizing the border of the zebrafish hypothalamus. ‘Multi-point’ function was used for labeling the GFP positive cells in the zebrafish brain. After that, these locations were added to the ‘ROI Manager’. ‘Measure’ function was then used to quantify the number of microglia. High resolution confocal images were taken and used for the analysis of the morphology of microglia. Parameters of microglia (including microglial soma area, number of microglial main processes and average process length of microglia) were measured and quantified. Overall, 50 microglia (from 10 zebrafish) were measured and quantified in each group.

2.2.8 Whole-mount neuromuscular junctions staining

8 dpf and 16 dpf larvae were fixed in 4% PFA at 4 °C for 15-24 hours. Zebrafish samples were washed 3 X 10 min in PBS and incubated in pre-chilled acetone at -20 °C for 15 hours. After 2 X 5 min PBS washes, samples were incubated in 2 mg/mL collagenase (in PBS) for 40 min and washed 2 X 10 min with PBS. Blocking solution that contained 10% newborn calf serum in PBS, 1% DMSO, 0.8% Triton X-100, and 0.1% Tween-20 was used for blocking (40 min) at room temperature. Primary antibody ZNP-1 and Alexa Fluor 488-α-bungarotoxin diluted in blocking solution were added to samples and incubated at 4 °C for 2 nights. Samples were washed 3 X 10 min in blocking solution and then incubated (2 nights at 4 °C) in goat anti-mouse Alexa Fluor antibody diluted in blocking solution was used for incubation of samples. Finally, samples were washed 3 X 10 min in PBS and were ready for imaging steps.

2.2.9 Confocal microscopy and NMJ analysis

Glass bottom petri dishes were used for mounting 8 dpf and 16 dpf larvae. Larvae were placed on dishes and topped with1.5% (w/v) low melting agarose for mounting. During mounting, larvae were fast and gently moved in the desired orientation. Larvae' sagittal planes were imaged parallel to the glass slide of glass dishes. An inverted Zeiss LSM800 confocal was used for larvae imaging. Samples were scanned with a 10x objective. ImageJ 2.3.0 was used for quantifications of pre- and post-synaptic stainings at NMJ co-localization. During analysis, the 'measure' and 'color threshold' functions were used.

2.2.10 Scanning Electron Microscopy

Sample preparation and EM imaging was performed by Dr. Martina Schifferer, DZNE Munich. 8 dpf and 16 dpf zebrafish larvae were fixed in fixation buffer (4% PFA and 2.5% glutaraldehyde in 0.1 M sodium cacodylate buffer, adjusted to pH 7.4) in a microwave. The heads and tails of zebrafish were dissected, and the remaining larvae were fixed for 5 days. A standard rOTO microwave staining protocol was used (*157*) including a post fixation step. Post fixation buffer was 2% osmium tetroxide, 1.5% potassium ferricyanide in 0.1 M sodium cacodylate buffer (pH7.4). To enhance staining, samples were incubated in 1% thiocarbohydrazide at 40°C for 45 min. The samples were washed in water and 2% aqueous osmium tetroxide was used for the next incubation and washes. After that, samples were further contrasted by using 1% aqueous uranyl acetate for overnight incubation at 4°C and followed by 2h incubation at 50°C. An ascending ethanol series was applied for dehydration of samples and samples were infiltrated with LX112. Blocks were left to cure for 48h, then trimmed. A 35° ultra-diamond knife on ultramicrotome was used to cut the sample sections (thickness 100 nm). Carbon nanotube tape strips were used for sections' collections and then collected sections were used for scanning EM (SEM) acquisition. Adhesive carbon tape on

4-inch silicon wafers was used for attaching all samples. Crossbeam Gemini 340 SEM that contained a four-quadrant backscatter detector was used for acquiring EM micrographs, ATLAS5 Array Tomography was used in the process of acquiring EM micrographs. Regions of interest were identified by medium lateral resolution images (100 nm) and 4-10 nm lateral resolution was applied for imaging. Fiji was used for image analysis (*158*).

2.2.11 Behavioral assays

5 dpf and 8 dpf larvae were used for behavior tests. One larva was placed in one well of a 24-well plate for analysis. The Zebrabox tracking device was used for tracking their activity automatically. Larvae' moving distances and moving time were recorded and measured for 1 hour. A transparent background mode was used for larvae detection and the detection threshold was set to 18.

2.2.12 RNA isolation and library preparation

Library preparation and sequencing was performed at the Helmholtz Zentrum München by the Genomics Core Facility. Every sample contained 3 larvae (1.5 dpf) and samples were frozen in liquid nitrogen. All samples were homogenized in QIAzol with a homogenizer. The miRNeasy Micro Kit was used for the samples' total RNA extractions based on the manufacturer's instructions. An Agilent 2100 BioAnalyzer was used for controlling RNA quality and quantity. RIN values of all samples were tested and only RNA samples with a RIN value of 10 were used for total RNA sequencing. The TruSeq stranded total RNA Sample Preparation kit was used for preparing the libraries based on the kit's instructions. Following a final QC, a Novaseq6000 sequencer was used for sequencing by pooling the libraries and sequencing them in a 150 bp paired-end mode. The depth of every sample was around 120 million reads. FastQC 1.9 was used for checking raw

fastq files generated from sequencing. The zebrafish genome annotation GRCz11 from Ensembl was used for the raw data mapping and gene annotations.

2.2.13 Data analysis

Differential expression analysis and PCA analysis was performed by Özge Burhan, DZNE Munich. Differential expression analysis was done in R environment using the DESeq2 pipeline based on raw counts from RNAseq results (*159*). The cutoff of the differentially regulated genes was set based on adjusted p value equivalent to the 5% false discovery rate (padj ≤ 0.05). ClusterProfiler package in R environment was used for gene ontology analysis. In the pipeline of gene ontology analysis, groups which have more than four significant genes compared to control groups were analyzed. Cytoscape plugin cytoHubba was used for Hubgene analysis (*160*).

2.2.14 Glycogen quantification

Multi-well spectrophotometer was operated by Brigitte Nuscher, DZNE Munich. 5 dpf larvae were collected and frozen in liquid nitrogen. For sample preparation, chilled water was added to the 5 frozen larvae and homogenized rapidly. Glycogen was measured by the Glycogen Assay Kit II based on the manufacturer's instructions.

2.2.15 Statistics

GraphPad Prism 9.3.0. was used for statistical analyses. Survival analysis was performed using the Mantel-Cox test. Shapiro-Wilk test was used for checking

normality of data distributions. If variables of data were normally distributed, two-tailed T tests were used to compare two groups, and ANOVAs were used to compare more than two groups. If variable of data is not normally distributed, Mann-Whitney tests were used to compare two groups, and Kruskal-Wallis tests were used to compare more than two groups.

3. Results

Please note: some figures and descriptions used in this part have similarities to a paper in the journal "Molecular Neurodegeneration", where I am the first author, primarily generated the storyline and wrote the first draft of the manuscript. As the first author of this paper, I was involved in all experiments and designed and performed most of the experiments. Results that are not mainly produced by me are marked clearly in this results section.

3.1 Generation of the ΔNLS-Tardbp mutation in zebrafish

P0 and F1 ΔNLS-Tardbp fish were generated by Alexander Hruscha. Two orthologs of human *TARDBP* (*tardbp* and *tardbpl*) exist in zebrafish. Similar to human TARDBP, zebrafish Tardbp contains a bipartite NLS and both parts of the NLS are required for nuclear localization of Tardbp (Figure 3.1). Consequently, mutations in either segment of the NLS motif result in the accumulation of TDP-43 in the cytoplasm (*161*). To induce cytoplasmic translocation of endogenous Tardbp, a ΔNLS-Tardbp KI line was generated by genome engineering using CRISPR/Cas9. The amino acids of Tardbp NLS 1 were mutated from KRK to AAA (Figure 3.1).

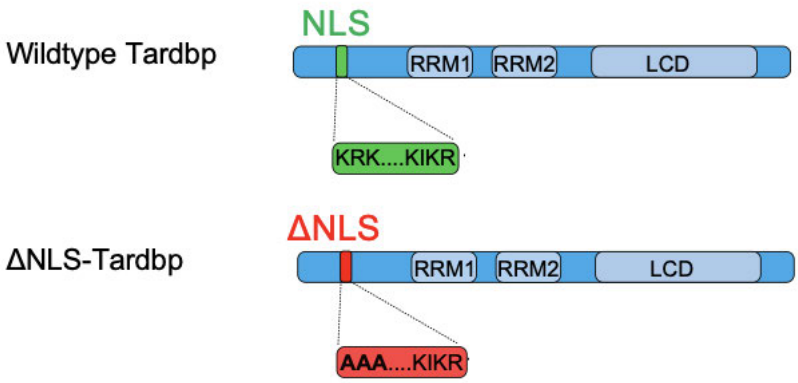

Figure 3.1: Mutation in ΔNLS-Tardbp (Figure from Hu, et al. Mol Neurodegener. 2024 (*107*)).

Schematic illustration emphasizes bipartite nuclear localization sequence (NLS) of zebrafish Tardbp. The ΔNLS-Tardbp mutation was introduced in the NLS by replacing the amino acids KRK with AAA.

Complete loss of Tardbp function does not result in any morphological phenotype because Tardbpl_tv1 is upregulated to functionally compensate Tardbp loss of function (*136, 137*). In this thesis, two zebrafish lines (1. *tardbp ΔNLS/ΔNLS; tardbpl +/+*. and 2. *tardbp ΔNLS/ΔNLS; tardbpl -/-*) were generated. I found that the *tardbp ΔNLS/ΔNLS*; *tardbpl +/+* fish look indistinguishable from wildtype fish from embryonic to adult stages (Figure 3.2A). I next analyzed the survival rates of *tardbp ΔNLS/ΔNLS; tardbp ΔNLS/+* and *tardbp +/+* and found that they had no statistically significant differences in survival compared to their siblings (Fig. 3.2 B).

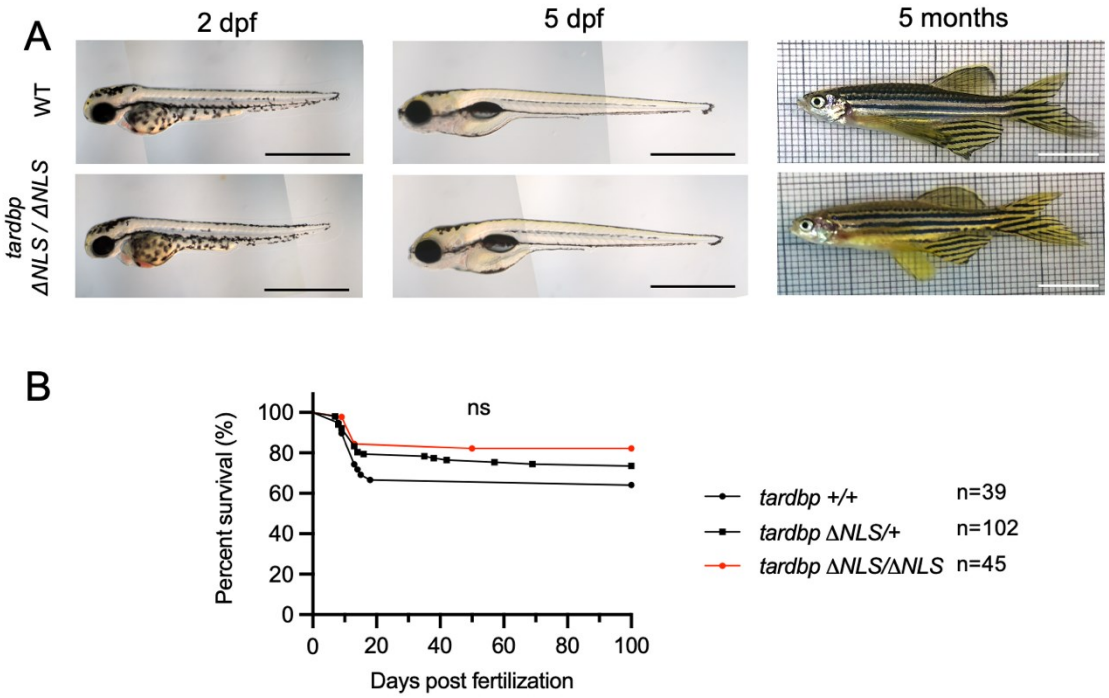

Figure 3.2: *tardbp ΔNLS/ΔNLS* fish do not exhibit noticeable morphological phenotypes (Figure from Hu, et al. Mol Neurodegener. 2024 (*107*)).

(A) Comparison between *tardbp* +/+ and *tardbp ΔNLS/ΔNLS* fish (2 dpf, 5 dpf and 5 months of age). Lateral view. (B) Percent survival rates of *tardbp* +/+ (n=39), *tardbp ΔNLS/+* (n=102) and *tardbp ΔNLS/ΔNLS* (n=45) animals from 0 dpf to 100 dpf revealed no significant difference, Mantel-Cox test.

To demonstrate that there is upregulation of Tardbpl_tv1 in *ΔNLS/ΔNLS*; *tardbpl* +/+ fish, I performed a WB with a Tardbpl_tv1 specific antibody. I found that the Tardbpl_tv1 levels were elevated in homozygous ΔNLS-Tardbp fish and Tardbp KO zebrafish compared to wildtype fish, consistent with previous findings (*136*). This suggested that *tardbpl* rescued the ΔNLS-Tardbp phenotype by promoting splicing towards the functionally equivalent Tardbpl_tv1 variant (Figure 3.3).

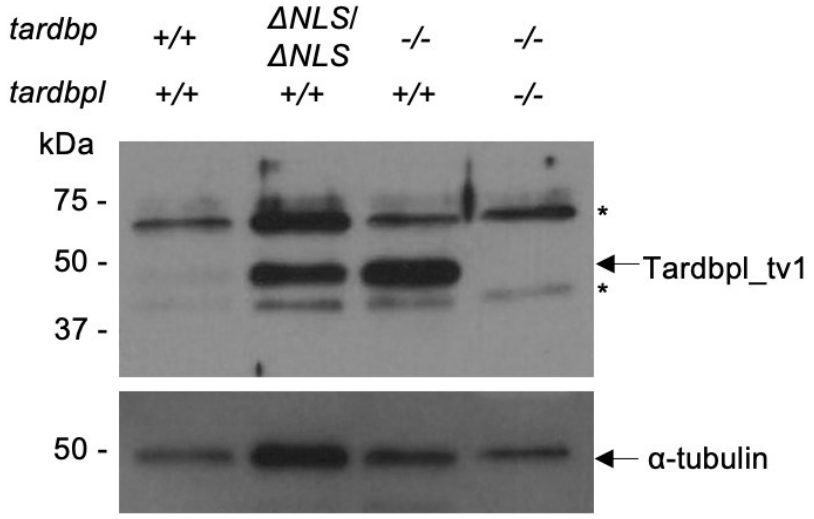

Figure 3.3: Tardbpl_tv1 is upregulated in tardbp ΔNLS/ΔNLS fish to compensate Tardbp loss of function (Figure from Hu, et al. Mol Neurodegener. 2024(*107*)).

Utilizing the Tardbpl_tv1 specific antibody 16C8, WB analysis revealed elevated Tardbpl_tv1 levels in *tardbp ΔNLS/ΔNLS* and *tardbp -/-* embryos compared to wildtype embryos. TDP DKO larvae shown in lane 4 were serving as a control to confirm the specificity of the Tardbpl_tv1 antibody, asterisks denoted unspecific bands. α-tubulin is utilized as a loading control.

The increase of Tardbpl-tv1 in a *tardbp ΔNLS/ΔNLS* background indicated rescue of a *tardbp ΔNLS/ΔNLS* phenotype. Thus, my next experiment was to investigate the phenotype of the *tardbp ΔNLS/ΔNLS* mutation in a *tardbpl -/-* background. For simplicity and conciseness, the *tardbp ΔNLS/ΔNLS; tardbpl -/-* larvae were designated CytoTDP and the *tardbp +/+; tardbpl -/-* larvae as Control. I discovered that the molecular weight of ΔNLS-Tardbp shifted from approximately 43kDa to a higher molecular weight by performing a WB with a Tardbp-specific antibody, accompanied by an 82% decrease in overall protein level (Figure 3.4).

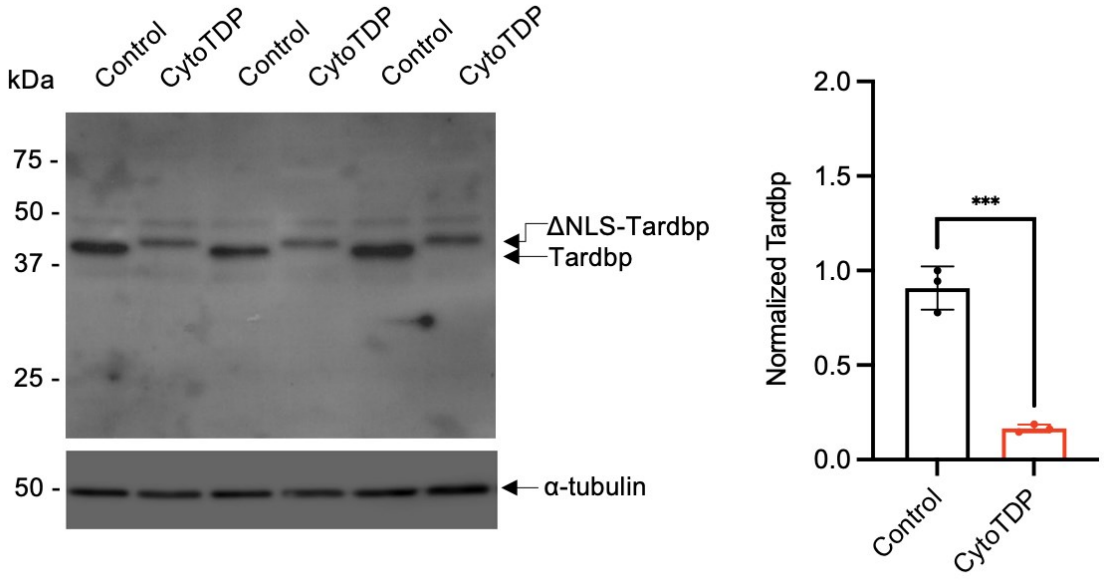

Figure 3.4: Tardbp has a molecular size shift and decreased levels in CytoTDP (Figure from Hu, et al. Mol Neurodegener. 2024 (*107*)).

WB analysis was conducted on 3 biological replicates using the Tardbp antibody 4A12, revealing diminished Tardbp levels and a molecular weight shift to a higher value in CytoTDP embryos when compared to Control (*tardbp* +/+; *tardbpl* -/-) embryos. Quantification of the WB showed that the Tardbp levels normalized to α-tubulin in CytoTDP embryos (5 dpf, n=3) were only 18% in comparison to Control (5 dpf, n=3), Unpaired T test.

I aimed to validate this result with commercially available antibodies against TDP-43 but they did not show any cross reactivity with ΔNLS-Tardbp. Fortunately, I obtained the custom made TDP-43 antibody 30G5 made by the Helmholtz Center Munich from Prof. Edbauer and Henrick Riemenschneider. I carefully optimized the WB conditions by titrating the antibody (Figure 3.5A) and comparing I-block versus milk as a blocking agent (Figure 3.5B).

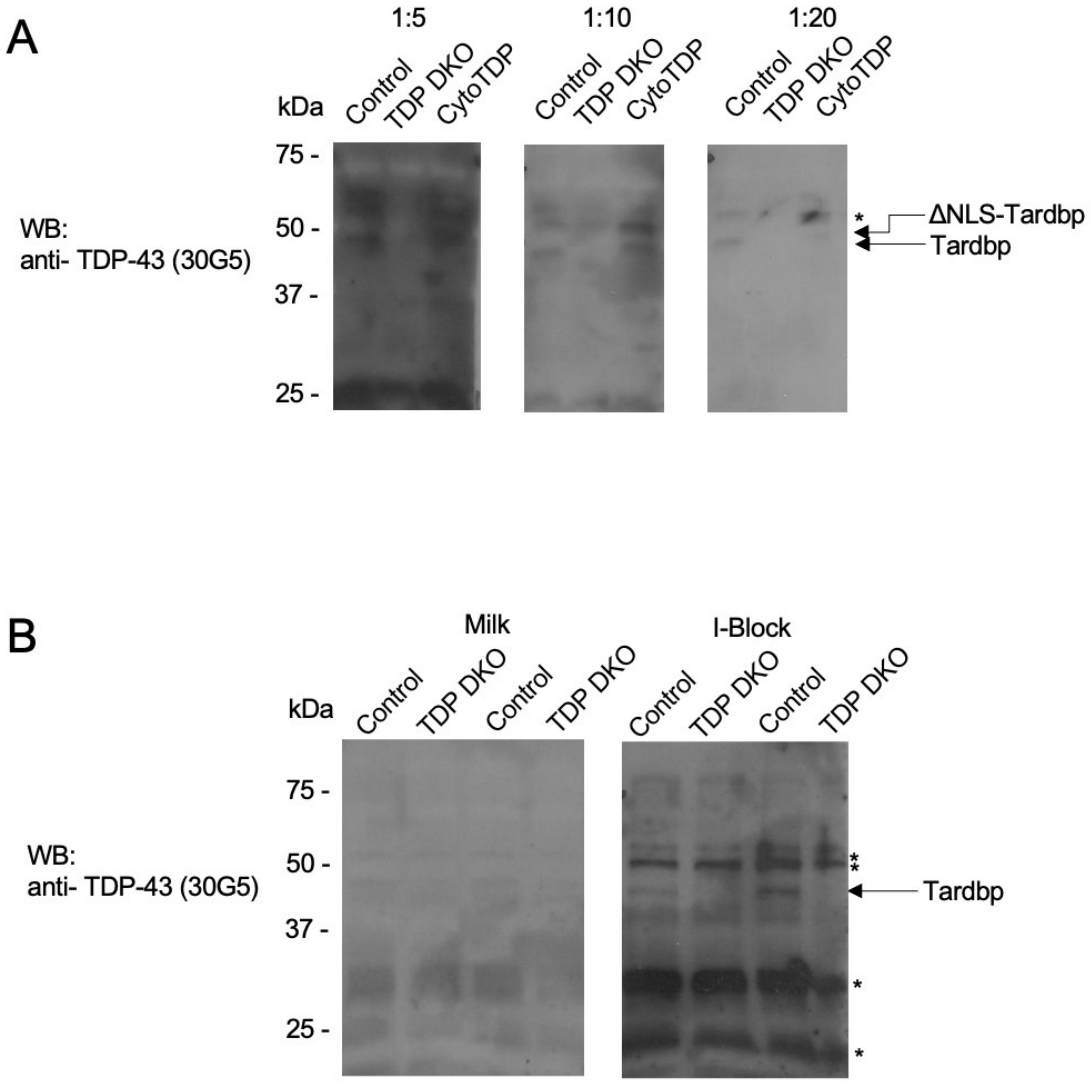

Figure 3.5: Diluting the 30G5 antibody and changing the blocking do not improve WB quality.

(A) WB analysis was conducted on Control, TDP DKO and CytoTDP fish using the Tardbp antibody 30G5 with different concentrations (1:5, 1:10, 1:20), revealing 30G5 can detect zebrafish Tardbp. Exposure time: 30 seconds. (B) Different block solutions (3% milk in PBST and 0.2% I-block in PBST) were used to improve the 30G5 (dilution 1:20) results. Exposure time: 3 minutes.

Since the level of TDP-43 in the CytoTDP line were severely reduced compared to Control fish, using the 30G5 antibody with the current WB protocol did not allow

clear visualization of a ΔNLS-Tardbp band, this antibody needed further optimization. I increased the blocking time between the primary and secondary antibodies (2 hours and 2.5 hours compared to the previous 1 hour), and I found that the WB background significantly decreased (Figure 3.6). Therefore, by optimizing the protocol, I was able to use a second TDP-43 antibody to verify the specificity of the ΔNLS-Tardbp band by WB.

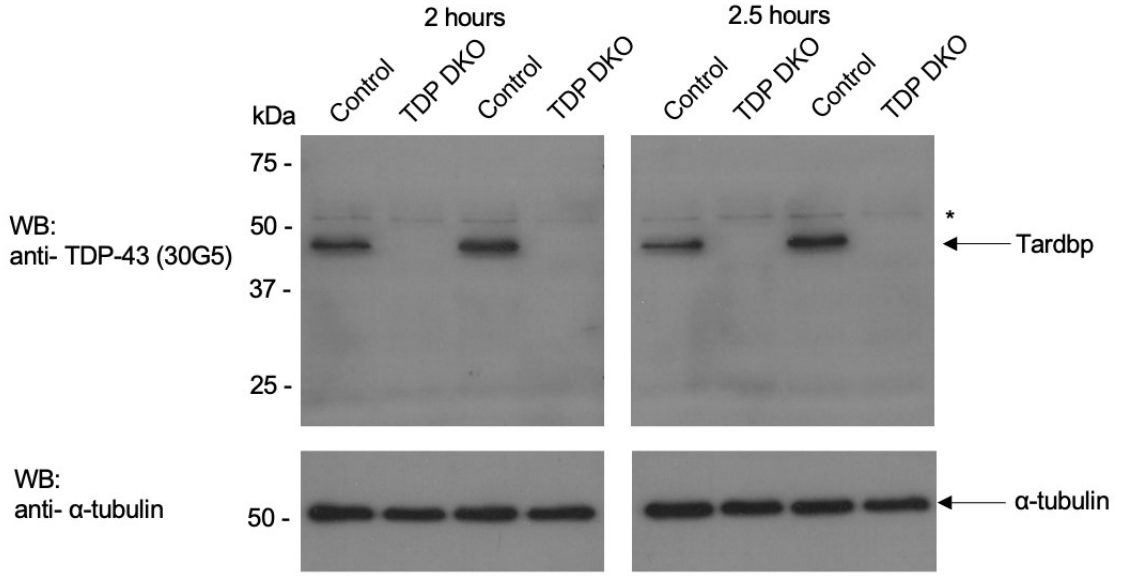

Figure 3.6: Increasing blocking time between primary and secondary antibody can decrease background.

WB analysis was conducted on Control and TDP DKO fish using the Tardbp antibody 30G5 (1:20) with increased blocking time (0.2% I-Block solution in PBST for 2 hours and 2.5 hours) between primary and secondary antibody. Exposure time: 30 seconds.

Two distinct TDP-43 antibodies (Figure 3.7A) were used on 2 days post fertilization (dpf), 3 dpf, 4 dpf, and 5 dpf Control and CytoTDP to confirm the ΔNLS-Tardbp band in CytoTDP fish (Figure 3.7B). The observed higher molecular weight of Tardbp in CytoTDP fish relative to Control indicated post-

translational modifications (ubiquitination or phosphorylation), as a consequence of the ΔNLS-Tardbp mutation.

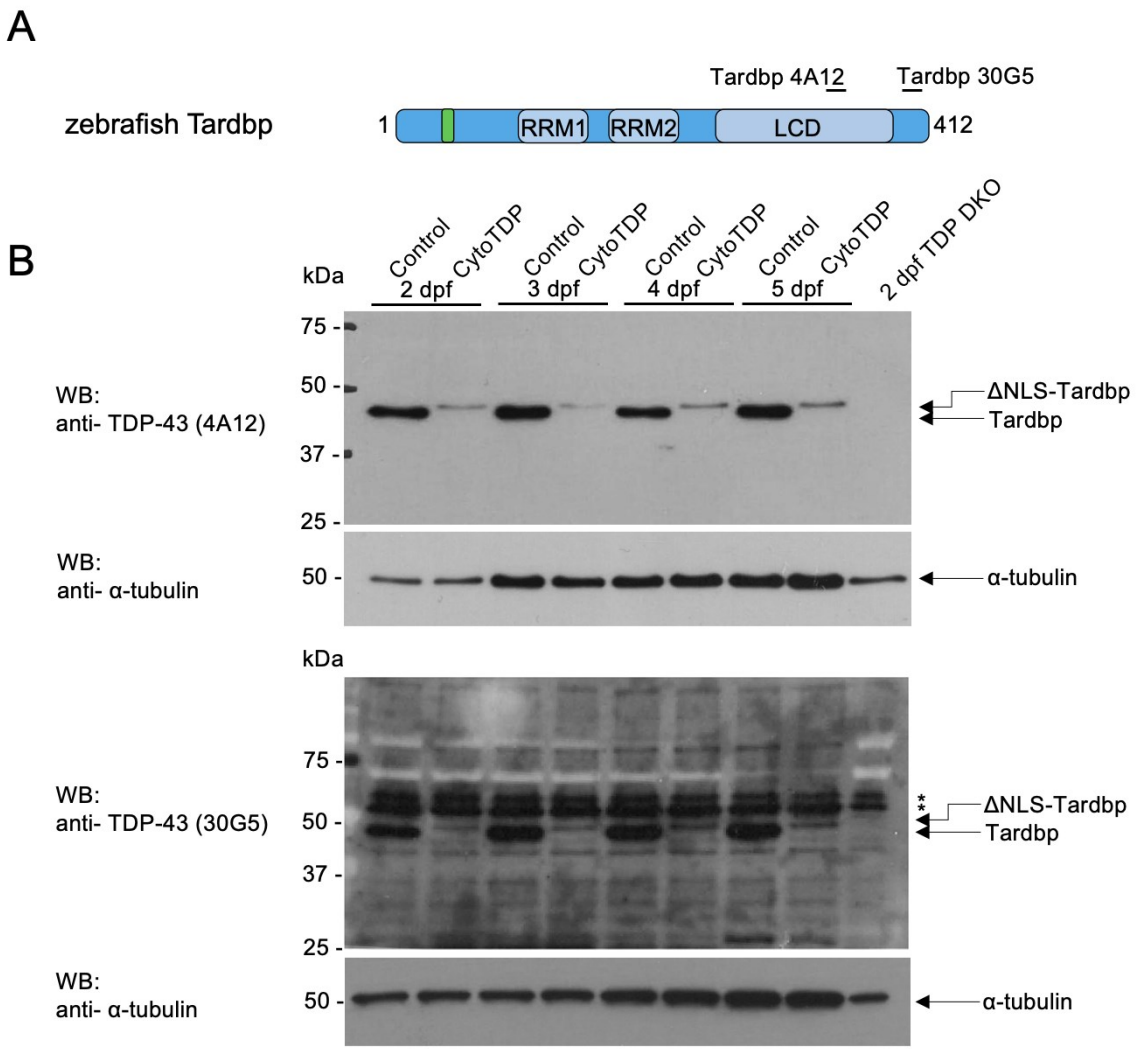

Figure 3.7: ΔNLS-Tardbp protein can be detected by two distinct TDP-43 antibodies (Figure from Hu, et al. Mol Neurodegener. 2024 (*107*)).

(A) Schematic illustration represents two different binding sites targeted by the 4A12 and 30G5 Tardbp antibody. (B) WB analysis was conducted on CytoTDP and Control embryos (2 dpf, 3 dpf, 4 dpf and 5 dpf) by using the 4A12 and 30G5 Tardbp antibodies. Unspecific bands are denoted by asterisks, with α-tubulin used as a loading control.

One of the reasons for the reduced ΔNLS-Tardbp levels could be increased degradation of Tardbp when forced to the cytoplasm. Proteasomal degradation is one of the main mechanisms for protein degradation. To test whether ΔNLS-Tardbp in CytoTDP fish is degraded by the proteasome, I treated CytoTDP with the proteasome inhibitor MG132. I first tested 100μM MG132 and performed WB analysis with an anti-ubiquitinated antibody to check for accumulation of ubiquitinated proteins. This did not show the expected smear of ubiquitinated proteins on the membrane but had an increase of high molecular weight ubiquitinated proteins, indicating of successful proteasome inhibition. There was no significant increase in TDP-43 levels compared to the untreated group (Figure 3.8A). I continued testing with 200μM MG132 but found that TDP-43 levels remained unchanged (Figure 3.8B). Higher concentrations of MG132 turned out to be toxic in zebrafish, so I could not further increase the MG132 concentration or treatment duration. These findings indicate that reduced amounts of ΔNLS-Tardbp may not a consequence of increased proteasomal degradation.

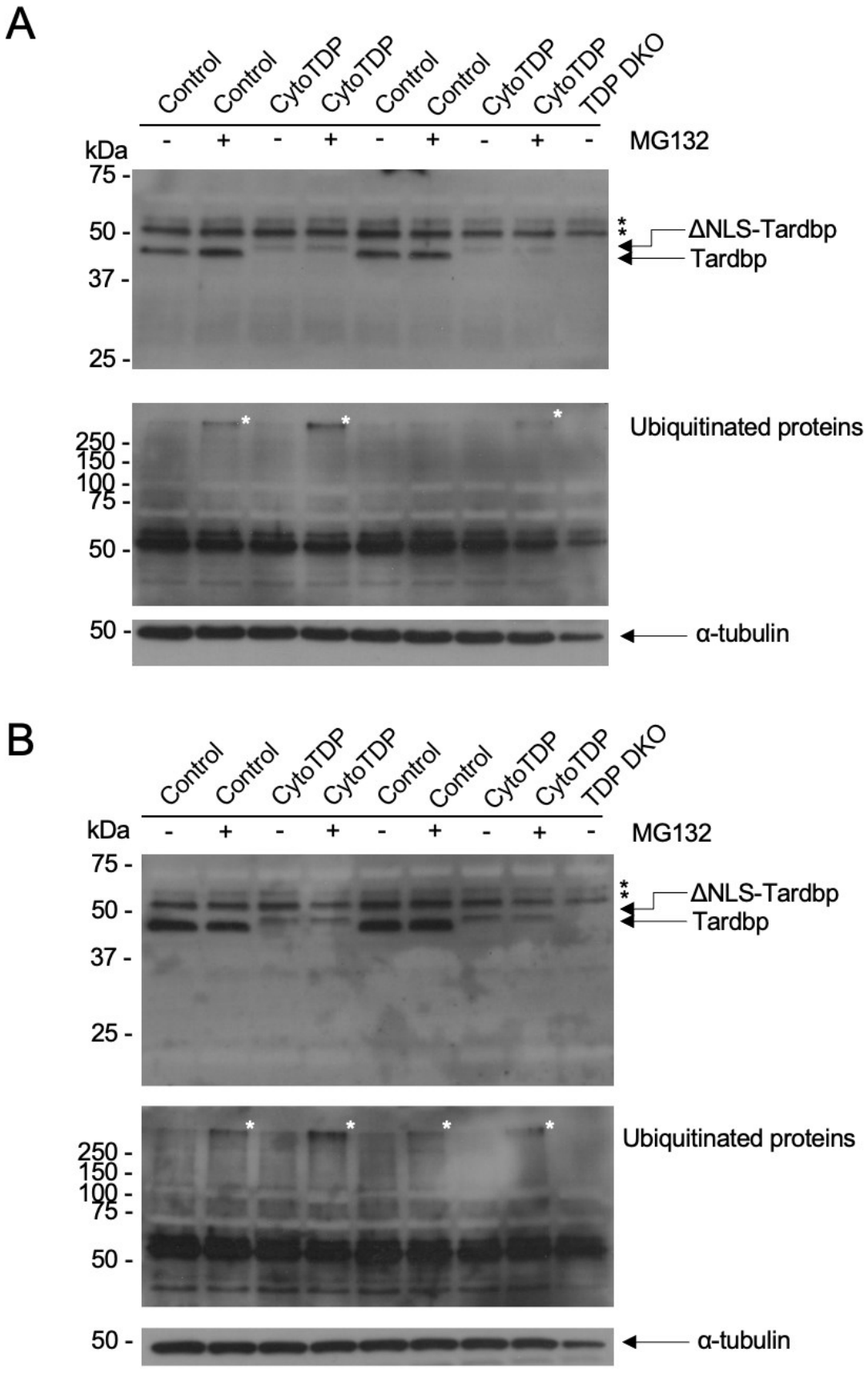
A
Control
Control
CytoTDP
CytoTDP
Control
Control
CytoTDP
CytoTDP
TDP DKO
kDa
- + - + - + - + -
MG132
75 -
50 -
37 -
25 -
**
ΔNLS-Tardbp
Tardbp
*
*
*
250 -
150 -
100 -
75 -
50 -
Ubiquitinated proteins
50 -
α-tubulin
B
Control
Control
CytoTDP
CytoTDP
Control
Control
CytoTDP
CytoTDP
TDP DKO
kDa
- + - + - + - + -
MG132
75 -
50 -
37 -
25 -
**
ΔNLS-Tardbp
Tardbp
*
*
*
*
250 -
150 -
100 -
75 -
50 -
Ubiquitinated proteins
50 -
α-tubulin

Figure 3.8: MG132 treatment does not change Tardbp level in CytoTDP line.

WB analysis was conducted on (A) 100μM MG132 and (B) 200μM MG132 treated Control and CytoTDP embryos (3 dpf) by using the anti-Tardbp antibody 30G5 and anti-ubiquitinated proteins antibody. White asterisks mark differences in WB with anti-ubiquitinated proteins antibody between treated and untreated fish. Unspecific bands are denoted by black asterisks, with α-tubulin used as a loading control.

I next investigated the morphology of CytoTDP and noticed that some CytoTDP fish displayed a clear hypopigmentation phenotype, which can be used as a distinctive morphological marker for their identification solely through visual inspection. This finding is very helpful and time saving in CytoTDP fish selection (Figure 3.9).

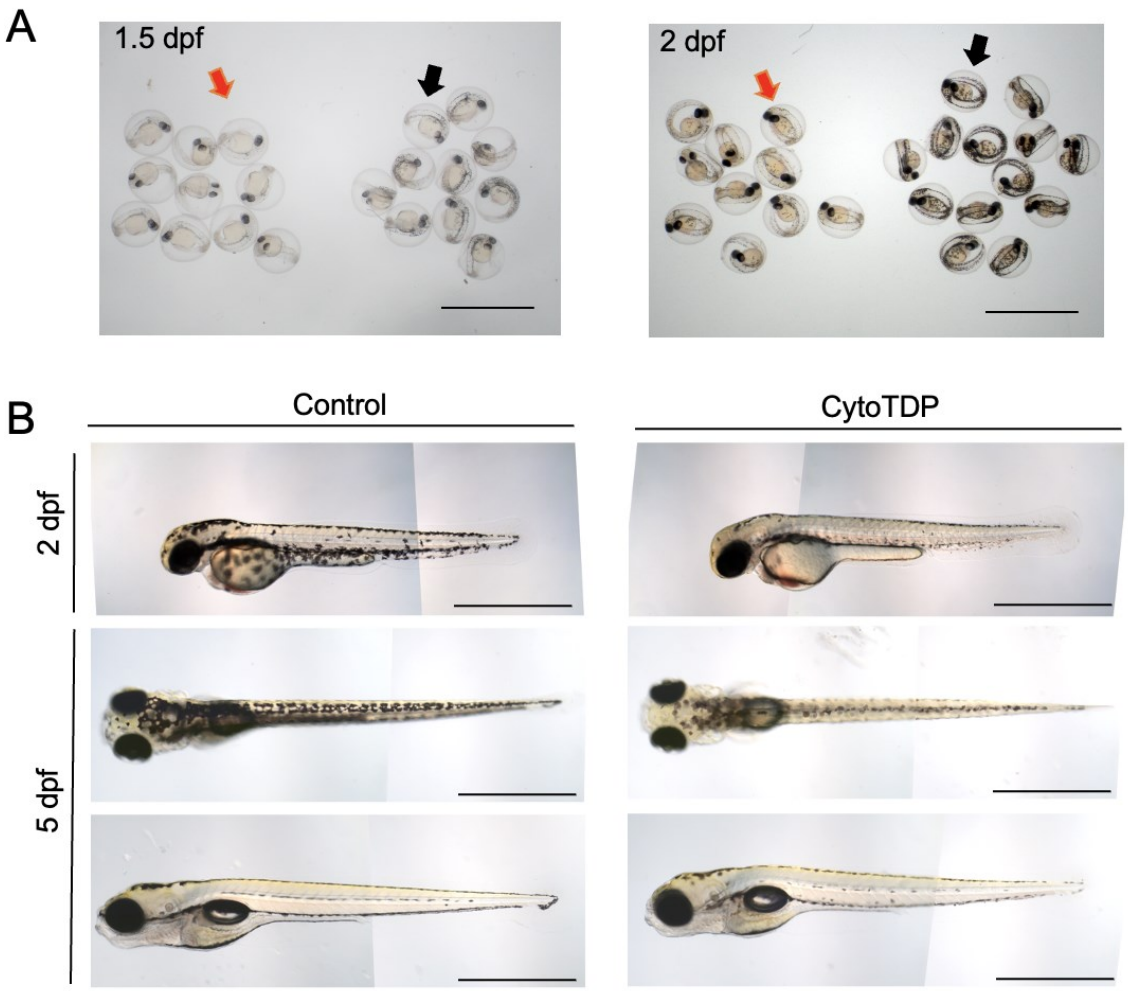

Figure 3.9: Pigmentation phenotype of CytoTDP fish (Figure adapted from Hu, et al. Mol Neurodegener. 2024 (*107*)).

(A) Pictures of petri dishes that contain sorted 1.5 dpf and 2 dpf CytoTDP larvae (red arrow) based on the pigmentation phenotype and their siblings (black arrow). Scale bar=2mm. (B) Hypopigmented CytoTDP embryos exhibited significantly decreased pigmentation compared to their siblings (2 dpf), as seen from a lateral view in the top panel. At 5 dpf, the hypopigmentation remained evident from a dorsal perspective (middle panel) but appeared less pronounced from a lateral view (bottom panel). Scale bar=1mm.

I also observed that CytoTDP fish exhibited a similar body length compared to their siblings at 2 dpf, but were notably smaller at 5 dpf and 14 dpf (Figure 3.10A).

The majority of the CytoTDP fish died within the first 4 weeks post-birth, with only a few surviving beyond that period (Figure 3.10B). These survivors were significantly smaller than their siblings (Figure 3.10C).

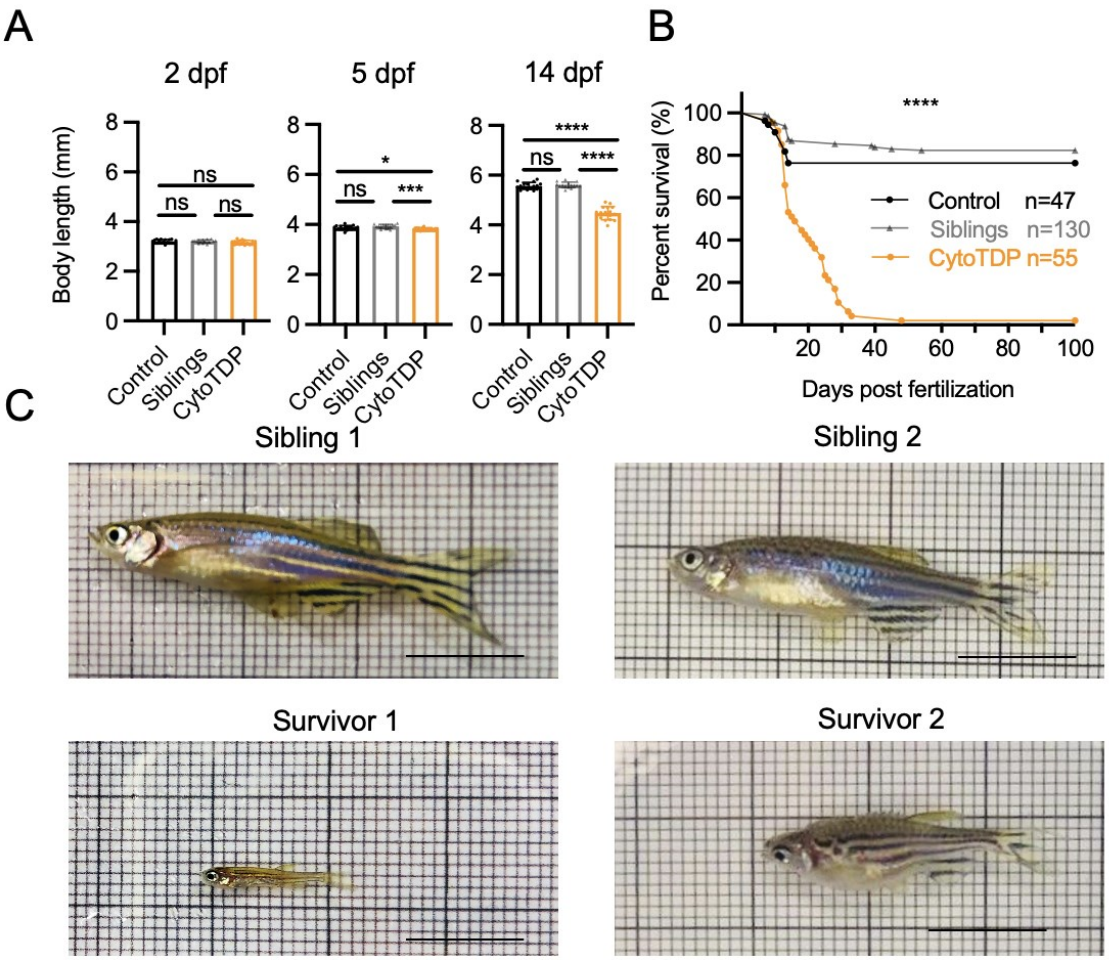

Figure 3.10: CytoTDP fish have shorter body lengths compared to siblings and are lethal (Figure from Hu, et al. Mol Neurodegener. 2024 (*107*)).

(A) Measurement of body length of CytoTDP (orange dots) and their siblings [Control (black dots): *tardbp +/+; tardbpl -/-*, Siblings (grey arrow heads): *tardbp ΔNLS/+; tardbpl -/-*] at 2 dpf, 5 dpf and 14 dpf. ANOVA test, n=16 (Control), n=15 (Siblings), n=16 (CytoTDP). (B) Kaplan-Meier analysis of CytoTDP (orange line, n=47) and its siblings [Siblings (tardbp ΔNLS/+; tardbpl-/-) (grey line, n=130), Control (tardbp +/+; tardbpl-/-) (black line, n=55)]. Within one month, 94.55% of CytoTDP larvae do not survive, with only 1.82% of them surviving beyond 3 months. Mantel-Cox test. (C) Images of two

CytoTDP survivors (5 months old fish in the left panel and 6 months old fish in the right panel). These survivors exhibit smaller sizes compared to their siblings. Scale bar=1cm.

To verify that the ΔNLS-Tardbp mutation leads to Tardbp cytoplasmic mis-localization, I performed TDP-43 stainings on CytoTDP and Control fish. Stainings of Tardbp have been shown in the past to be very challenging and sensitive in zebrafish. In addition, I was facing the fact that there are only a limited availability of antibodies that cross-react with zebrafish. I teamed up with Dr. Arzberger, an experienced neuropathology specialist, and successfully established a staining pipeline for TDP-43 stainings in zebrafish (Figure 3.11).

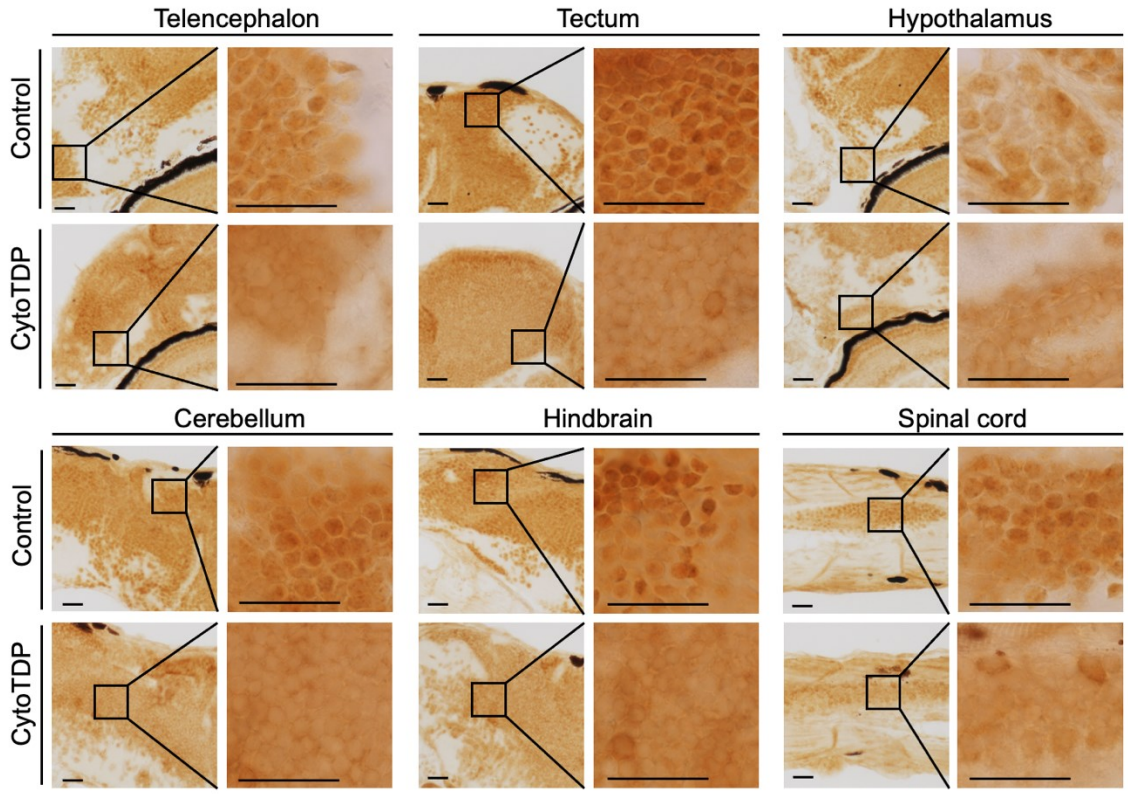

Figure 3.11: Mis-localization of Tardbp in CytoTDP fish (Figure from Hu, et al. Mol Neurodegener. 2024 (*107*)).

Images of Tardbp immunohistochemical stainings of 5 dpf CytoTDP fish and Control fish showed reduced level of Tardbp in the nucleus and an increased cytoplasmic Tardbp level in CytoTDP fish. Scale bar=100μm.

3.2 Age dependent movement phenotypes in CytoTDP line

Patients with ALS suffer from progressive motor deficits and muscle weakness (*2*). A zebrafish model of ALS should exhibit a progressive decreased swimming performance. At 5 dpf, zebrafish larvae have depleted their yolk and actively swim while searching for food. I used video recordings to track spontaneous locomotor activity of 5 and 8 dpf old zebrafish larvae for a period of one hour to evaluate the swimming performance. CytoTDP fish displayed swimming deficits at 5 dpf and 8 dpf. They exhibited reduced total displacement distance (Figure 3.12A, B) compared to their siblings as early as 5 dpf, indicating a motor neuron dysfunction in CytoTDP. Additionally, the velocity was also reduced in CytoTDP (Figure 3.12C). The decrease in both displacement distance and velocity became more noticeable at 8 dpf (Figure 3.12B, C) and indicated a progressive nature of degeneration. Interestingly, CytoTDP larvae exhibited only a slightly decreased duration compared to their siblings at both 5 dpf and 8 dpf (Figure 3.12D).

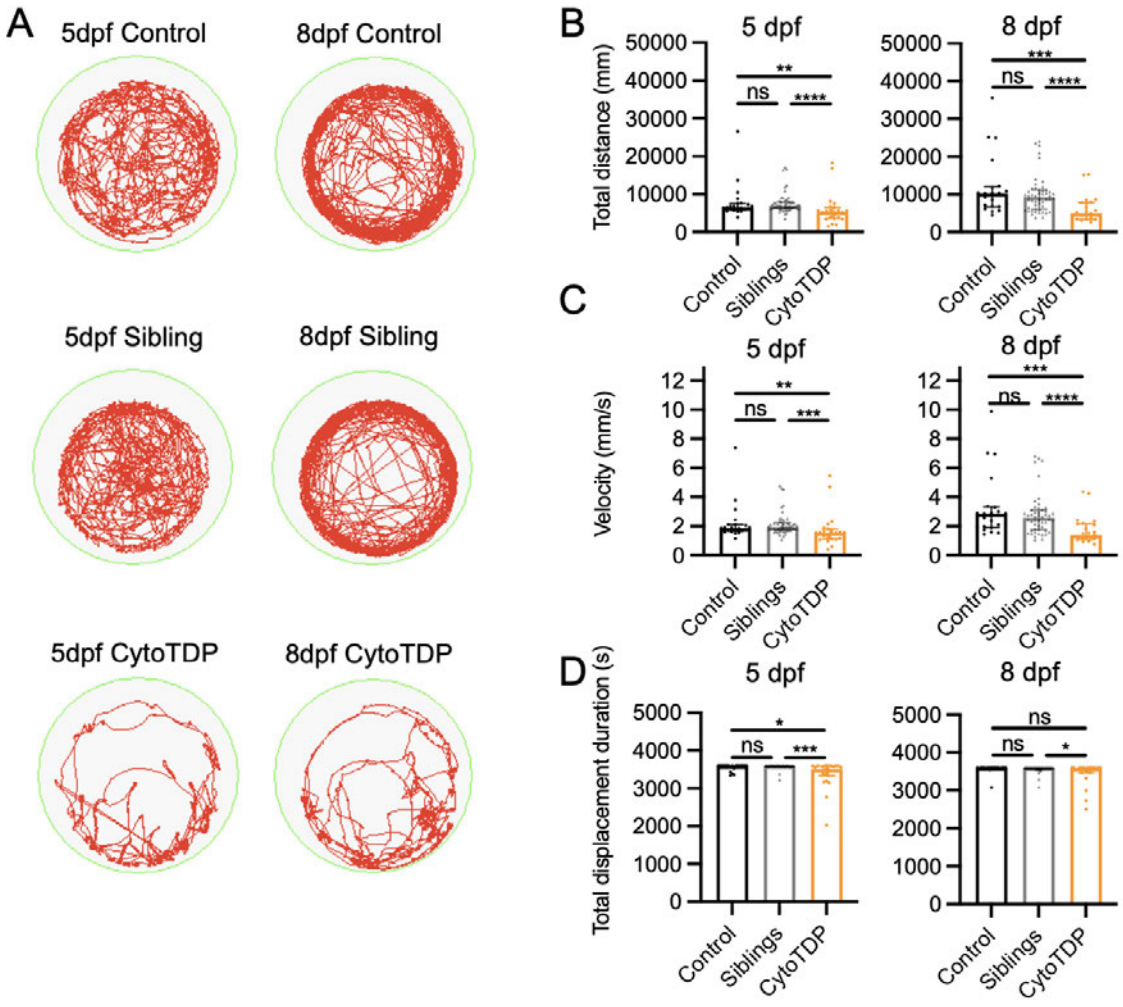

Figure 3.12: Age dependent locomotor activity phenotypes in CytoTDP line (Figure from Hu, et al. Mol Neurodegener. 2024 (*107*)).

(A) Pictures of one hour recordings of a representative locomotor activity path (red path) of one larva, including 5 dpf and 8 dpf CytoTDP and its siblings [Control (*tardbp +/+; tardbpl -/-*) and Siblings (*tardbp ΔNLS/+; tardbpl -/-*)]. (B-D) CytoTDP (orange dots) and its siblings [Control (black dots): *tardbp +/+; tardbpl -/-* and Siblings (grey arrow heads): *tardbp ΔNLS/+; tardbpl -/-*] were quantified for total displacement distance, velocity and duration at 5 dpf and 8 dpf. Statistical analysis was performed using Kruskal-Wallis test for comparisons among three groups and Mann-Whitney test for two groups. n=21 (Control), n=50 (Siblings), n=23 (CytoTDP).

Moreover, I found CytoTDP fish exhibited difficulties maintaining proper postures and swam shorter distances once they started a swimming bout (characterized

by short bursts of movement). To quantify my observations, I set a threshold based on the moving distance per swimming bout to divide swimming bouts to small-bouts (<4mm) and large-bouts (≥4mm). Remarkably, 5 dpf CytoTDP fish showed significant reduction in both the amount and proportion of large swimming bouts when compared to their siblings. This deficit in movement became more pronounced at 8 dpf (Figure 3.13A-D).

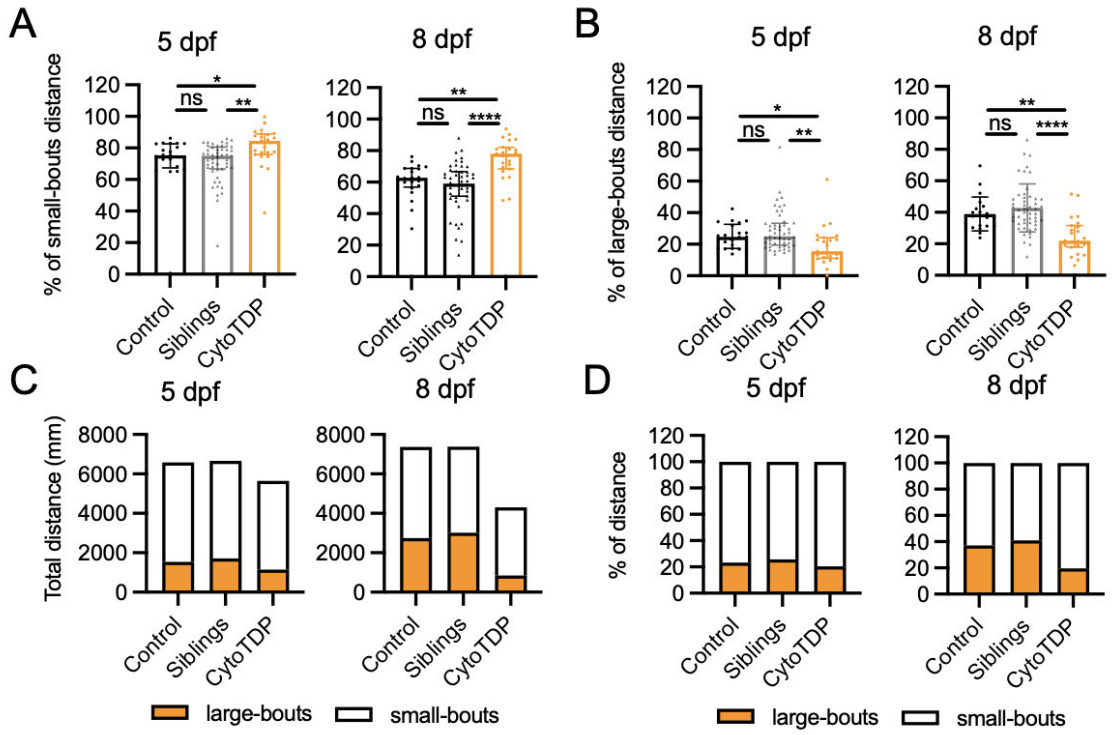

Figure 3.13: Quantifications of small-bouts and large-bouts distance percentages for CytoTDP and its siblings (Figure from Hu, et al. Mol Neurodegener., 2024 (*107*)).

(A-B) Quantifications of 5 dpf and 8 dpf CytoTDP's (orange dots) and its siblings' [Control (black dots): *tardbp +/+; tardbpl -/-* and Siblings (grey arrow heads): *tardbp ΔNLS/+; tardbpl -/-*] small-bouts and large-bouts distance percentage. Statistical analysis was performed using Kruskal-Wallis test for comparisons among three groups and Mann-Whitney test for two groups. n=21 (Control), n=50 (Siblings), n=23 (CytoTDP). (C) The

stacked bar graph illustrates mean distribution of large-bouts distance (orange bar) and small-bouts distance (white bar) at 5 dpf and 8 dpf. n=21 (Control), n=50 (Siblings), n=23 (CytoTDP). (D) The 100% stacked bar graph displays CytoTDP's and its siblings' mean distribution of large-bouts (orange bar) and small-bouts (white bar) swimming distance percentages at 5 dpf and 8 dpf. n=21 (Control), n=50 (Siblings), n=23 (CytoTDP).

Moreover, CytoTDP fish displayed a significant reduction in both the amount and proportion of time spent in large-bouts compared to their siblings, and this phenotype became more severe at 8 dpf (Figure 3.14A-D). These findings suggested that CytoTDP fish have a potential motor neuron, neuromuscular junction or muscular dysfunction.

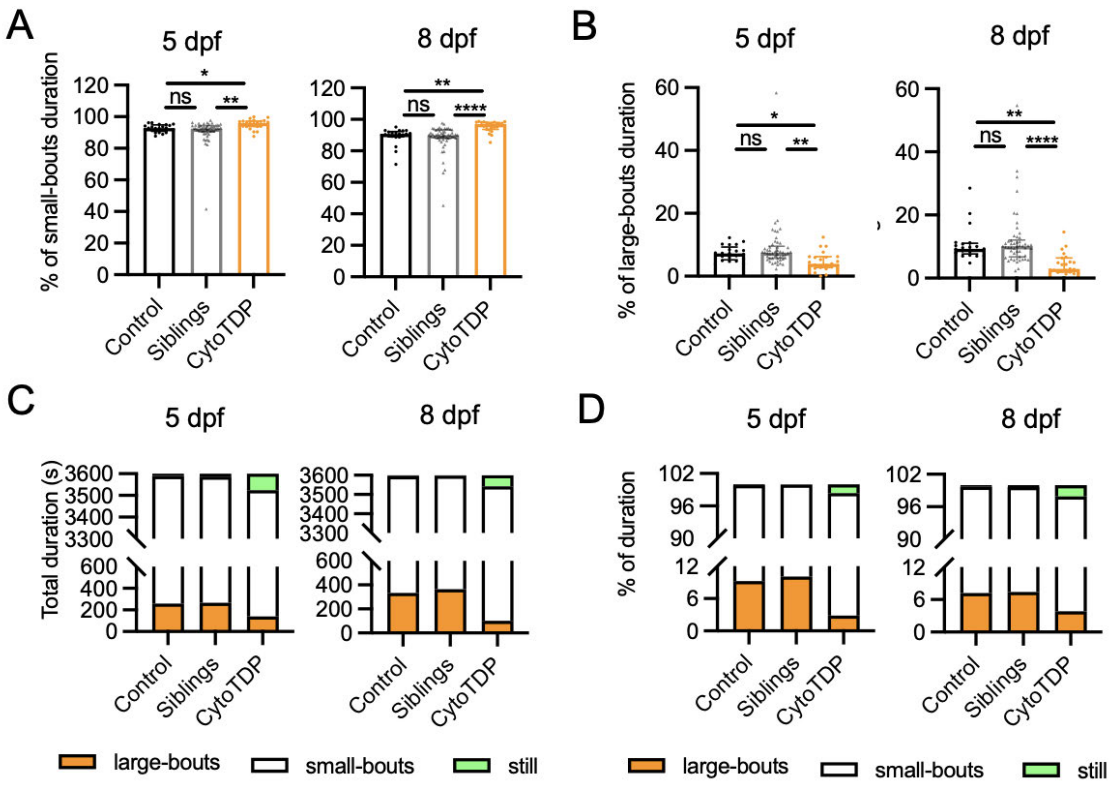

Figure 3.14: Quantifications of small-bouts and large-bouts duration percentages for CytoTDP and its siblings (Figure from Hu, et al. Mol Neurodegener. 2024 (*107*)).

(A-B) Quantifications of 5 dpf and 8 dpf CytoTDP's (orange dots) and its siblings' [Control (black dots): *tardbp +/+; tardbpl -/-* and Siblings (grey arrow heads): *tardbp ΔNLS/+; tardbpl -/-*] small-bouts and large-bouts duration percentage. Statistical analysis was performed using Kruskal-Wallis test for comparisons among three groups and Mann-Whitney test for two groups. n=21 (Control), n=50 (Siblings), n=23 (CytoTDP). (C) The stacked bar graph illustrates CytoTDP's and its siblings' mean distribution of large-bouts duration (orange bar), small-bouts (white bar) duration and still duration (green bar) at 5 dpf and 8 dpf. (D) The 100% stacked bar graph displays CytoTDP's and its siblings' mean distribution of durations of large-bouts (orange bar), small-bouts (white bar) and still time (green bar) percentages at 5 dpf and 8 dpf. n=21 (Control), n=50 (Siblings), n=23 (CytoTDP).

3.3 CytoTDP fish displayed degeneration of neuromuscular junctions and muscle atrophy

Muscle atrophy resulting from the loss of neuromuscular junctions (NMJs) is an important feature of ALS (*2, 162*). Therefore, I conducted the analysis of NMJs and muscles. To analyze NMJs, I quantified the colocalization of postsynaptic structures (stained with bungarotoxin (BTX)) and presynaptic structures (stained with an anti-synaptotagmin 2 antibody) in the last ventral half portion of the fish somite before the end of the fish gut (Figure 3.15). This analysis served as an indicator of NMJ integrity.

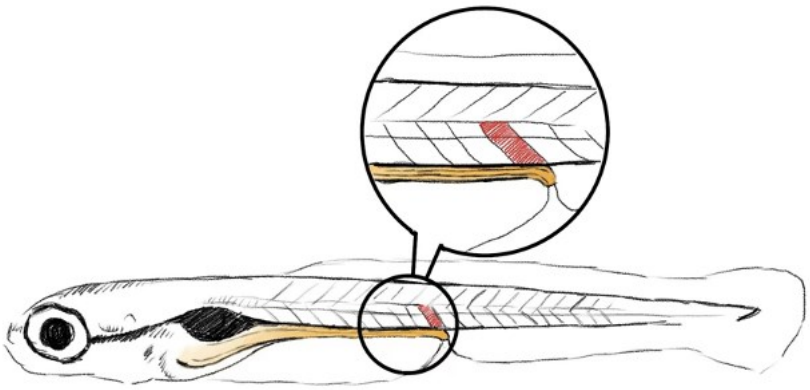

Hand-painted by Yang Wang

Figure 3.15: Schematic drawing of an 8 dpf larva (Figure from Hu, et al Mol Neurodegener. 2024 (*107*)).

A schematic representation of an 8 dpf larva highlighted the most caudal ventral half of the fish somite (red) before the end of the gut (yellow).

However, the only available method for NMJ staining 5 dpf larvae required peeling off the fish skin before staining (*163*). Although removing the skin can solve the permeability issue, it has two major drawbacks: firstly, it damages the fish muscle tissue (Figure 3.16); secondly, it is time-consuming to peel the skin off from the 3-4mm long larva. Therefore, after careful consideration, I decided to establish a new protocol for NMJ staining in zebrafish older than 5 dpf without the need for skin peeling.

I believe that achieving NMJ staining without skin peeling requires addressing the permeability problems at 5 dpf. Using strong chemical reagent to increase permeability may also cause tissue damage, especially since zebrafish tissue is more susceptible to damage compared to other animals like mouse. I believe balance is crucial for the whole mount staining technique. Therefore, I decided to make three modifications to the original protocol without skin peeling: 1. Treating the zebrafish in acetone at -20 degrees overnight; 2. Treating the zebrafish with 2mg/ml collagenase for 40 minutes; 3. Adding 0.8% TritonX-100 to the block

solution. Although making three modifications to a protocol at the same time is risky, fortunately, this protocol succeeded in the first attempt.

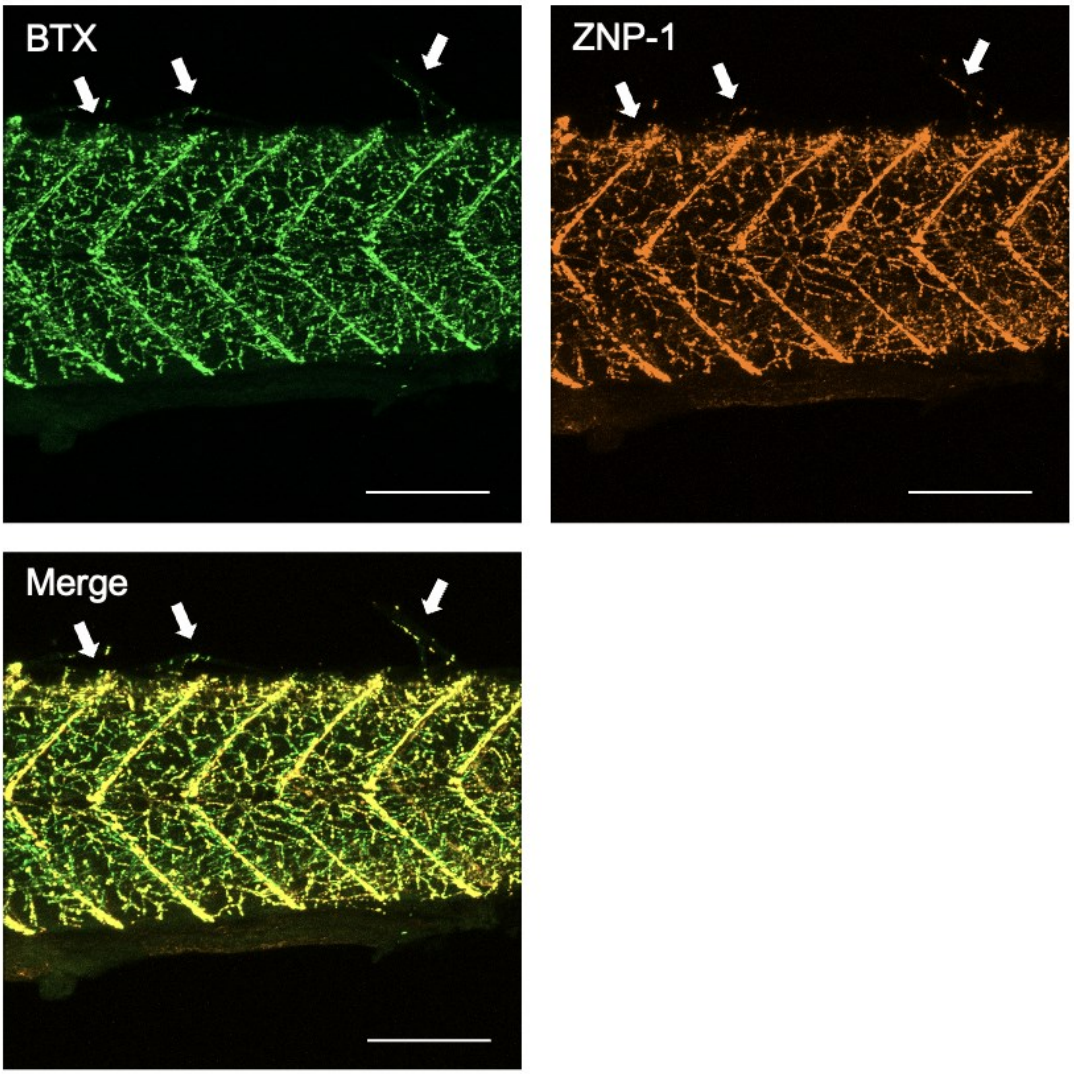

Figure 3.16: Removing skin of zebrafish disrupted tissue.

Pictures of zebrafish (5 dpf) whole-mount immunostainings with old protocol for synaptotagmin 2 (ZNP1, orange) and bungarotoxin (BTX, green) represents the NMJ of zebrafish, scale bar=150µm. Arrows shows disrupted tissues by removing skin.

Using the newly established protocol, I stained the NMJ in CytoTDP fish and Control fish at 8 dpf and 16 dpf, CytoTDP fish showed a significant overlap of the

presynaptic and postsynaptic marker and no irregularities of the NMJ stainings compared to Control fish at 8 dpf. However, at 16 dpf CytoTDP fish displayed a notable decrease in the colocalization of presynaptic and postsynaptic markers, suggesting NMJ defects in CytoTDP fish (Figure 3.17A, B). This indicated that while the NMJs are initially properly formed at 8 dpf, they undergo degeneration over time as observed in ALS.

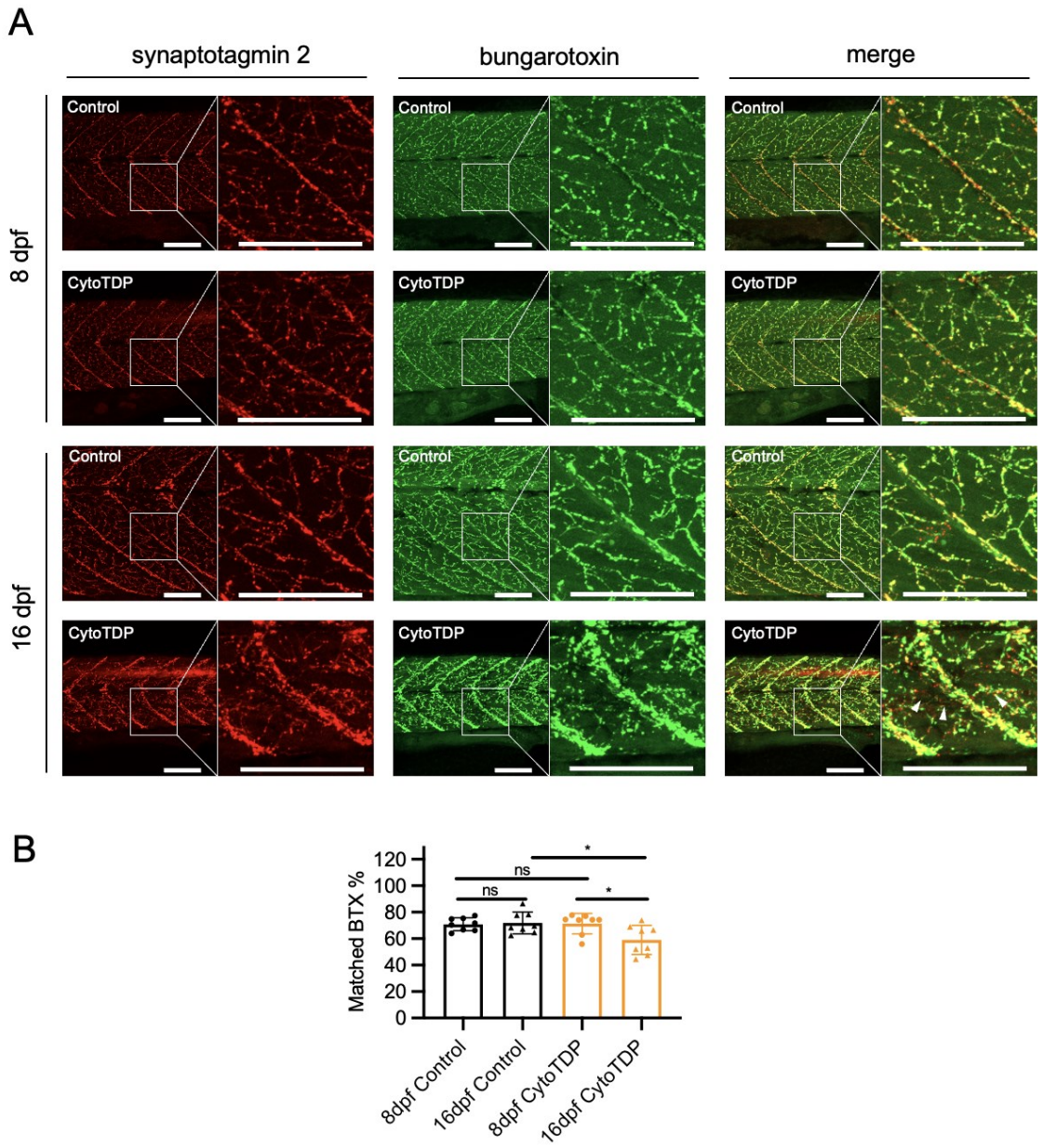

Figure 3.17: NMJ degeneration in CytoTDP fish (Figure from Hu, et al. Mol Neurodegener. 2024 (*107*)).

(A) Representative images of double whole-mount immunostainings for presynaptic marker synaptotagmin 2 (red) and postsynaptic marker bungarotoxin (green) labeling the NMJ of CytoTDP and Control (8 dpf and 16 dpf). At 8 dpf, CytoTDP and Control fish exhibited similar NMJ structure, whereas at 16 dpf, CytoTDP displayed mis-aligned presynaptic and postsynaptic structures, which indicated a degenerated NMJ. Arrowheads point to non-overlapping synaptotagmin 2 and bungarotoxin stainings. Scale bar=150μm. (B) Quantification shows presynaptic and postsynaptic markers which are colocalized in the most caudal ventral half of the fish somite before the end of the fish gut in CytoTDP line and Control line at 8 dpf and 16 dpf. Unpaired T test: n=8 (each group).

To evaluate muscle size in CytoTDP fish, the area of the most caudal somite dorsal to the end of the gut was quantified. I observed that the somite area in CytoTDP fish was smaller compared to Control fish at 8 dpf and 16 dpf. Notably, at 16 dpf, the somite area in CytoTDP fish exhibited not only a reduction compared to Control fish, but also a significant decrease compared to CytoTDP at 8 dpf (Figure 3.18), indicating progressive muscle wasting.

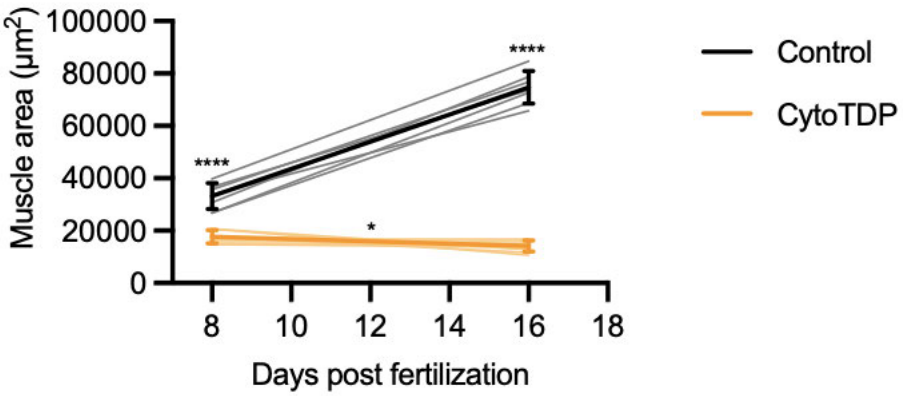

Figure 3.18: Decreased muscle area in CytoTDP fish (Figure from Hu, et al. Mol Neurodegener. 2024 (*107*)).

Quantitative analysis was conducted on musculature area of the most caudal ventral half of the somite before the end of the fish gut in both CytoTDP and Control fish (8 dpf and 16 dpf). Unpaired T test. n=7 (each group).

Our collaborator Dr. Schifferer helped me to further investigate potential muscle wasting in CytoTDP fish on at an ultrastructural level by performing scanning electron microscopy (SEM) on CytoTDP fish and Control fish. In line with the NMJ findings, no indications of ultrastructural muscle wasting were observed in CytoTDP at 8 dpf (Figure 3.19A). However, 16 dpf CytoTDP fish exhibited varying degrees of muscle wasting when compared to Control fish. We observed a slight dilation of the sarcoplasmic reticulum (SR) in the mildly affected area and these dilated SR became more pronounced in the moderately affected area. In the severely affected area, the muscle cells' structure in the cytoplasm were entirely disrupted (Figure 3.19B).

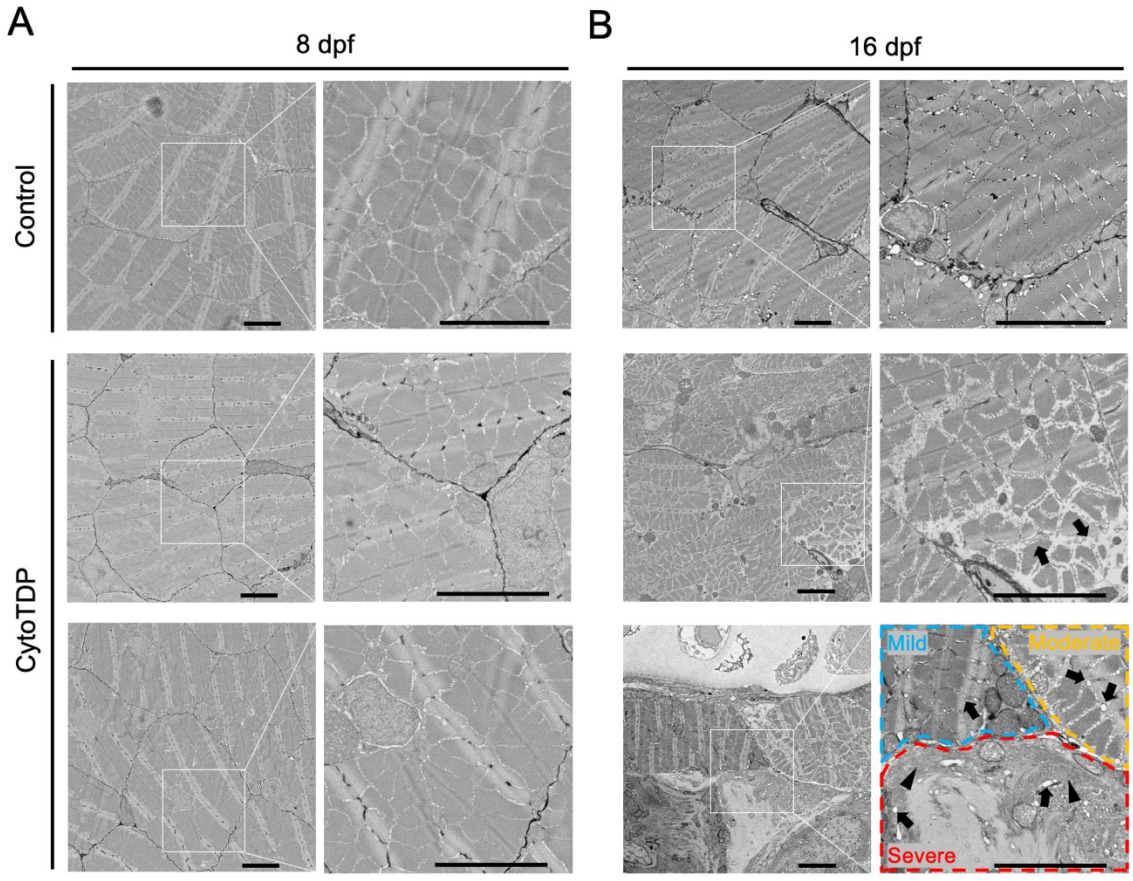

Sample preparation and EM imaging was performed by Dr. Martina Schifferer

Figure 3.19: CytoTDP fish have muscle atrophy (Figure from Hu, et al. Mol Neurodegener. 2024 (*107*)).

(A) Representative pictures of electron microscopy (EM) images for skeletal muscle in 8 dpf CytoTDP and Control fish. At 8 dpf, CytoTDP fish exhibited well-organized myofibrils and lack obvious signs of muscle atrophy similar to Control. (B) Representative pictures of EM images of skeletal muscle in 16 dpf CytoTDP and Control fish. At 16 dpf, compared to Control fish, CytoTDP fish displayed a dilation of the sarcoplasmic reticulum (SR) (indicated by arrows), along with substantial muscle atrophy. The mildly affected muscle fiber is highlighted in blue, the moderately affected muscle fiber is highlighted in orange and the severely affected muscle fiber is highlighted in red (Scale bar=5 µm).

3.4 Microglia proliferation and activation in the hypothalamus of CytoTDP

When studying animal models of TDP-43, most scientists tend to focus on the condition of motor neurons. Scientists who are doing research using zebrafish models often use the length of primary motor neuron axons at 28 hours post fertilization as a readout of motor neuron dysfunction. However, I believe this phenotype of shorter length of primary motor neuron axons compared to controls is likely due to developmental delays in these zebrafish animal models. In addition, the pathological manifestations of TDP-43 occur not only in ALS patients but also in about half of FTD patients. Importantly, in FTD patients, only about 30% have accompanying motor defects. Thus, I think it is important to investigate non motor cells in the CytoTDP model, in particular brain areas that are selectively affected in CytoTDP.

Microglia have sentinel functions and can sense environmental changes (*164*). Therefore, I chose to observe the changes in microglia within different brain regions of CytoTDP. In the zebrafish field, most scientists observe microglia in the forebrain of zebrafish in the early stages of development (mostly at 3 dpf) taking advantage of the zebrafish's transparency. Using zebrafish to study neurodegenerative diseases inevitably means studying the progression of the disease, but as zebrafish develop, the advantage of transparency gradually disappears. The disappearance of transparency weakens the advantage of zebrafish. Fortunately, I started to collaborate with Dr. Pan, an expert in tissue clearing to overcome this limitation. We analyzed the changes in microglia in the early and late stages of the whole brain in the CytoTDP line. I generated CytoTDP and control fish with the Tg(mpeg1.1: EGFP-CAAX) background and he performed whole-mount immunostaining and tissue clearing on CytoTDP and Control fish at 5 dpf and 8 dpf.

We conducted a comparison of microglial abundance in CytoTDP fish and Control fish at 5 dpf and 8 dpf. We observed a remarkable increase in total microglia in the whole brain in CytoTDP fish compared to Control fish (Figure 3.20A, B). In

addition, we also observed a notable accumulation of microglia in the hypothalamus in the CytoTDP fish compared to Control fish at 5 dpf, with an increase in severity of the phenotype at 8 dpf (Figure 3.20A, C).

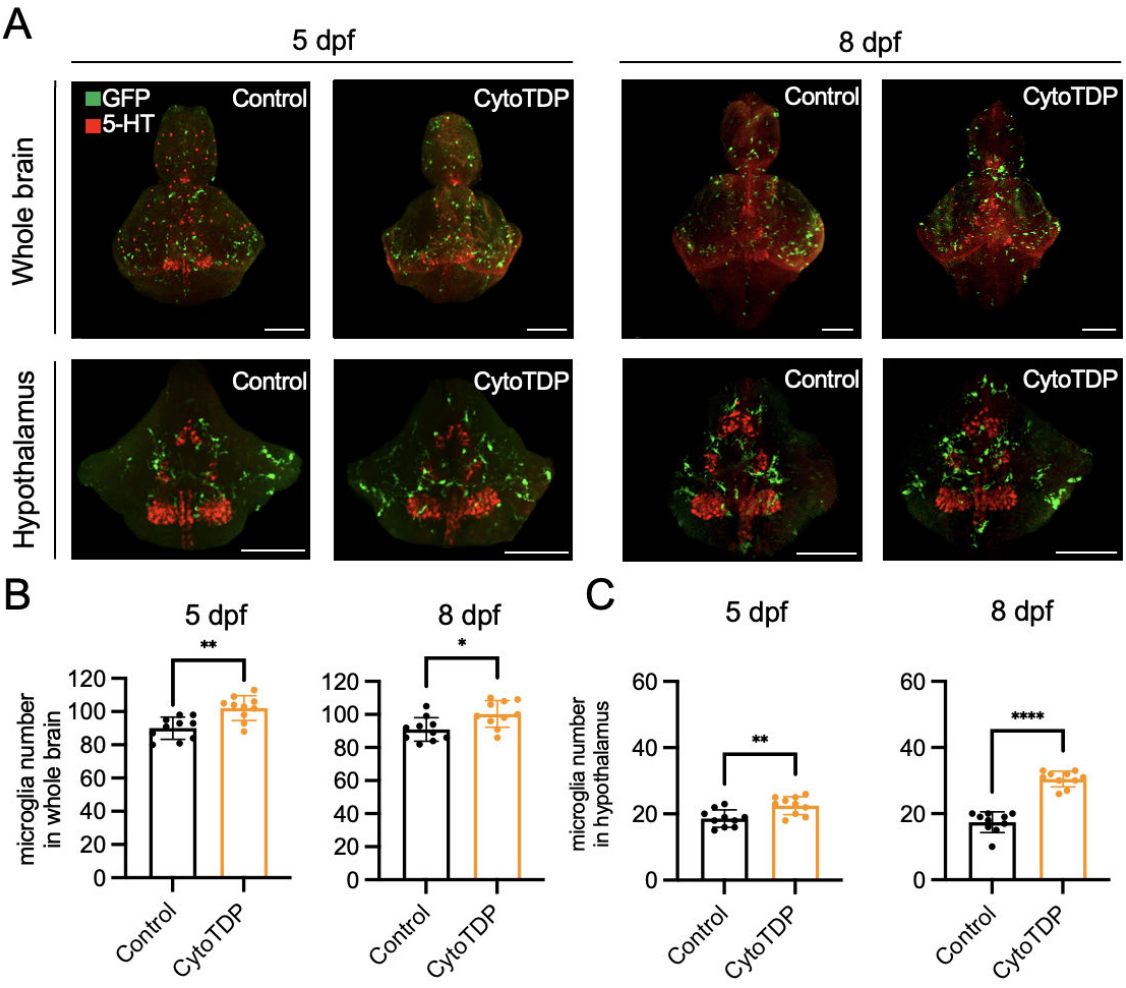

The original data and this figure were produced by Dr. Chenchen Pan

Figure 3.20: CytoTDP fish have microglia proliferation in the hypothalamus (Figure from Hu, et al. Mol Neurodegener. 2024 (*107*)).

(A) The top panel shows representative pictures of segmented zebrafish whole-brains from dorsal views and the lower panel shows segmented zebrafish hypothalamus images at 5 dpf and 8 dpf (CytoTDP fish and Control fish). Co-staining against 5-

hydroxytryptamine (5-HT) was utilized as a counterstain to confirm the segmentation of hypothalamus in zebrafish (*165*). Scale bars=100 μm. (B) The whole-brain's microglia cell number was quantified at 5 dpf and 8 dpf (CytoTDP fish and Control fish), each group has 10 larvae, unpaired T test. (C) Microglia cell number in the hypothalamus was quantified at 5 dpf and 8 dpf (CytoTDP fish and Control fish), unpaired T test, each group has 10 larvae.

Furthermore, we also noted morphological changes of microglia in CytoTDP fish compared to Control fish. Microglia in CytoTDP fish showed enlarged somata bodies, shorter processes and a decreased number of processes compared to Control fish (Figure 3.21). These changes indicated microglia activation in the hypothalamus. The hypothalamus is notably selectively impacted by the re-location of Tardbp in CytoTDP fish.

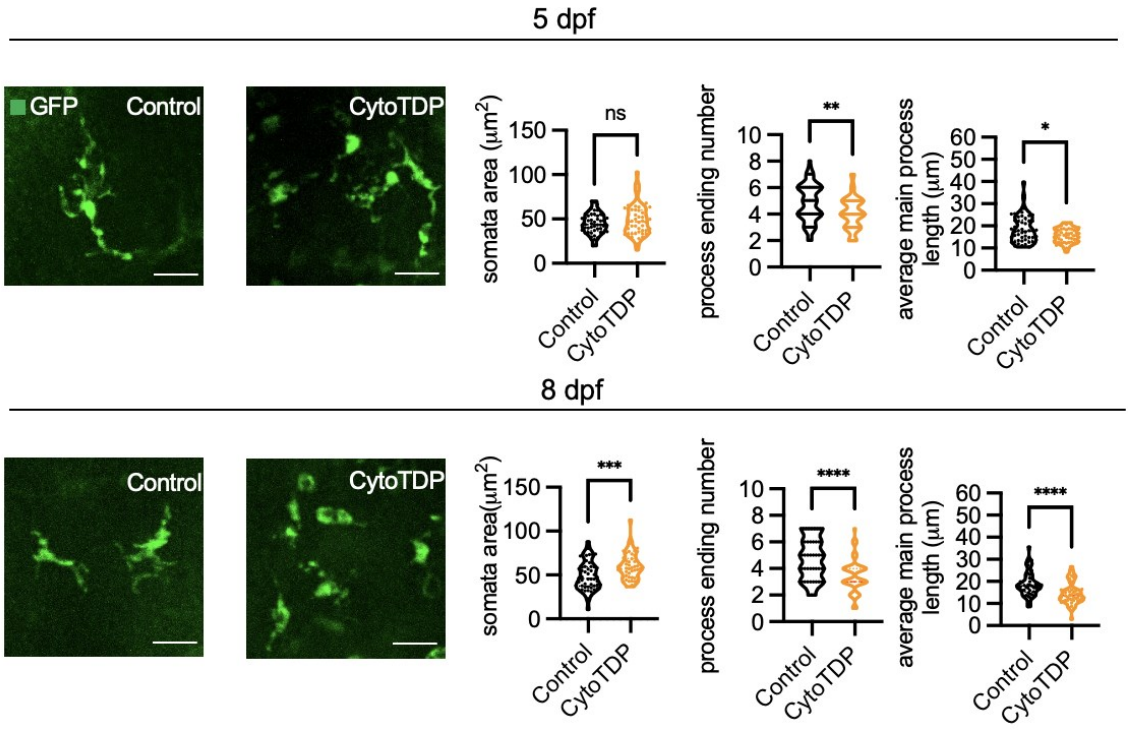

The original data and this figure were produced by Dr. Chenchen Pan

Figure 3.21: CytoTDP fish shows microglia activation in the hypothalamus (Figure from Hu, et al. Mol Neurodegener. 2024 (*107*)).

The top panel shows representative images of mpeg1.1-eGFP positive microglia in hypothalamus at 5 dpf (Control fish and CytoTDP fish), the bottom panel shows pictures at 8 dpf. Scale bars=20 μm. Quantifications of microglia's area of somata, number of main processes, and average main process length were showed by violin plots (top panel represents 5 dpf fish and bottom panel represents 8 dpf fish). For each group, 50 microglia were quantified, unpaired T test.

3.5 CytoTDP affects key metabolic processes

In the past, our lab generated a TDP DKO line and investigated the consequences of combined Tardbp and Tarbpl loss of function. I was interested to know the molecular changes at an early stage in CytoTDP fish and compare these results to the TDP DKO line, because these molecular changes indicate selective gain of function contribution to CytoTDP phenotype rather than nuclear loss of function. Thus, RNA sequencing was conducted CytoTDP, Control and TDP DKO fish at 1.5 dpf. This is the earliest stage that I can select CytoTDP and TDP DKO fish out from their siblings based on CytoTDP fish having a pigmentation and TDP DKO fish having a hypoperfusion phenotype. Principal component analysis (PCA) was performed based on RNA sequencing results and displayed a strong separation of these three genotypes (Figure 3.22).

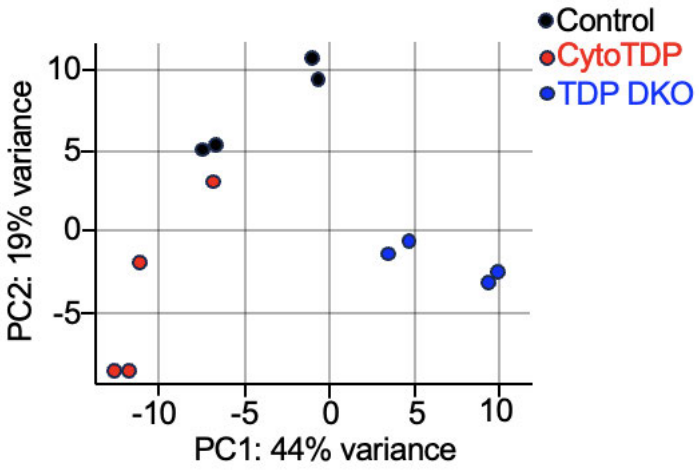

This original figure was produced by Özge Burhan

Figure 3.22: CytoTDP, DKO and Control fish have a clear separation in gene expressions (Figure from Hu, et al. Mol Neurodegener. 2024 (*107*)).

Principal component analysis (PCA) based on RNA sequencing results from TDP DKO fish, CytoTDP fish and Control fish.

I then performed a Venn analysis to study the number of overlapping dysregulated genes between TDP DKO and CytoTDP line (representing loss of Tardbp nuclear function) and number of dysregulated genes only shown in CytoTDP fish (representing gain of cytoplasmic Tardbp function). I found 179 overlapping dysregulated genes in CytoTDP and TDP DKO, with 1467 genes only dysregulated in TDP DKO and 273 genes only dysregulated in CytoTDP.

I performed a gene ontology (GO) analysis and found the enriched dysregulated biological processes of overlapping genes mainly were found in visual perception, lens development in camera-type eye, sensory perception of light stimulus and sensory perception (Figure 3.23).

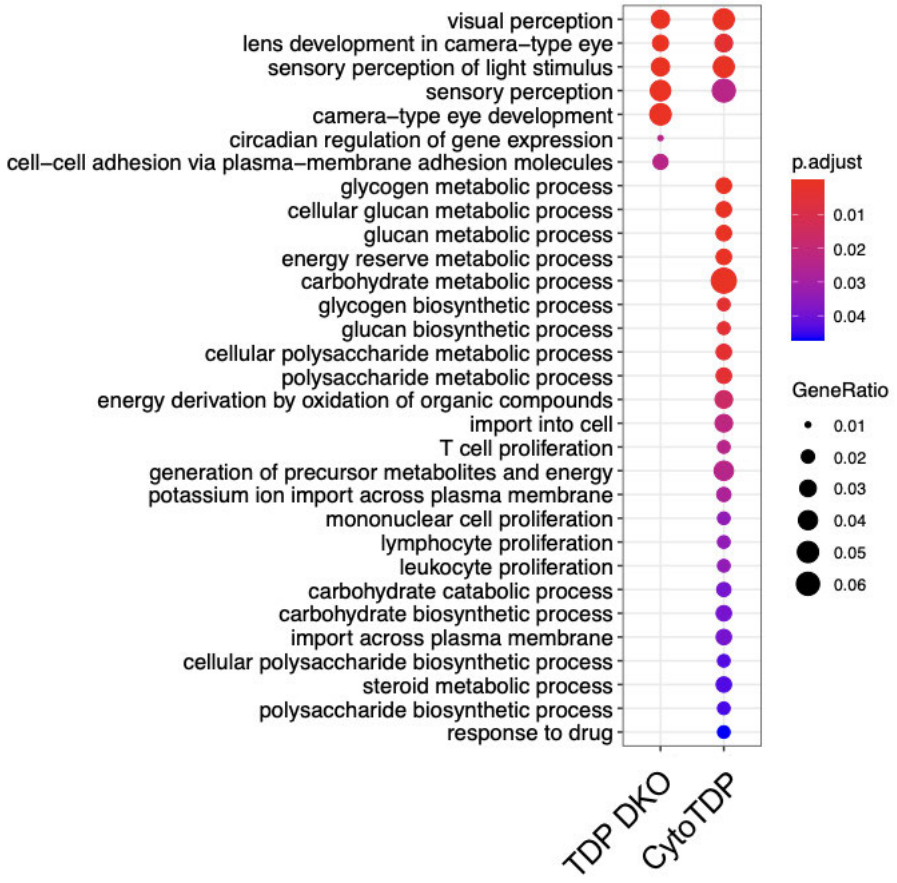

Figure 3.23: CytoTDP affects many key metabolic processes (Figure from Hu, et al. Mol Neurodegener. 2024 (*107*)).

Gene ontology analysis (biological process) was performed based on differentially expressed genes from TDP DKO and CytoTDP compared to Control, respectively.

In addition, GO analysis showed that the dysregulation of many metabolic pathways was only found in the CytoTDP line, indicating that Tardbp cytoplasmic toxicity can cause metabolic dysfunction. I also found many affected pathways concentrated around glycogen and carbohydrate metabolism, such as glycogen metabolic process, glycogen biosynthetic process, carbohydrate metabolic process, as well as immune cell related processes, including T-cell proliferation, leukocyte proliferation, and lymphocyte proliferation, and sterol metabolic processes (Figure 3.23). In all affected pathways, carbohydrate metabolic processes had the biggest number of mis-regulated genes. I wanted next to evaluate which genes play the most important role and used the hub gene

analysis tool (*160*) to identify which genes have the highest connectivity within gene networks. I performed hub gene calculations and identified hub genes (Figure 3.24A) and found that the top ranked gene in hub gene analysis was muscle glycogen phosphorylase b (*pygmb*). *pygmb* is a one of the key enzymes in glycogenolysis and its function is to release glucose from glycogen. To determine the consequences of glycogen metabolic process dysfunction in CytoTDP, I measured the glycogen levels with the help from Brigitte Nuscher. CytoTDP fish showed increased glycogen levels compared to Control fish (Figure 3.24B). This result confirmed my finding that mis-localization of Tardbp significantly changed glycogen levels in the CytoTDP line.

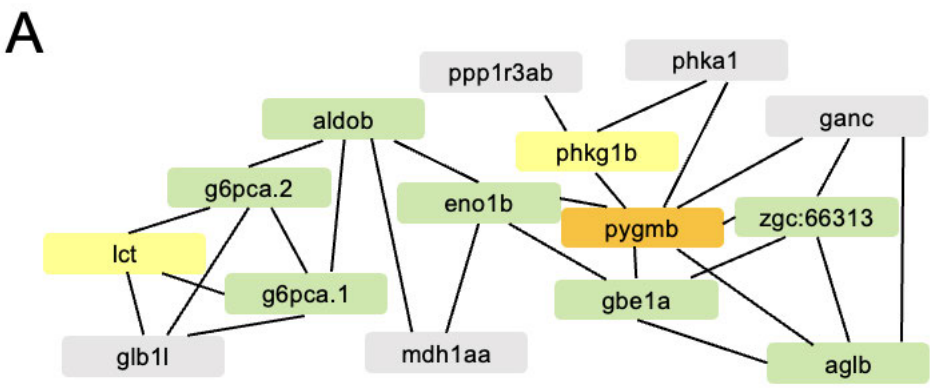

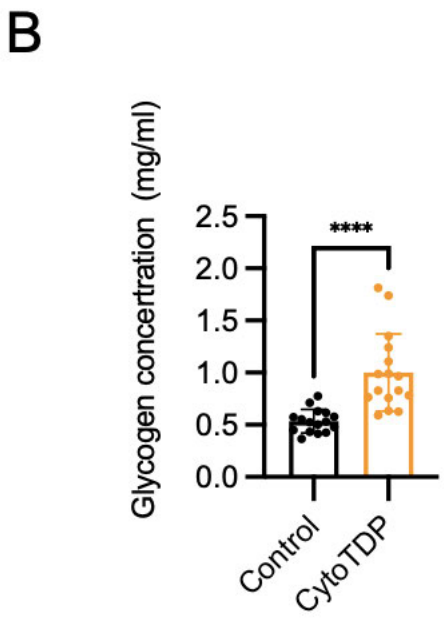

Multi-well spectrophotometer was operated by Brigitte Nuscher

Figure 3.24: Mis-localization of Tardbp alters metabolic processes (Figure from Hu, et al. Mol Neurodegener. 2024 (*107*)).

(A) Hub genes were identified using Cytoscape, where the color intensity reflects the gene's ranking (1=orange, 2=green, 9=yellow). (B) Glycogen concentrations were measured in 5 dpf CytoTDP and Control fish. Each group has 16 samples, unpaired T test.

4. Discussion

A crucial but still missing part in ALS research is an animal model that recapitulates nuclear clearing of TDP-43 and increased endogenous cytoplasmic TDP-43. In this thesis, I analyzed a novel animal model called CytoTDP, which shifts endogenous Tardbp from the nucleus to the cytoplasm. I showed that combination of both nuclear clearing of TDP-43 and endogenous accumulation of cytoplasmic TDP-43 result in multiple early phenotypes (Figure 4.1), such as motor defects, disruption of the neuromuscular junction, muscle wasting and metabolic changes. Imaging of whole-brain microglia in the hypothalamus showed microglia proliferation and activation prior food intake at 5 dpf. Moreover, these observations indicated that the CytoTDP line, unlike the TDP DKO line, displayed early onset dysregulation of metabolic carbohydrate pathways reminiscent of the early stages of ALS/FTLD. Thus, the CytoTDP animal model presents a valuable resource for studying pathological mechanisms and devising new treatments targeting metabolism in the early phases of ALS.

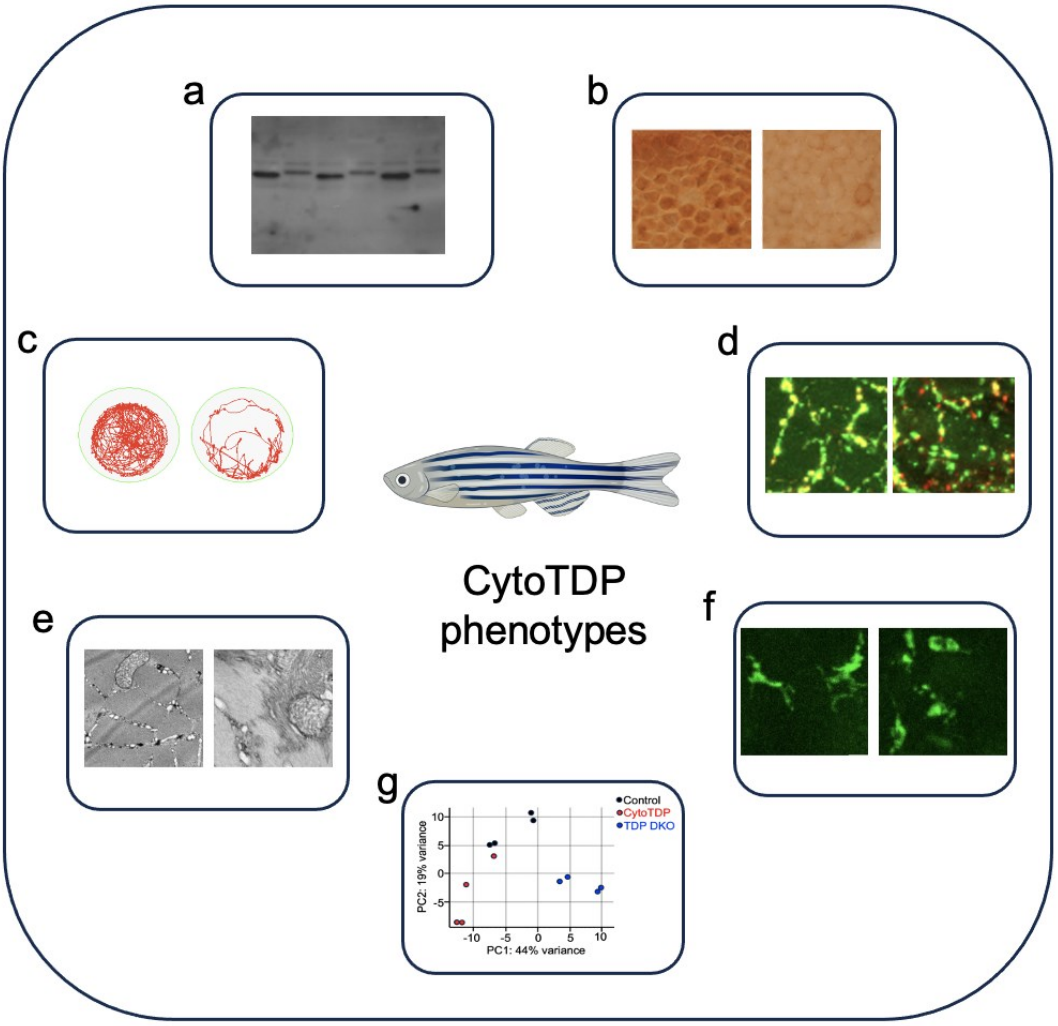

Figure 4.1: Summary of CytoTDP features.

(a) Identification of a Tardbp protein modification when translocated to the cytoplasm, (b) Re-localization of TDP-43 from the nucleus to the cytoplasm, (c) ALS-like motor phenotypes, (d) Mis-matched presynaptic and postsynaptic structures, (e) Muscle atrophy, (f) Microglia proliferation and activation in the metabolic regulatory center prior food intake, (g) Transcriptional differences of the CytoTDP compared to TDP DKO line.

4.1 Limitations of current TDP-43 animal models

Endogenous TDP-43 nuclear clearing and cytoplasmic TDP-43 inclusions were discovered to be a hallmark of ALS/FTLD in 2006 (*47*). But for a long time, it was not clear whether the loss of TDP-43 function or gain of cytosolic toxic TDP-43 function was the main problem in causing ALS/FTLD (*47, 48*). One important but still missing part in these studies are good animal models to mimic this TDP-43 pathology, which is found in about 97% ALS patients (*166*). This problem greatly slows down the understanding of TDP-43 function in ALS/FTLD.

The contributions of TDP-43 loss of nuclear function and gain of cytoplasmic function in ALS is an important and still not solved question is the ALS research field. There is increasing evidence for a loss of TDP-43 function contribution, such as *STMN2* and *UNC13A* mis-splicing (*147-149*). Unfortunately, the contribution of cytoplasmic TDP-43 gain of function has been less clearly shown (*129, 167-171*). To investigate the gain of cytoplasmic TDP-43 function, researchers have generated transgenic mice (rNLS8) which express human TDP-43-ΔNLS (hTDP-43-ΔNLS) in the mice' brain and spinal cord (*141*). These mice have over 10 times higher expression levels of TDP-43 compared to endogenous TDP-43 levels, which are much higher levels compared to human ALS patients. Importantly, other researchers showed that even 3.8 times higher overexpression of human WT TDP-43 in transgenic mice already resulted in mortality at around half a year of age, suggesting that the overexpression of TDP-43 is toxic (*117*). To solve this problem, several groups have generated new KI TDP-43 animal models to investigate the consequences of endogenous mutant TDP-43 expression. However, these models exhibit only a mild ALS-like motor phenotype and the onset of the phenotype is very late. Thus, they are not suitable to use for drug discovery (*138, 142, 172*).

Therefore, there is a need to generate a new KI TDP-43 animal model that can mimic both characteristics of TDP-43 nuclear clearing and elevated cytoplasmic TDP-43 levels. In this thesis, I describe a new animal model called CytoTDP which fulfills this need. In addition, mis-localization of TDP-43 to the cytoplasm

occurs prior cytoplasmic TDP-43 aggregation and can therefore be considered as an early disease signature.

4.2 CytoTDP zebrafish line recapitulates ALS in multiple important clinical aspects

I showed that the CytoTDP line effectively recapitulates several crucial clinical features of ALS during its very initial phases. These features include progressive motor impairments, neuromuscular junction degeneration and muscle wasting. In the past, researchers working on developing TDP-43 zebrafish animal models focused on KO or knockdown of TDP-43 (*136, 137, 173*). However, TDP-43 is essential for early embryonic development in zebrafish with severe phenotypes in several tissues. Therefore, I think it is highly likely that the observation of reduced axons growth in the caudal primary motor neuron in these TDP-43 loss of function zebrafish models is associated with developmental delay rather than neurodegeneration due to TDP-43 nuclear loss of function since they never form normal motor neurons. I found in the CytoTDP line, normal NMJ structures initially formed and subsequently underwent degeneration. I therefore believe this model better mimics the neurodegenerative aspects of ALS compared to previously reported zebrafish TDP-43 models (*174*).

Furthermore, motor phenotypes in the CytoTDP line started prior to the morphological changes of the NMJ, suggesting early-stage neuron dysfunction and not NMJ degeneration or muscle wasting as the reason of motor defects in ALS patients. Notably, I observed motor defects in the CytoTDP line at 5 dpf, which is significantly earlier compared to phenotypes that are detected in other previously reported endogenous TDP-43 human mutations KI animal models (*142, 145, 166*). This advantage is important for accelerating ALS drug screening. When the CytoTDP model is used for drug screening in the future, it will be possible to see if the drug improves the motor phenotype of ALS within 5 days.

The use of this animal model will greatly reduce human resources and field costs and facilitate rapid drug screening.

4.3 Metabolic dysfunction happens prior to decreased food intake in CytoTDP line

Whole-mount immunolabeling with tissue clearing is a very powerful technique in research, but rarely used in zebrafish. This is due to the transparent nature of zebrafish during early development, and researchers in the zebrafish field tend to focus on early development. Since I am working on an animal model which mimics neurodegenerative disease, it is necessary to work on late-stage zebrafish. Thus, I decided to use whole-mount immunolabeling with tissue clearing for the characterization of late-stage CytoTDP fish. For the first time in an ALS animal model, whole-mount immunolabeling and whole-brain microglia imaging was used, which allowed comprehensive analysis of microglia numbers and morphology in the entire brain. Increased numbers and activation of microglia was identified in CytoTDP fish, consistent with observations in human ALS and other animal models (*175-178*). Notably, there was a pronounced microglial activation in the hypothalamus, which is a key center for metabolic regulation (*179, 180*).

In individuals with ALS, metabolic dysfunction is frequently observed as a primary feature during the early stages of ALS, sometimes even prior motor defects (*181-183*). A crucial unresolved question in human studies is the determination of whether metabolic dysfunction is influenced by factors such as reduced food intake resulting from muscle weakness, swallowing difficulties, or potential depression (Figure 4.2) (*184, 185*). Interestingly, in zebrafish embryos at 5 dpf, hypothalamic microglial activation is observed before the initiation of food intake, with its severity increasing over time. This observation supports that mis-localization of TDP-43 has a direct impact on the hypothalamus. Notably, atrophy and TDP-43 pathology has been observed in the hypothalamus of ALS patients

(Figure 4.3) (*186-189*), emphasizing the potential involvement of the hypothalamus in the etiology of the disease.

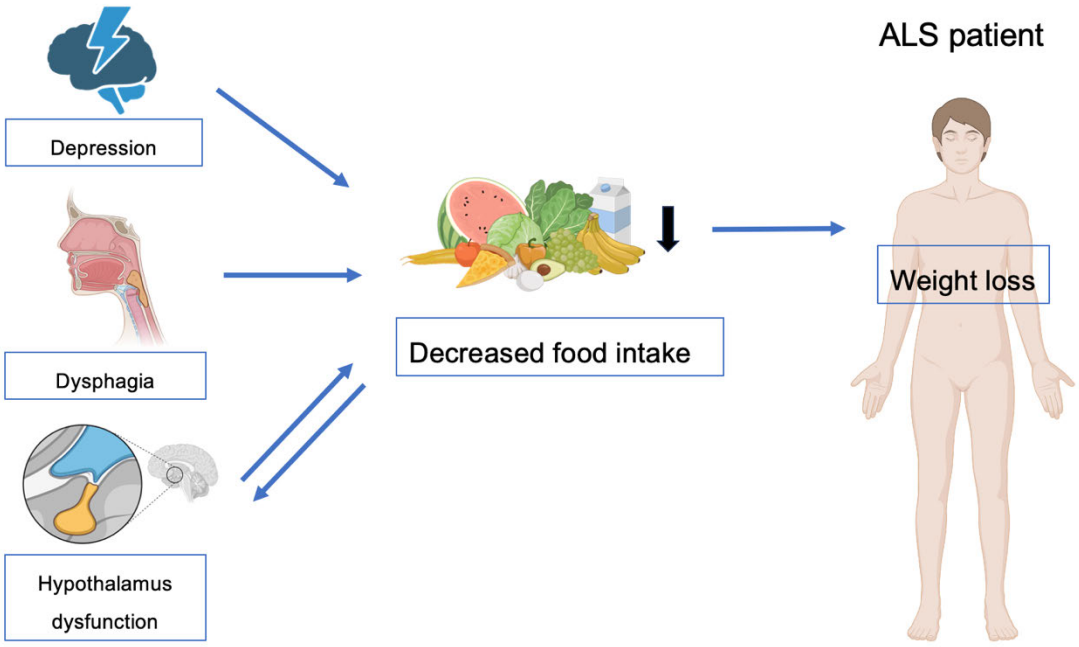

Figure 4.2: Schematic image shows reasons of decreased food intake in ALS patients (generated by Biorender)**.**

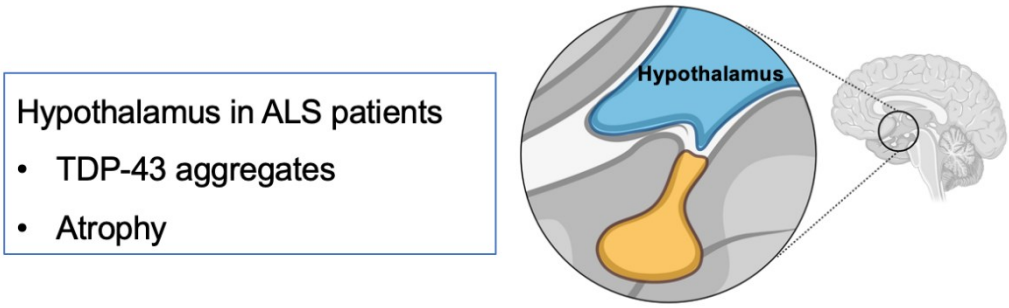

Figure 4.3: Hypothalamus alterations in ALS patients (generated by Biorender)**.**

In ALS patients, weight loss has been shown as a notable feature directly linked to poor prognosis (*182, 185, 190-193*). Reduced food intake can result in weight loss and many factors may contribute to ALS patients' reduced food intake, including diminished appetite and dysphagia or metabolic imbalances (*182, 185, 190-193*). However, the temporal relationship between reduced food intake, metabolic dysfunction and weight loss in ALS patients remained unclear in previous studies. Through the analysis of the CytoTDP line, along with a combination of whole-mount immunostaining and tissue clearing techniques, I managed to identify that microglia activation in the hypothalamus in the CytoTDP line occurs prior to the initiation of food intake. These findings suggest that the observed weight loss in patients could be independent of food intake mediated by a direct metabolic mechanism mediated by hypothalamic pathology (Figure 4.4). This finding offers new insights for future development of ALS drugs that can help ALS patients to correct metabolic dysfunction at an early stage, thereby slowing down or stopping disease progression.

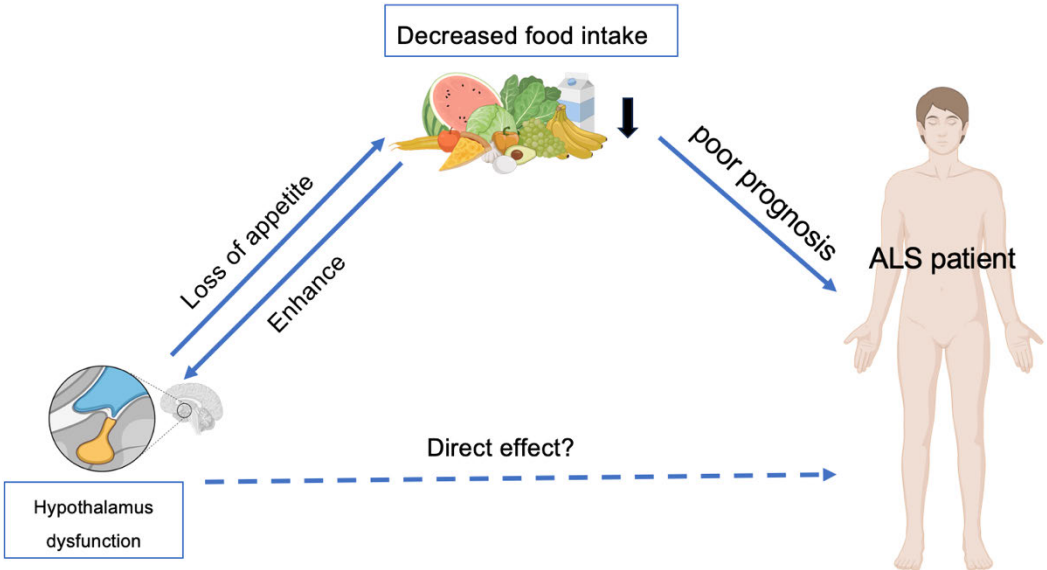

Figure 4.4 Schematic image highlighting potential direct effect of hypothalamic dysfunction on ALS progression rather than an indirect effect by loss of appetite and decreased food intake (generated by Biorender)**.**

4.4 Gain of function or loss of function?

Over the last two decades, many scientists have been working on determining whether loss of TDP-43 nuclear function or gain of TDP-43 cytoplasmic toxicity function plays the more important role in TDP-43-mediated neurodegenerative diseases. However, advancements in this area have been hindered by the embryonic lethality observed in TDP-43 KO rodent models and the absence of animal models exhibiting mis-localized endogenous TDP-43 (*112-114*).

The work presented in my thesis makes an advancement in answering this question. I analyzed the transcriptomes of the CytoTDP line and compared it to

our previously reported TDP DKO line (*136*). I found that, compared to the TDP DKO line, the CytoTDP line displayed dysregulation in many key metabolic pathways, particularly in glycogen storage and degradation. This finding aligns with the observed muscle atrophy and the activation of microglia in the brain center for energy homoeostasis. By analyzing hub genes, I identified the significant involvement of *pygmb* in the metabolic dysfunction observed in the CytoTDP line. Thus, my thesis shows that TDP-43 gain of function is an essential contributing factor for TDP-43-mediated neurodegenerative diseases.

4.5 *PYGM* function in ALS

Zebrafish have 2 orthologous of human muscle form of glycogen phosphorylase (*PYGM*), referred to as *pygma* and *pygmb*. Both encode the muscle isoform of glycogen phosphorylase and have significant similarity to the human *PYGM* gene. I observed a reduced level of *pygmb* in CytoTDP fish compared to Control fish. I analyzed differentially expressed genes in C9ORF72 ALS patients and found a downregulation of the *PYGM* gene in the motor cortex of patients' brain (*177*). A previous study has shown that the pathology of TDP-43 in ALS appears first in the motor cortex (*194*), indicating that the downregulation of *PYGM* in this region could provide crucial insights into the early ALS pathomechanism.

PYGM serves as a crucial enzyme in glycogen metabolism. The function of PYGM is catalyzing glycogen to be cleaved into glucose-1-phosphate. Its expression is not limited to skeletal and cardiac muscles (*195*), but has also been reported in the brain, particularly in astrocytes (*196-199*). Although the functional implications of *PYGM* downregulation in ALS patients are still uncertain, a study using astrocytes differentiated from C9ORF72 ALS patients has demonstrated that the *PYGM* downregulation is linked to a reduction in mitochondrial energy production and dysfunction in glycolytic metabolism (*200*). In conclusion, the findings in my thesis support the hypothesis that glycogen processing and energy homeostasis are affected by mis-regulation of *PYGM*. In the future, it would be

very interesting to further explore the effects of cellular energy metabolism of glia cells in ALS.

4.6 Associations between insulin resistance and ALS

PYGM also plays a role in insulin and glucagon signaling, as well as in the insulin resistance pathway involved in glycogen level regulation (*201*). Insulin resistance is a common feature in many neurodegenerative diseases, including Alzheimer's disease, Huntington's disease, Parkinson's disease and ALS (*202*).

Insulin resistance is the main hallmark of type 2 diabetes and occurs in many neurodegenerative diseases. Several studies have demonstrated that poorly controlled diabetes is associated with an increased risk of Alzheimer's disease (*203-205*). Type 2 diabetes also increases the risk of Parkinson's disease (*206-209*).

Interestingly, it has been observed that type II diabetes is associated with a reduced risk of ALS (odds ratio 0.79, 95% confidence interval: 0.68-0.91) (*210*), while type I diabetes is associated with an increased risk (odds ratio 5.38, 95% confidence interval: 1.87-15.51) (*211*). In addition, another study has demonstrated a 4-year delay in the onset of motor symptoms in patients with ALS and type 2 diabetes (*30*). These studies suggest that the protective effect of diabetes on ALS likely presents only in type 2 diabetes, rather than type 1 diabetes. In addition, it has been shown that insulin resistance occurs in ALS patients (*212*). However, since ALS patients with diabetes use medications to control their diabetes, it is difficult to tell whether it is the medications the patient use or the insulin resistance itself that effects the progress of ALS. In this newly established CytoTDP line, dysregulation of *pygmb*, which is associated with the insulin resistance pathway, was found for the first time in an animal model of ALS. Therefore, the CytoTDP model may allow to identify the molecular pathways mediating this potential protective effect of insulin resistance.

4.7 CytoTDP line is helpful for the development of future nutritional interventions

In line with our findings, previous research had demonstrated increased glycogen storage in the CNS among individuals diagnosed with ALS and ALS animal models (*213*). Additionally, several FDG-PET studies conducted on ALS patients have associated decreased glucose uptake and phosphorylation with disease severity and early ALS diagnosis (*214, 215*). Several clinical studies have also reported that nutritional interventions in ALS patients may extend survival or exhibit a disease-modulating effect. Ideally, it would be beneficial to continue this research in ALS patients. However, these studies face limitations, such as small group sizes, higher dropout rates compared to typical drug trials, challenges in achieving good nutritional balance, and modest observed benefits (*216-219*).

In advancing our understanding, the CytoTDP ALS model presents a promising path for future research. Specifically, this model offers the opportunity of unraveling the complicated molecular mechanisms through which mis-localization of TDP-43 interacts with glycogen metabolism. By using CytoTDP, we may gain valuable more insights that could contribute to the refinement of therapeutic approaches and interventions for ALS.

4.8 Limitations of CytoTDP and hope for the future

Although CytoTDP not only successfully shifted endogenous TDP-43 from the nucleus to the cytoplasm and mimics several clinical features of ALS/FTD, like other TDP-43 animal models, it also has limitations. On the one hand, it is difficult to test the CytoTDP line for dementia or anxiety and depression because the CytoTDP line has strong motor phenotypes at an early age, and it is difficult to determine whether the CytoTDP line has dementia or just motor deficits. Motor deficits are indeed a typical clinical feature in ALS patients, but around 70% of

FTD patients can be free of any motor problems, and the pathologic manifestations of TDP-43 occur not only in ALS patients, but also in FTD patients who do not present motor deficits. Therefore, the study of FTD using the CytoTDP line may suffer from a lack of evaluation readouts. On the other hand, although zebrafish are vertebrates like humans, it cannot be denied that there are still huge species differences between zebrafish and humans. Even effective drugs found using mice are not guaranteed to be effective in ALS patients. Therefore, researchers not only need to continue to develop new animal models, but also to look for new biomarkers and potential therapeutic targets from affected patients.

Currently there are only two drugs approved for clinical use in the treatment of ALS: edaravone and riluzole. However, both drugs have very limited efficacy (especially edaravone) (*220-224*). Silencing of toxic gain of function genes using antisense oligonucleotides (ASOs) is currently a very promising therapeutic strategy (*225-227*), and monoclonal antibodies against mutant TDP-43 and C9ORF72 are in clinical trials (*228*). Neurofilaments in cerebrospinal fluid and plasma have been shown to be effective biomarkers for ALS (*219, 225, 229-233*). More validated ALS diagnostic biomarkers are needed to evaluate ALS progression as well as to test potential therapeutic efficacy more effectively. It has also been demonstrated that magnetic resonance imaging (MRI) combined with fluid-attenuated inversion recovery (FLAIR) or diffusion tensor imaging (DTI) can be used to monitor abnormalities in ALS patients (*234-236*). PET-CT has also provided new insights into the mechanisms of ALS (*237, 238*). By combining animal models and clinical advances, effective drugs for ALS will hopefully be discovered in the near future.

References

1. R. M. Ahmed *et al.*, Amyotrophic lateral sclerosis and frontotemporal dementia: distinct and overlapping changes in eating behaviour and metabolism. *Lancet Neurol* **15**, 332-342 (2016).
2. E. L. Feldman *et al.*, Amyotrophic lateral sclerosis. *Lancet* **400**, 1363-1380 (2022).
3. J. Bang, S. Spina, B. L. Miller, Frontotemporal dementia. *Lancet* **386**, 1672-1682 (2015).
4. S. C. Ling, M. Polymenidou, D. W. Cleveland, Converging mechanisms in ALS and FTD: disrupted RNA and protein homeostasis. *Neuron* **79**, 416-438 (2013).
5. S. A. Goutman *et al.*, Recent advances in the diagnosis and prognosis of amyotrophic lateral sclerosis. *Lancet Neurol* **21**, 480-493 (2022).
6. M. A. del Aguila, W. T. Longstreth, V. McGuire, T. D. Koepsell, G. van Belle, Prognosis in amyotrophic lateral sclerosis: a population-based study. *Neurology* **60**, 813-819 (2003).
7. S. A. Goutman *et al.*, Emerging insights into the complex genetics and pathophysiology of amyotrophic lateral sclerosis. *Lancet Neurol* **21**, 465-479 (2022).
8. B. Marin *et al.*, Age-specific ALS incidence: a dose-response meta-analysis. *Eur J Epidemiol* **33**, 621-634 (2018).
9. A. Chiò *et al.*, Global epidemiology of amyotrophic lateral sclerosis: a systematic review of the published literature. *Neuroepidemiology* **41**, 118-130 (2013).
10. B. Marin *et al.*, Variation in worldwide incidence of amyotrophic lateral sclerosis: a meta-analysis. *Int J Epidemiol* **46**, 57-74 (2017).
11. E. Longinetti, F. Fang, Epidemiology of amyotrophic lateral sclerosis: an update of recent literature. *Curr Opin Neurol* **32**, 771-776 (2019).
12. K. C. Arthur *et al.*, Projected increase in amyotrophic lateral sclerosis from 2015 to 2040. *Nat Commun* **7**, 12408 (2016).
13. P. Mehta *et al.*, Prevalence of amyotrophic lateral sclerosis - United States, 2010-2011. *MMWR Suppl* **63**, 1-14 (2014).
14. A. Chiò *et al.*, ALS phenotype is influenced by age, sex, and genetics: A population-based study. *Neurology* **94**, e802-e810 (2020).

15. A. Chiò *et al.*, Phenotypic heterogeneity of amyotrophic lateral sclerosis: a population based study. *J Neurol Neurosurg Psychiatry* **82**, 740-746 (2011).
16. C. Crockford *et al.*, ALS-specific cognitive and behavior changes associated with advancing disease stage in ALS. *Neurology* **91**, e1370-e1380 (2018).
17. M. Pinto-Grau *et al.*, Patterns of Language Impairment in Early Amyotrophic Lateral Sclerosis. *Neurol Clin Pract* **11**, e634-e644 (2021).
18. T. Burke *et al.*, A Cross-sectional population-based investigation into behavioral change in amyotrophic lateral sclerosis: subphenotypes, staging, cognitive predictors, and survival. *Ann Clin Transl Neurol* **4**, 305-317 (2017).
19. M. Elamin *et al.*, Identifying behavioural changes in ALS: Validation of the Beaumont Behavioural Inventory (BBI). *Amyotroph Lateral Scler Frontotemporal Degener* **18**, 68-73 (2017).
20. E. Beeldman *et al.*, Progression of cognitive and behavioural impairment in early amyotrophic lateral sclerosis. *J Neurol Neurosurg Psychiatry* **91**, 779-780 (2020).
21. N. Pender, M. Pinto-Grau, O. Hardiman, Cognitive and behavioural impairment in amyotrophic lateral sclerosis. *Curr Opin Neurol* **33**, 649-654 (2020).
22. E. Bersano *et al.*, Decline of cognitive and behavioral functions in amyotrophic lateral sclerosis: a longitudinal study. *Amyotroph Lateral Scler Frontotemporal Degener* **21**, 373-379 (2020).
23. Y. Park, J. Park, Y. Kim, H. Baek, S. H. Kim, Association between nutritional status and disease severity using the amyotrophic lateral sclerosis (ALS) functional rating scale in ALS patients. *Nutrition* **31**, 1362-1367 (2015).
24. P. Kühnlein *et al.*, Diagnosis and treatment of bulbar symptoms in amyotrophic lateral sclerosis. *Nat Clin Pract Neurol* **4**, 366-374 (2008).
25. T. Holm *et al.*, Severe loss of appetite in amyotrophic lateral sclerosis patients: online self-assessment study. *Interact J Med Res* **2**, e8 (2013).
26. M. H. Huisman *et al.*, Effect of Presymptomatic Body Mass Index and Consumption of Fat and Alcohol on Amyotrophic Lateral Sclerosis. *JAMA Neurol* **72**, 1155-1162 (2015).
27. C. Bouteloup *et al.*, Hypermetabolism in ALS patients: an early and persistent phenomenon. *J Neurol* **256**, 1236-1242 (2009).
28. N. Vaisman *et al.*, Do patients with amyotrophic lateral sclerosis (ALS) have increased energy needs? *J Neurol Sci* **279**, 26-29 (2009).

29. J. STEINKE, H. R. TYLER, THE ASSOCIATION OF AMYOTROPHIC LATERAL SCLEROSIS (MOTOR NEURON DISEASE) AND CARBOHYDRATE INTOLERANCE, A CLINICAL STUDY. *Metabolism* **13**, 1376-1381 (1964).
30. A. Jawaid *et al.*, ALS disease onset may occur later in patients with pre-morbid diabetes mellitus. *Eur J Neurol* **17**, 733-739 (2010).
31. E. T. Reyes, O. H. Perurena, B. W. Festoff, R. Jorgensen, W. V. Moore, Insulin resistance in amyotrophic lateral sclerosis. *J Neurol Sci* **63**, 317-324 (1984).
32. A. E. Renton, A. Chiò, B. J. Traynor, State of play in amyotrophic lateral sclerosis genetics. *Nat Neurosci* **17**, 17-23 (2014).
33. L. P. Rowland, N. A. Shneider, Amyotrophic lateral sclerosis. *N Engl J Med* **344**, 1688-1700 (2001).
34. F. Akçimen *et al.*, Amyotrophic lateral sclerosis: translating genetic discoveries into therapies. *Nat Rev Genet* **24**, 642-658 (2023).
35. D. R. Rosen *et al.*, Mutations in Cu/Zn superoxide dismutase gene are associated with familial amyotrophic lateral sclerosis. *Nature* **362**, 59-62 (1993).
36. Z. Y. Zou *et al.*, Genetic epidemiology of amyotrophic lateral sclerosis: a systematic review and meta-analysis. *J Neurol Neurosurg Psychiatry* **88**, 540-549 (2017).
37. W. Robberecht, T. Philips, The changing scene of amyotrophic lateral sclerosis. *Nat Rev Neurosci* **14**, 248-264 (2013).
38. S. Yamashita, Y. Ando, Genotype-phenotype relationship in hereditary amyotrophic lateral sclerosis. *Transl Neurodegener* **4**, 13 (2015).
39. C. F. Tan *et al.*, TDP-43 immunoreactivity in neuronal inclusions in familial amyotrophic lateral sclerosis with or without SOD1 gene mutation. *Acta Neuropathol* **113**, 535-542 (2007).
40. I. R. Mackenzie *et al.*, Pathological TDP-43 distinguishes sporadic amyotrophic lateral sclerosis from amyotrophic lateral sclerosis with SOD1 mutations. *Ann Neurol* **61**, 427-434 (2007).
41. M. DeJesus-Hernandez *et al.*, Expanded GGGGCC hexanucleotide repeat in noncoding region of C9ORF72 causes chromosome 9p-linked FTD and ALS. *Neuron* **72**, 245-256 (2011).
42. A. E. Renton *et al.*, A hexanucleotide repeat expansion in C9ORF72 is the cause of chromosome 9p21-linked ALS-FTD. *Neuron* **72**, 257-268 (2011).
43. E. L. van der Ende *et al.*, Unravelling the clinical spectrum and the role of repeat length in. *J Neurol Neurosurg Psychiatry* **92**, 502-509 (2021).

44. I. Gijselinck *et al.*, The C9orf72 repeat size correlates with onset age of disease, DNA methylation and transcriptional downregulation of the promoter. *Mol Psychiatry* **21**, 1112-1124 (2016).
45. A. Nordin *et al.*, Extensive size variability of the GGGGCC expansion in C9orf72 in both neuronal and non-neuronal tissues in 18 patients with ALS or FTD. *Hum Mol Genet* **24**, 3133-3142 (2015).
46. L. J. Schipper *et al.*, Prevalence of brain and spinal cord inclusions, including dipeptide repeat proteins, in patients with the C9ORF72 hexanucleotide repeat expansion: a systematic neuropathological review. *Neuropathol Appl Neurobiol* **42**, 547-560 (2016).
47. M. Neumann *et al.*, Ubiquitinated TDP-43 in frontotemporal lobar degeneration and amyotrophic lateral sclerosis. *Science (New York, N.Y.)* **314**, 130-133 (2006).
48. T. Arai *et al.*, TDP-43 is a component of ubiquitin-positive tau-negative inclusions in frontotemporal lobar degeneration and amyotrophic lateral sclerosis. *Biochem Biophys Res Commun* **351**, 602-611 (2006).
49. E. Kabashi *et al.*, TARDBP mutations in individuals with sporadic and familial amyotrophic lateral sclerosis. *Nat Genet* **40**, 572-574 (2008).
50. M. A. Gitcho *et al.*, TDP-43 A315T mutation in familial motor neuron disease. *Ann Neurol* **63**, 535-538 (2008).
51. V. M. Van Deerlin *et al.*, TARDBP mutations in amyotrophic lateral sclerosis with TDP-43 neuropathology: a genetic and histopathological analysis. *Lancet Neurol* **7**, 409-416 (2008).
52. A. Yokoseki *et al.*, TDP-43 mutation in familial amyotrophic lateral sclerosis. *Ann Neurol* **63**, 538-542 (2008).
53. A. Chiò *et al.*, Extensive genetics of ALS: a population-based study in Italy. *Neurology* **79**, 1983-1989 (2012).
54. E. Buratti, Functional Significance of TDP-43 Mutations in Disease. *Adv Genet* **91**, 1-53 (2015).
55. G. S. Pesiridis, V. M. Lee, J. Q. Trojanowski, Mutations in TDP-43 link glycine-rich domain functions to amyotrophic lateral sclerosis. *Hum Mol Genet* **18**, R156-162 (2009).
56. E. Buratti *et al.*, TDP-43 binds heterogeneous nuclear ribonucleoprotein A/B through its C-terminal tail: an important region for the inhibition of cystic fibrosis

transmembrane conductance regulator exon 9 splicing. *J Biol Chem* **280**, 37572-37584 (2005).

57. Y. M. Ayala *et al.*, Structural determinants of the cellular localization and shuttling of TDP-43. *J Cell Sci* **121**, 3778-3785 (2008).
58. B. S. Johnson *et al.*, TDP-43 is intrinsically aggregation-prone, and amyotrophic lateral sclerosis-linked mutations accelerate aggregation and increase toxicity. *J Biol Chem* **284**, 20329-20339 (2009).
59. T. Nonaka, F. Kametani, T. Arai, H. Akiyama, M. Hasegawa, Truncation and pathogenic mutations facilitate the formation of intracellular aggregates of TDP-43. *Hum Mol Genet* **18**, 3353-3364 (2009).
60. W. Guo *et al.*, An ALS-associated mutation affecting TDP-43 enhances protein aggregation, fibril formation and neurotoxicity. *Nat Struct Mol Biol* **18**, 822-830 (2011).
61. T. J. Kwiatkowski *et al.*, Mutations in the FUS/TLS gene on chromosome 16 cause familial amyotrophic lateral sclerosis. *Science* **323**, 1205-1208 (2009).
62. C. Vance *et al.*, Mutations in FUS, an RNA processing protein, cause familial amyotrophic lateral sclerosis type 6. *Science* **323**, 1208-1211 (2009).
63. H. Deng, K. Gao, J. Jankovic, The role of FUS gene variants in neurodegenerative diseases. *Nat Rev Neurol* **10**, 337-348 (2014).
64. A. Hirano, Neuropathology of ALS: an overview. *Neurology* **47**, S63-66 (1996).
65. N. Shibata, K. Asayama, A. Hirano, M. Kobayashi, Immunohistochemical study on superoxide dismutases in spinal cords from autopsied patients with amyotrophic lateral sclerosis. *Dev Neurosci* **18**, 492-498 (1996).
66. S. Kato, M. Saito, A. Hirano, E. Ohama, Recent advances in research on neuropathological aspects of familial amyotrophic lateral sclerosis with superoxide dismutase 1 gene mutations: neuronal Lewy body-like hyaline inclusions and astrocytic hyaline inclusions. *Histol Histopathol* **14**, 973-989 (1999).
67. N. Jankovska, R. Matej, Molecular Pathology of ALS: What We Currently Know and What Important Information Is Still Missing. *Diagnostics (Basel)* **11**, (2021).
68. M. Neumann *et al.*, Phosphorylation of S409/410 of TDP-43 is a consistent feature in all sporadic and familial forms of TDP-43 proteinopathies. *Acta Neuropathol* **117**, 137-149 (2009).
69. A. Ratti, E. Buratti, Physiological functions and pathobiology of TDP-43 and FUS/TLS proteins. *J Neurochem* **138 Suppl 1**, 95-111 (2016).

70. S. Pun, A. F. Santos, S. Saxena, L. Xu, P. Caroni, Selective vulnerability and pruning of phasic motoneuron axons in motoneuron disease alleviated by CNTF. *Nat Neurosci* **9**, 408-419 (2006).
71. M. Neumann, M. Tolnay, I. R. Mackenzie, The molecular basis of frontotemporal dementia. *Expert Rev Mol Med* **11**, e23 (2009).
72. C. U. Onyike, J. Diehl-Schmid, The epidemiology of frontotemporal dementia. *Int Rev Psychiatry* **25**, 130-137 (2013).
73. R. T. Vieira *et al.*, Epidemiology of early-onset dementia: a review of the literature. *Clin Pract Epidemiol Ment Health* **9**, 88-95 (2013).
74. M. A. Lambert *et al.*, Estimating the burden of early onset dementia; systematic review of disease prevalence. *Eur J Neurol* **21**, 563-569 (2014).
75. D. S. Knopman, R. O. Roberts, Estimating the number of persons with frontotemporal lobar degeneration in the US population. *J Mol Neurosci* **45**, 330-335 (2011).
76. J. R. Hodges, R. Davies, J. Xuereb, J. Kril, G. Halliday, Survival in frontotemporal dementia. *Neurology* **61**, 349-354 (2003).
77. M. L. Gorno-Tempini *et al.*, Classification of primary progressive aphasia and its variants. *Neurology* **76**, 1006-1014 (2011).
78. K. Rascovsky *et al.*, Sensitivity of revised diagnostic criteria for the behavioural variant of frontotemporal dementia. *Brain* **134**, 2456-2477 (2011).
79. M. M. Mesulam, Primary progressive aphasia. *Ann Neurol* **49**, 425-432 (2001).
80. B. F. Boeve, A. L. Boxer, F. Kumfor, Y. Pijnenburg, J. D. Rohrer, Advances and controversies in frontotemporal dementia: diagnosis, biomarkers, and therapeutic considerations. *Lancet Neurol* **21**, 258-272 (2022).
81. J. R. Burrell, M. C. Kiernan, S. Vucic, J. R. Hodges, Motor neuron dysfunction in frontotemporal dementia. *Brain* **134**, 2582-2594 (2011).
82. K. A. Josephs *et al.*, Clinically undetected motor neuron disease in pathologically proven frontotemporal lobar degeneration with motor neuron disease. *Arch Neurol* **63**, 506-512 (2006).
83. M. Ikeda, J. Brown, A. J. Holland, R. Fukuhara, J. R. Hodges, Changes in appetite, food preference, and eating habits in frontotemporal dementia and Alzheimer's disease. *J Neurol Neurosurg Psychiatry* **73**, 371-376 (2002).
84. O. Piguet, M. Hornberger, B. P. Shelley, C. M. Kipps, J. R. Hodges, Sensitivity of current criteria for the diagnosis of behavioral variant frontotemporal dementia. *Neurology* **72**, 732-737 (2009).

85. J. D. Woolley *et al.*, Binge eating is associated with right orbitofrontal-insular-striatal atrophy in frontotemporal dementia. *Neurology* **69**, 1424-1433 (2007).
86. J. S. Snowden *et al.*, Distinct behavioural profiles in frontotemporal dementia and semantic dementia. *J Neurol Neurosurg Psychiatry* **70**, 323-332 (2001).
87. R. M. Ahmed *et al.*, Quantifying the eating abnormalities in frontotemporal dementia. *JAMA Neurol* **71**, 1540-1546 (2014).
88. S. Shinagawa *et al.*, Characteristics of abnormal eating behaviours in frontotemporal lobar degeneration: a cross-cultural survey. *J Neurol Neurosurg Psychiatry* **80**, 1413-1414 (2009).
89. S. E. Langmore, R. K. Olney, C. Lomen-Hoerth, B. L. Miller, Dysphagia in patients with frontotemporal lobar dementia. *Arch Neurol* **64**, 58-62 (2007).
90. R. M. Ahmed *et al.*, Systemic metabolism in frontotemporal dementia. *Neurology* **83**, 1812-1818 (2014).
91. A. Golimstok *et al.*, Cardiovascular risk factors and frontotemporal dementia: a case-control study. *Transl Neurodegener* **3**, 13 (2014).
92. D. A. Olszewska, R. Lonergan, E. M. Fallon, T. Lynch, Genetics of Frontotemporal Dementia. *Curr Neurol Neurosci Rep* **16**, 107 (2016).
93. M. Hutton *et al.*, Association of missense and 5'-splice-site mutations in tau with the inherited dementia FTDP-17. *Nature* **393**, 702-705 (1998).
94. M. G. Spillantini, T. D. Bird, B. Ghetti, Frontotemporal dementia and Parkinsonism linked to chromosome 17: a new group of tauopathies. *Brain Pathol* **8**, 387-402 (1998).
95. P. Poorkaj *et al.*, Tau is a candidate gene for chromosome 17 frontotemporal dementia. *Ann Neurol* **43**, 815-825 (1998).
96. A. Benussi, A. Padovani, B. Borroni, Phenotypic Heterogeneity of Monogenic Frontotemporal Dementia. *Front Aging Neurosci* **7**, 171 (2015).
97. A. Sieben *et al.*, The genetics and neuropathology of frontotemporal lobar degeneration. *Acta Neuropathol* **124**, 353-372 (2012).
98. L. Sun, J. L. Eriksen, Recent insights into the involvement of progranulin in frontotemporal dementia. *Curr Neuropharmacol* **9**, 632-642 (2011).
99. H. R. Morris *et al.*, The genetic and pathological classification of familial frontotemporal dementia. *Arch Neurol* **58**, 1813-1816 (2001).
100. I. R. Mackenzie *et al.*, Nomenclature for neuropathologic subtypes of frontotemporal lobar degeneration: consensus recommendations. *Acta Neuropathol* **117**, 15-18 (2009).

101. N. J. Cairns *et al.*, Neuropathologic diagnostic and nosologic criteria for frontotemporal lobar degeneration: consensus of the Consortium for Frontotemporal Lobar Degeneration. *Acta Neuropathol* **114**, 5-22 (2007).
102. I. R. Mackenzie *et al.*, Nomenclature and nosology for neuropathologic subtypes of frontotemporal lobar degeneration: an update. *Acta Neuropathol* **119**, 1-4 (2010).
103. E. Buratti *et al.*, Nuclear factor TDP-43 and SR proteins promote in vitro and in vivo CFTR exon 9 skipping. *EMBO J* **20**, 1774-1784 (2001).
104. H. Y. Wang, I. F. Wang, J. Bose, C. K. Shen, Structural diversity and functional implications of the eukaryotic TDP gene family. *Genomics* **83**, 130-139 (2004).
105. Y. M. Ayala *et al.*, Human, Drosophila, and C.elegans TDP43: nucleic acid binding properties and splicing regulatory function. *J Mol Biol* **348**, 575-588 (2005).
106. M. J. Winton *et al.*, Disturbance of nuclear and cytoplasmic TAR DNA-binding protein (TDP-43) induces disease-like redistribution, sequestration, and aggregate formation. *J Biol Chem* **283**, 13302-13309 (2008).
107. Y. Hu *et al.*, Mis-localization of endogenous TDP-43 leads to ALS-like early-stage metabolic dysfunction and progressive motor deficits. *Mol Neurodegener* **19**, 50 (2024).
108. E. Buratti, F. E. Baralle, Multiple roles of TDP-43 in gene expression, splicing regulation, and human disease. *Front Biosci* **13**, 867-878 (2008).
109. C. Lagier-Tourenne, M. Polymenidou, D. W. Cleveland, TDP-43 and FUS/TLS: emerging roles in RNA processing and neurodegeneration. *Hum Mol Genet* **19**, R46-64 (2010).
110. E. Buratti *et al.*, Nuclear factor TDP-43 can affect selected microRNA levels. *FEBS J* **277**, 2268-2281 (2010).
111. Z. S. Xu, Does a loss of TDP-43 function cause neurodegeneration? *Mol Neurodegener* **7**, 27 (2012).
112. C. F. Sephton *et al.*, TDP-43 is a developmentally regulated protein essential for early embryonic development. *J Biol Chem* **285**, 6826-6834 (2010).
113. L. S. Wu *et al.*, TDP-43, a neuro-pathosignature factor, is essential for early mouse embryogenesis. *Genesis* **48**, 56-62 (2010).
114. B. C. Kraemer *et al.*, Loss of murine TDP-43 disrupts motor function and plays an essential role in embryogenesis. *Acta Neuropathol* **119**, 409-419 (2010).

115. Y. M. Ayala *et al.*, TDP-43 regulates its mRNA levels through a negative feedback loop. *EMBO J* **30**, 277-288 (2011).
116. S. E. Avendaño-Vázquez *et al.*, Autoregulation of TDP-43 mRNA levels involves interplay between transcription, splicing, and alternative polyA site selection. *Genes Dev* **26**, 1679-1684 (2012).
117. H. Wils *et al.*, TDP-43 transgenic mice develop spastic paralysis and neuronal inclusions characteristic of ALS and frontotemporal lobar degeneration. *Proc Natl Acad Sci U S A* **107**, 3858-3863 (2010).
118. M. Hasegawa *et al.*, Phosphorylated TDP-43 in frontotemporal lobar degeneration and amyotrophic lateral sclerosis. *Ann Neurol* **64**, 60-70 (2008).
119. H. Tsuji *et al.*, Molecular analysis and biochemical classification of TDP-43 proteinopathy. *Brain* **135**, 3380-3391 (2012).
120. S. Xiao *et al.*, Low molecular weight species of TDP-43 generated by abnormal splicing form inclusions in amyotrophic lateral sclerosis and result in motor neuron death. *Acta Neuropathol* **130**, 49-61 (2015).
121. Y. Davidson *et al.*, Ubiquitinated pathological lesions in frontotemporal lobar degeneration contain the TAR DNA-binding protein, TDP-43. *Acta Neuropathol* **113**, 521-533 (2007).
122. F. Geser *et al.*, Pathological TDP-43 in parkinsonism-dementia complex and amyotrophic lateral sclerosis of Guam. *Acta Neuropathol* **115**, 133-145 (2008).
123. M. Hasegawa *et al.*, TDP-43 is deposited in the Guam parkinsonism-dementia complex brains. *Brain* **130**, 1386-1394 (2007).
124. C. Amador-Ortiz *et al.*, TDP-43 immunoreactivity in hippocampal sclerosis and Alzheimer's disease. *Ann Neurol* **61**, 435-445 (2007).
125. A. Probst, K. I. Taylor, M. Tolnay, Hippocampal sclerosis dementia: a reappraisal. *Acta Neuropathol* **114**, 335-345 (2007).
126. S. H. Freeman, T. Spires-Jones, B. T. Hyman, J. H. Growdon, M. P. Frosch, TAR-DNA binding protein 43 in Pick disease. *J Neuropathol Exp Neurol* **67**, 62-67 (2008).
127. K. Uryu *et al.*, Concomitant TAR-DNA-binding protein 43 pathology is present in Alzheimer disease and corticobasal degeneration but not in other tauopathies. *J Neuropathol Exp Neurol* **67**, 555-564 (2008).
128. S. Nag, J. A. Schneider, Limbic-predominant age-related TDP43 encephalopathy (LATE) neuropathological change in neurodegenerative diseases. *Nat Rev Neurol* **19**, 525-541 (2023).

129. I. R. Mackenzie, R. Rademakers, M. Neumann, TDP-43 and FUS in amyotrophic lateral sclerosis and frontotemporal dementia. *Lancet Neurol* **9**, 995-1007 (2010).
130. R. Pamphlett, N. Luquin, C. McLean, S. K. Jew, L. Adams, TDP-43 neuropathology is similar in sporadic amyotrophic lateral sclerosis with or without TDP-43 mutations. *Neuropathol Appl Neurobiol* **35**, 222-225 (2009).
131. G. G. Kovacs *et al.*, TARDBP variation associated with frontotemporal dementia, supranuclear gaze palsy, and chorea. *Mov Disord* **24**, 1843-1847 (2009).
132. D. M. Sampathu *et al.*, Pathological heterogeneity of frontotemporal lobar degeneration with ubiquitin-positive inclusions delineated by ubiquitin immunohistochemistry and novel monoclonal antibodies. *Am J Pathol* **169**, 1343-1352 (2006).
133. I. R. Mackenzie *et al.*, Heterogeneity of ubiquitin pathology in frontotemporal lobar degeneration: classification and relation to clinical phenotype. *Acta Neuropathol* **112**, 539-549 (2006).
134. K. A. Josephs, A. Stroh, B. Dugger, D. W. Dickson, Evaluation of subcortical pathology and clinical correlations in FTLD-U subtypes. *Acta Neuropathol* **118**, 349-358 (2009).
135. M. Neumann *et al.*, TDP-43 in the ubiquitin pathology of frontotemporal dementia with VCP gene mutations. *J Neuropathol Exp Neurol* **66**, 152-157 (2007).
136. B. Schmid *et al.*, Loss of ALS-associated TDP-43 in zebrafish causes muscle degeneration, vascular dysfunction, and reduced motor neuron axon outgrowth. *Proc Natl Acad Sci U S A* **110**, 4986-4991 (2013).
137. C. A. Hewamadduma *et al.*, Tardbpl splicing rescues motor neuron and axonal development in a mutant tardbp zebrafish. *Hum Mol Genet* **22**, 2376-2386 (2013).
138. T. W. Todd, L. Petrucelli, Modelling amyotrophic lateral sclerosis in rodents. *Nat Rev Neurosci* **23**, 231-251 (2022).
139. L. S. Wu *et al.*, Transcriptomopathies of pre- and post-symptomatic frontotemporal dementia-like mice with TDP-43 depletion in forebrain neurons. *Acta Neuropathol Commun* **7**, 50 (2019).
140. L. S. Wu, W. C. Cheng, C. K. Shen, Targeted depletion of TDP-43 expression in the spinal cord motor neurons leads to the development of amyotrophic

lateral sclerosis-like phenotypes in mice. *J Biol Chem* **287**, 27335-27344 (2012).

141. A. K. Walker *et al.*, Functional recovery in new mouse models of ALS/FTLD after clearance of pathological cytoplasmic TDP-43. *Acta Neuropathol* **130**, 643-660 (2015).
142. M. A. White *et al.*, TDP-43 gains function due to perturbed autoregulation in a Tardbp knock-in mouse model of ALS-FTD. *Nat Neurosci* **21**, 552-563 (2018).
143. S. L. Huang *et al.*, A robust TDP-43 knock-in mouse model of ALS. *Acta Neuropathol Commun* **8**, 3 (2020).
144. S. Watanabe *et al.*, ALS-linked TDP-43. *Mol Brain* **13**, 8 (2020).
145. S. Y. Ebstein, I. Yagudayeva, N. A. Shneider, Mutant TDP-43 Causes Early-Stage Dose-Dependent Motor Neuron Degeneration in a TARDBP Knockin Mouse Model of ALS. *Cell Rep* **26**, 364-373.e364 (2019).
146. H. P. Müller *et al.*, Longitudinal diffusion tensor magnetic resonance imaging analysis at the cohort level reveals disturbed cortical and callosal microstructure with spared corticospinal tract in the. *Transl Neurodegener* **8**, 27 (2019).
147. Z. Melamed *et al.*, Premature polyadenylation-mediated loss of stathmin-2 is a hallmark of TDP-43-dependent neurodegeneration. *Nat Neurosci* **22**, 180-190 (2019).
148. J. R. Klim *et al.*, ALS-implicated protein TDP-43 sustains levels of STMN2, a mediator of motor neuron growth and repair. *Nat Neurosci* **22**, 167-179 (2019).
149. X. R. Ma *et al.*, TDP-43 represses cryptic exon inclusion in the FTD-ALS gene UNC13A. *Nature* **603**, 124-130 (2022).
150. A. Villani *et al.*, Clearance by Microglia Depends on Packaging of Phagosomes into a Unique Cellular Compartment. *Dev Cell* **49**, 77-88.e77 (2019).
151. C. Lawrence, E. Sanders, E. Henry, Methods for culturing saltwater rotifers (Brachionus plicatilis) for rearing larval zebrafish. *Zebrafish* **9**, 140-146 (2012).
152. C. Lawrence, A. James, S. Mobley, Successful Replacement of Artemia salina nauplii with Marine Rotifers (Brachionus plicatilis) in the Diet of Preadult Zebrafish (Danio rerio). *Zebrafish* **12**, 366-371 (2015).
153. C. Lawrence *et al.*, The Complete and Updated "Rotifer Polyculture Method" for Rearing First Feeding Zebrafish. *J Vis Exp*, e53629 (2016).
154. C. B. Kimmel, W. W. Ballard, S. R. Kimmel, B. Ullmann, T. F. Schilling, Stages of embryonic development of the zebrafish. *Dev Dyn* **203**, 253-310 (1995).

155. A. Hruscha, B. Schmid, Generation of zebrafish models by CRISPR /Cas9 genome editing. *Methods Mol Biol* **1254**, 341-350 (2015).
156. M. Pende *et al.*, A versatile depigmentation, clearing, and labeling method for exploring nervous system diversity. *Science advances* **6**, eaba0365 (2020).
157. G. Kislinger *et al.*, ATUM-FIB microscopy for targeting and multiscale imaging of rare events in mouse cortex. *STAR Protocols* **1**, 100232 (2020).
158. J. Schindelin *et al.*, Fiji: an open-source platform for biological-image analysis. *Nat Methods* **9**, 676-682 (2012).
159. M. I. Love, W. Huber, S. Anders, Moderated estimation of fold change and dispersion for RNA-seq data with DESeq2. *Genome Biol* **15**, 550 (2014).
160. C. H. Chin *et al.*, cytoHubba: identifying hub objects and sub-networks from complex interactome. *BMC Syst Biol* **8 Suppl 4**, S11 (2014).
161. M. J. Winton *et al.*, Disturbance of nuclear and cytoplasmic TAR DNA-binding protein (TDP-43) induces disease-like redistribution, sequestration, and aggregate formation. *Journal of Biological Chemistry* **283**, 13302-13309 (2008).
162. A. Ionescu, T. Altman, E. Perlson, Looking for answers far away from the soma-the (un)known axonal functions of TDP-43, and their contribution to early NMJ disruption in ALS. *Mol Neurodegener* **18**, 35 (2023).
163. J. A. Panzer *et al.*, Neuromuscular synaptogenesis in wild-type and mutant zebrafish. *Dev Biol* **285**, 340-357 (2005).
164. M. Colonna, O. Butovsky, Microglia Function in the Central Nervous System During Health and Neurodegeneration. *Annu Rev Immunol* **35**, 441-468 (2017).
165. O. Ronneberger *et al.*, ViBE-Z: a framework for 3D virtual colocalization analysis in zebrafish larval brains. *Nat Methods* **9**, 735-742 (2012).
166. E. M. C. Fisher *et al.*, Opinion: more mouse models and more translation needed for ALS. *Mol Neurodegener* **18**, 30 (2023).
167. G. Kim, O. Gautier, E. Tassoni-Tsuchida, X. R. Ma, A. D. Gitler, ALS Genetics: Gains, Losses, and Implications for Future Therapies. *Neuron* **108**, 822-842 (2020).
168. M. Baralle, E. Buratti, F. E. Baralle, The role of TDP-43 in the pathogenesis of ALS and FTLD. *Biochem Soc Trans* **41**, 1536-1540 (2013).
169. R. A. Fuentealba *et al.*, Interaction with polyglutamine aggregates reveals a Q/N-rich domain in TDP-43. *J Biol Chem* **285**, 26304-26314 (2010).

170. E. B. Lee, V. M. Lee, J. Q. Trojanowski, Gains or losses: molecular mechanisms of TDP43-mediated neurodegeneration. *Nat Rev Neurosci* **13**, 38-50 (2011).
171. E. L. Scotter, H. J. Chen, C. E. Shaw, TDP-43 Proteinopathy and ALS: Insights into Disease Mechanisms and Therapeutic Targets. *Neurotherapeutics* **12**, 352-363 (2015).
172. P. Fratta *et al.*, Mice with endogenous TDP-43 mutations exhibit gain of splicing function and characteristics of amyotrophic lateral sclerosis. *The EMBO journal* **37**, (2018).
173. E. Kabashi *et al.*, Gain and loss of function of ALS-related mutations of TARDBP (TDP-43) cause motor deficits in vivo. *Hum Mol Genet* **19**, 671-683 (2010).
174. K. Chia, A. Klingseisen, D. Sieger, J. Priller, Zebrafish as a model organism for neurodegenerative disease. *Front Mol Neurosci* **15**, 940484 (2022).
175. M. R. Turner *et al.*, Evidence of widespread cerebral microglial activation in amyotrophic lateral sclerosis: an [11C](R)-PK11195 positron emission tomography study. *Neurobiol Dis* **15**, 601-609 (2004).
176. M. E. Alexianu, M. Kozovska, S. H. Appel, Immune reactivity in a mouse model of familial ALS correlates with disease progression. *Neurology* **57**, 1282-1289 (2001).
177. K. D. LaClair *et al.*, Congenic expression of poly-GA but not poly-PR in mice triggers selective neuron loss and interferon responses found in C9orf72 ALS. *Acta neuropathologica* **140**, 121-142 (2020).
178. L. M. Igaz *et al.*, Dysregulation of the ALS-associated gene TDP-43 leads to neuronal death and degeneration in mice. *J Clin Invest* **121**, 726-738 (2011).
179. A. Kalsbeek *et al.*, Hypothalamic control of energy metabolism via the autonomic nervous system. *Ann N Y Acad Sci* **1212**, 114-129 (2010).
180. M. Valdearcos, M. G. Myers, S. K. Koliwad, Hypothalamic microglia as potential regulators of metabolic physiology. *Nat Metab* **1**, 314-320 (2019).
181. J. Y. Li *et al.*, Correlation of weight and body composition with disease progression rate in patients with amyotrophic lateral sclerosis. *Sci Rep* **12**, 13292 (2022).
182. S. Körner *et al.*, Weight loss, dysphagia and supplement intake in patients with amyotrophic lateral sclerosis (ALS): impact on quality of life and therapeutic options. *BMC Neurol* **13**, 84 (2013).

183. Q. Q. Wei *et al.*, Early weight instability is associated with cognitive decline and poor survival in amyotrophic lateral sclerosis. *Brain Res Bull* **171**, 10-15 (2021).
184. A. Ludolph *et al.*, Nutritional and metabolic factors in amyotrophic lateral sclerosis. *Nature reviews. Neurology* **19**, 511-524 (2023).
185. R. S. Peter *et al.*, Life course body mass index and risk and prognosis of amyotrophic lateral sclerosis: results from the ALS registry Swabia. *Eur J Epidemiol* **32**, 901-908 (2017).
186. M. D. Cykowski, H. Takei, P. E. Schulz, S. H. Appel, S. Z. Powell, TDP-43 pathology in the basal forebrain and hypothalamus of patients with amyotrophic lateral sclerosis. *Acta Neuropathol Commun* **2**, 171 (2014).
187. M. Gorges *et al.*, Hypothalamic atrophy is related to body mass index and age at onset in amyotrophic lateral sclerosis. *Journal of neurology, neurosurgery, and psychiatry* **88**, 1033-1041 (2017).
188. O. Piguet *et al.*, Eating and hypothalamus changes in behavioral-variant frontotemporal dementia. *Ann Neurol* **69**, 312-319 (2011).
189. S. Gabery *et al.*, Loss of the metabolism and sleep regulating neuronal populations expressing orexin and oxytocin in the hypothalamus in amyotrophic lateral sclerosis. *Neuropathol Appl Neurobiol* **47**, 979-989 (2021).
190. J. C. Desport *et al.*, Nutritional status is a prognostic factor for survival in ALS patients. *Neurology* **53**, 1059-1063 (1999).
191. J. C. Desport *et al.*, Nutritional assessment and survival in ALS patients. *Amyotroph Lateral Scler Other Motor Neuron Disord* **1**, 91-96 (2000).
192. É. O'Reilly *et al.*, Premorbid body mass index and risk of amyotrophic lateral sclerosis. *Amyotroph Lateral Scler Frontotemporal Degener* **14**, 205-211 (2013).
193. V. Gallo *et al.*, Prediagnostic body fat and risk of death from amyotrophic lateral sclerosis: the EPIC cohort. *Neurology* **80**, 829-838 (2013).
194. J. Brettschneider *et al.*, Stages of pTDP-43 pathology in amyotrophic lateral sclerosis. *Ann Neurol* **74**, 20-38 (2013).
195. E. S. David, M. M. Crerar, Quantitation of muscle glycogen phosphorylase mRNA and enzyme amounts in adult rat tissues. *Biochim Biophys Acta* **880**, 78-90 (1986).
196. B. Pfeiffer-Guglielmi, B. Fleckenstein, G. Jung, B. Hamprecht, Immunocytochemical localization of glycogen phosphorylase isozymes in rat

nervous tissues by using isozyme-specific antibodies. *J Neurochem* **85**, 73-81 (2003).

197. B. Pfeiffer-Guglielmi, S. Bröer, A. Bröer, B. Hamprecht, Isozyme pattern of glycogen phosphorylase in the rat nervous system and rat astroglia-rich primary cultures: electrophoretic and polymerase chain reaction studies. *Neurochem Res* **25**, 1485-1491 (2000).
198. E. Jakobsen *et al.*, Glycogen Shunt Activity and Glycolytic Supercompensation in Astrocytes May Be Distinctly Mediated via the Muscle Form of Glycogen Phosphorylase. *Neurochem Res* **42**, 2490-2494 (2017).
199. R. Pinacho *et al.*, The glial phosphorylase of glycogen isoform is reduced in the dorsolateral prefrontal cortex in chronic schizophrenia. *Schizophr Res* **177**, 37-43 (2016).
200. S. P. Allen *et al.*, C9orf72 expansion within astrocytes reduces metabolic flexibility in amyotrophic lateral sclerosis. *Brain* **142**, 3771-3790 (2019).
201. M. Kanehisa, S. Goto, M. Furumichi, M. Tanabe, M. Hirakawa, KEGG for representation and analysis of molecular networks involving diseases and drugs. *Nucleic Acids Res* **38**, D355-360 (2010).
202. S. C. Cunnane *et al.*, Brain energy rescue: an emerging therapeutic concept for neurodegenerative disorders of ageing. *Nat Rev Drug Discov* **19**, 609-633 (2020).
203. S. Li, I. Laher, Exercise Pills: At the Starting Line. *Trends Pharmacol Sci* **36**, 906-917 (2015).
204. M. N. N. Vieira, R. A. S. Lima-Filho, F. G. De Felice, Connecting Alzheimer's disease to diabetes: Underlying mechanisms and potential therapeutic targets. *Neuropharmacology* **136**, 160-171 (2018).
205. C. A. Castellano *et al.*, A 3-Month Aerobic Training Program Improves Brain Energy Metabolism in Mild Alzheimer's Disease: Preliminary Results from a Neuroimaging Study. *J Alzheimers Dis* **56**, 1459-1468 (2017).
206. J. K. Morris *et al.*, Measures of striatal insulin resistance in a 6-hydroxydopamine model of Parkinson's disease. *Brain Res* **1240**, 185-195 (2008).
207. D. Bosco *et al.*, Dementia is associated with insulin resistance in patients with Parkinson's disease. *J Neurol Sci* **315**, 39-43 (2012).

208. Y. Pang *et al.*, Intranasal insulin protects against substantia nigra dopaminergic neuronal loss and alleviates motor deficits induced by 6-OHDA in rats. *Neuroscience* **318**, 157-165 (2016).
209. H. Green, P. Tsitsi, I. Markaki, D. Aarsland, P. Svenningsson, Novel Treatment Opportunities Against Cognitive Impairment in Parkinson's Disease with an Emphasis on Diabetes-Related Pathways. *CNS Drugs* **33**, 143-160 (2019).
210. D. Mariosa, F. Kamel, R. Bellocco, W. Ye, F. Fang, Association between diabetes and amyotrophic lateral sclerosis in Sweden. *Eur J Neurol* **22**, 1436-1442 (2015).
211. M. R. Turner, R. Goldacre, S. Ramagopalan, K. Talbot, M. J. Goldacre, Autoimmune disease preceding amyotrophic lateral sclerosis: an epidemiologic study. *Neurology* **81**, 1222-1225 (2013).
212. P. F. Pradat *et al.*, Impaired glucose tolerance in patients with amyotrophic lateral sclerosis. *Amyotroph Lateral Scler* **11**, 166-171 (2010).
213. J. C. Dodge *et al.*, Metabolic signatures of amyotrophic lateral sclerosis reveal insights into disease pathogenesis. *Proceedings of the National Academy of Sciences of the United States of America* **110**, 10812-10817 (2013).
214. M. C. Dalakas, J. Hatazawa, R. A. Brooks, G. Di Chiro, Lowered cerebral glucose utilization in amyotrophic lateral sclerosis. *Ann Neurol* **22**, 580-586 (1987).
215. K. Van Laere *et al.*, Value of 18fluorodeoxyglucose-positron-emission tomography in amyotrophic lateral sclerosis: a prospective study. *JAMA Neurol* **71**, 553-561 (2014).
216. A. M. Wills *et al.*, Hypercaloric enteral nutrition in patients with amyotrophic lateral sclerosis: a randomised, double-blind, placebo-controlled phase 2 trial. *Lancet* **383**, 2065-2072 (2014).
217. J. Dorst *et al.*, Percutaneous endoscopic gastrostomy in amyotrophic lateral sclerosis: a prospective observational study. *J Neurol* **262**, 849-858 (2015).
218. A. C. Ludolph *et al.*, Effect of High-Caloric Nutrition on Survival in Amyotrophic Lateral Sclerosis. *Ann Neurol* **87**, 206-216 (2020).
219. J. Dorst *et al.*, Effect of high-caloric nutrition on serum neurofilament light chain levels in amyotrophic lateral sclerosis. *Journal of neurology, neurosurgery, and psychiatry* **91**, 1007-1009 (2020).

220. T. Fang *et al.*, Stage at which riluzole treatment prolongs survival in patients with amyotrophic lateral sclerosis: a retrospective analysis of data from a dose-ranging study. *Lancet Neurol* **17**, 416-422 (2018).
221. J. A. Andrews *et al.*, Real-world evidence of riluzole effectiveness in treating amyotrophic lateral sclerosis. *Amyotroph Lateral Scler Frontotemporal Degener* **21**, 509-518 (2020).
222. J. Shefner *et al.*, Long-term edaravone efficacy in amyotrophic lateral sclerosis: Post-hoc analyses of Study 19 (MCI186-19). *Muscle Nerve* **61**, 218-221 (2020).
223. C. Lunetta *et al.*, The Italian multicenter experience with edaravone in amyotrophic lateral sclerosis. *J Neurol* **267**, 3258-3267 (2020).
224. S. Witzel *et al.*, Safety and Effectiveness of Long-term Intravenous Administration of Edaravone for Treatment of Patients With Amyotrophic Lateral Sclerosis. *JAMA Neurol* **79**, 121-130 (2022).
225. T. M. Miller *et al.*, Trial of Antisense Oligonucleotide Tofersen for. *N Engl J Med* **387**, 1099-1110 (2022).
226. D. A. Amado, B. L. Davidson, Gene therapy for ALS: A review. *Mol Ther* **29**, 3345-3358 (2021).
227. A. Mullard, ALS antisense drug falters in phase III. *Nat Rev Drug Discov* **20**, 883-885 (2021).
228. A. Poulin-Brière, E. Rezaei, S. Pozzi, Antibody-Based Therapeutic Interventions for Amyotrophic Lateral Sclerosis: A Systematic Literature Review. *Front Neurosci* **15**, 790114 (2021).
229. F. Huang *et al.*, Longitudinal biomarkers in amyotrophic lateral sclerosis. *Ann Clin Transl Neurol* **7**, 1103-1116 (2020).
230. K. Poesen *et al.*, Neurofilament markers for ALS correlate with extent of upper and lower motor neuron disease. *Neurology* **88**, 2302-2309 (2017).
231. M. Benatar *et al.*, Validation of serum neurofilaments as prognostic and potential pharmacodynamic biomarkers for ALS. *Neurology* **95**, e59-e69 (2020).
232. M. Benatar, J. Wuu, P. M. Andersen, V. Lombardi, A. Malaspina, Neurofilament light: A candidate biomarker of presymptomatic amyotrophic lateral sclerosis and phenoconversion. *Ann Neurol* **84**, 130-139 (2018).
233. K. Bjornevik *et al.*, Prediagnostic Neurofilament Light Chain Levels in Amyotrophic Lateral Sclerosis. *Neurology* **97**, e1466-e1474 (2021).
234. J. Fabes *et al.*, Quantitative FLAIR MRI in Amyotrophic Lateral Sclerosis. *Acad Radiol* **24**, 1187-1194 (2017).

235. E. K. Weidman *et al.*, Diffusion tensor imaging and quantitative susceptibility mapping as diagnostic tools for motor neuron disorders. *Clin Imaging* **53**, 6-11 (2019).
236. T. Welton *et al.*, Diffusion kurtosis and quantitative susceptibility mapping MRI are sensitive to structural abnormalities in amyotrophic lateral sclerosis. *Neuroimage Clin* **24**, 101953 (2019).
237. L. D'hulst *et al.*, Multicenter validation of [*Amyotroph Lateral Scler Frontotemporal Degener* **19**, 570-577 (2018).
238. E. M. Ratai *et al.*, Integrated imaging of [*Neuroimage Clin* **20**, 357-364 (2018).

Acknowledgement

There are many people I would like to thank during this PhD journey.

First of all, I would like to express my sincere gratitude to Prof. Dr. Dr. h.c. Christian Haass for his continuous supervision, support and excellent advice throughout my Ph.D. He is a very wise and supportive leader and has an extremely broad knowledge of biology, biochemistry, medicine and clinical medicine. His guidance has made a profound impact on me and inspires me to become a clinician scientist.

I would like to thank Dr. Bettina Schmid for providing me with the opportunity to conduct my PhD research in a wonderful group with a very pleasant working atmosphere in the zebrafish group. I am also very grateful to Dr. Bettina Schmid for supervising my PhD project, she is a very good zebrafish expert and it was a very enjoyable journey to conduct zebrafish research.

I am very grateful to Dr. Thomas Arzberger for his advice and support on my PhD project, he is always very nice and willing to share his knowledge on pathology and ALS/FTLD.

I would also like to thank Prof. Dr. Dieter Edbauer, a member of my Thesis Advisory Committee (TAC), for his advice on my PhD project and for the excellent discussions with him.

I would like to thank my collaborator, Dr. Martina Schifferer, for her help with the EM parts of my project and her care during my entire PhD study.

I would like to thank all the members of the zebrafish group for their support of my PhD project, especially Alexander Hruscha for sharing his extensive experimental experience with me.

I would like to thank my friends Dr. Laura Strohm, Mareike Czuppa, Dr. Xianyuan Xiang, Dr. Ali Rezaei, Rong Fang, Dr. Lukai Zheng, Lizhen Cheng, Dr. Zhouyi Rong, Lin Zhang, Yang Wang and nice neighbors from Christian Behrends's lab

for their invaluable help and friendly companionship during my study. I would like to thank Brigitte Nuscher, Sabine Odoy, Marcel Matt, Wilhelm Tkocz, Dr. Manuela Schneider, Dr. Carolin Konrad and Arailym Aronova for their kind help.

I would like to thank China Scholarship Council (CSC) and Prof. Dr. Dr. h.c. Christian Haass for funding my PhD study.

I would like to thank my collaborator Dr. Chenchen Pan for the scientific discussions with me every day, which is very helpful for my scientific thinking, and I am also thankful for his experimental support of my project.

Finally, I would like to thank my family for their understanding, support and encouragement during my whole PhD. This is an unforgettable and amazing journey and the beginning of my academic career.

Affidavit

LMU LUDWIG-MAXIMILIANS-UNIVERSITÄT MÜNCHEN

Dekanat Medizinische Fakultät
Promotionsbüro

Affidavit

Hu, Yiying

Surname, first name

Feodor-Lynen-Str 17, 81377 Munich

Address

I hereby declare, that the submitted thesis entitled

Mis-localization of endogenous TDP-43 leads to ALS-like early-stage metabolic dysfunction and progressive motor deficits

is my own work. I have only used the sources indicated and have not made unauthorised use of services of a third party. Where the work of others has been quoted or reproduced, the source is always given.

I further declare that the dissertation presented here has not been submitted in the same or similar form to any other institution for the purpose of obtaining an academic degree.

Munich, 17.07.2024

Place, Date

Yiying Hu

Signature doctoral candidate

Confirmation of congruency

LMU LUDWIG-MAXIMILIANS-UNIVERSITÄT MÜNCHEN

Dean's Office Medical Faculty
Doctoral Office

Confirmation of congruency between printed and electronic version of the doctoral thesis

Doctoral candidate: Yiying Hu

Address: Feodor-Lynen-Str 17, 81377 Munich

I hereby declare that the electronic version of the submitted thesis, entitled

Mis-localization of endogenous TDP-43 leads to ALS-like early-stage metabolic dysfunction and progressive motor deficits

is congruent with the printed version both in content and format.

Munich, 17.07.2024 — Yiying Hu

Place, Date — Signature doctoral candidate

List of publications

1. **Yiying Hu**, Alexander Hruscha, Chenchen Pan, Thomas Arzberger, Martina Schifferer, Michael K. Schmidt, Özge Burhan, Brigitte Nuscher, Martin Giera, Sarantos Kostidis, Frauke van Bebber, Dieter Edbauer, Christian Haass, Bettina Schmid; Mis-localization of endogenous TDP-43 leads to ALS-like early-stage metabolic dysfunction and progressive motor deficits. Mol Neurodegener 19, 50 (2024). DOI: 10.1186/s13024-024-00735-7.
2. **Yiying Hu**; Yajun Lian; Hongliang Xu; Yake Zheng; Chenfei Li; Jiwei Zhang; Shuping Yan; Novel, de novo dysferlin gene mutations in a patient with Miyoshi myopathy. Neuroscience Letters.2018V664N:107-109, DOI: 10.1016/j.neulet.2017.10.048.
3. Jae-Sook Park; **Yiying Hu**; Nancy M Hollingsworth; Gabriel Miltenberger-Miltenyi; Aaron M Neiman; Interaction between VPS13A and the XK scramblase is important for VPS13A function in humans. Journal of Cell Science. 2022 Sep 1;135(17): jcs260227. DOI: 10.1242/jcs.260227.
4. Yuhan Wang; Wenchao Cheng; Yajun Lian; Jing Zhang; Yake Zheng; **Yiying Hu**; Yuan Chen; Shouyi Wu; Zhi Huang; Yinping Shi; Characteristics and Relative Factors of Headache Caused by Cervicocerebral Artery Dissection. Journal of Neurology. 2019 Feb;266(2):298-305. DOI: 10.1007/s00415-018-9111-5.
5. Wenchao Cheng; Yuhan Wang; Yajun Lian; Jing Zhang; Yake Zheng; **Yiying Hu**; Yuan Chen; Shouyi Wu; Zhi Huang; Yinping Shi; A Case-control Study of the Determinants for Cervicocerebral Artery Dissection. Journal of Neurology. 2019 Jan;266(1):119-123. DOI: 10.1007/s00415-018-9096-0.